ปริมาณรังสีที่ผู้ป่วยได้รับจากการตรวจ Whole brain Computed Tomography In Comprehensive Stroke Imaging ด้วยเครื่องเอกซเรย์คอมพิวเตอร์ชนิด320 สไลซ์ โดยเทคนิค Axial Volumetric Mode

นางสาวสายฝน อาจมนตรี

วิทยานิพนธ์นี้เป็นส่วนหนึ่งของการศึกษาตามหลักสูตรปริญญาวิทยาศาสตรมหาบัณฑิต
สาขาวิชาฉายาเวชศาสตร์ ภาควิชารังสีวิทยา
คณะแพทยศาสตร์ จุฬาลงกรณ์มหาวิทยาลัย
ปีการศึกษา 2556

RADIATION DOSE IN WHOLE BRAIN COMPUTED TOMOGRAPHY IN COMPREHENSIVE STROKE IMAGING USING AXIAL VOLUMETRIC 320-DETECTOR CT

Miss Saifhon Admontree

A Thesis Submitted in Partial Fulfillment of the Requirements
for the Degree of Master of Science Program in Medical Imaging
Department of Radiology
Faculty of Medicine
Chulalongkorn University
Academic Year 2013

Thesis Title	RADIATION DOSE IN WHOLE BRAIN COMPUTED TOMOGRAPHY IN COMPREHENSIVE STROKE IMAGING USING AXIAL VOLUMETRIC 320-DETECTOR CT
By	Miss Saifhon Admontree
Field of Study	Medical Imaging
Thesis Advisor	Associate Professor Anchali Krisanachinda, Ph.D.
Thesis Co-Advisor	Associate Professor Jiraporn Laothamatas, M.D.
	Associate Professor Panruethai Trinavarat, M.D.

Accepted by the Faculty of Medicine, Chulalongkorn University in Partial Fulfillment of the Requirements for the Master's Degree

....Dean of the Faculty of Medicine

(Associate Professor Sophon Napathorn, M.D.)

THESIS COMMITTEE

....Chairman

(Associate Professor Kiat Arjhansiri, M.D.)

....Thesis Advisor

(Associate Professor Anchali Krisanachinda, Ph.D.)

....Thesis Co-Advisor

(Associate Professor Jiraporn Laothamatas, M.D.)

....Thesis Co-Advisor

(Associate Professor Panruethai Trinavarat, M.D.)

....External Examiner

(Professor Franco Milano, Ph.D.)

สายฝน อาจมนตรี : ปริมาณรังสีที่ผู้ป่วยได้รับจากการตรวจ Whole brain Computed Tomography In Comprehensive Stroke Imaging ด้วยเครื่องเอกซเรย์คอมพิวเตอร์ชนิด320 สไลซ์ โดยเทคนิค Axial Volumetric Mode. (RADIATION DOSE IN WHOLE BRAIN COMPUTED TOMOGRAPHY IN COMPREHENSIVE STROKE IMAGING USING AXIAL VOLUMETRIC 320-DETECTOR CT) อ.ที่ปรึกษาวิทยานิพนธ์หลัก: รศ. ดร. อัญชลี กฤษณจินดา, อ.ที่ปรึกษาวิทยานิพนธ์ร่วม: รศ. พญ. จิรพร เหล่าธรรมทัศน์, รศ. พญ. ปานฤทัย ตรีนวรัตน์, 93 หน้า.

เครื่องเอกซเรย์คอมพิวเตอร์ชนิด 320 แถวหัววัดที่เปิดได้กว้างครอบคลุมแนวหัวท้าย (Z-direction) ของร่างกาย สามารถถ่ายภาพสมองทั้งศีรษะได้ ชุดการตรวจอย่างต่อเนื่องตามเวลา (Dynamic series) ของหลอดเลือดแดง (CT Angiography) หลอดเลือดดำ (CT Venography) และ CT Perfusion ที่ทำในครั้งเดียวกันหลังฉีดสารทึบรังสีเข้าทางหลอดเลือดดำ สามารถทำได้ภายในเวลาอันสั้น ช่วยเพิ่มประสิทธิผลในการตรวจผู้ป่วยโรคหลอดเลือดสมอง (Stroke)

ศูนย์รังสีวินิจฉัยก้าวหน้า (AIMC) โรงพยาบาลรามาธิบดี ได้ให้บริการตรวจวินิจฉัยผู้ป่วยโรคหลอดเลือดสมอง ด้วยเทคนิค Axial volume mode ซึ่งสัมพันธ์กับปริมาณรังสีที่ผู้ป่วยจะได้รับค่อนข้างสูง ดังนั้นจึงนำไปสู่วัตถุประสงค์ของการศึกษาในครั้งนี้ เพื่อหาปริมาณรังสีที่ผู้ป่วยโรคหลอดเลือดสมองจะได้รับจากการตรวจโดยใช้เทคนิค Axial volume mode ด้วยเครื่องเอกซเรย์คอมพิวเตอร์ชนิด 320 แถวหัววัด

ข้อมูลผู้ป่วย 21 ราย แบ่งเป็นเพศชาย 11 ราย และเพศหญิง 10 ราย โดยมีช่วงอายุระหว่าง 6-77 ปี และอายุเฉลี่ย 45.5 ปีถูกเก็บในด้านปัจจัยที่มีผลต่อเทคนิคการตรวจ และปริมาณรังสี ที่ได้รับจากการตรวจ CT Perfusion ของสมอง ด้วยเทคนิค Combo protocol โดยใช้ Axial volume mode ปริมาณรังสียังผล ได้จากการคำนวณและนำไปเปรียบเทียบกับค่ามาตรฐานอื่น ปริมาณรังสีสะสมรวม เมื่อพิจารณาเป็น CT Dose Index (CTDIvol) หน่วยเป็น มิลลิเกรย์ , Dose Length Product (DLP) หน่วยเป็น มิลลิเกรย์.ซม. และปริมาณรังสียังผล หน่วยเป็น มิลลิซีเวิร์ทมีค่าระหว่าง 142.9 -313.4 มิลลิเกรย์, 2286.6-5014.2 มิลลิเกรย์.ซม. และ 4.8-10.5 มิลลิซีเวิร์ท ตามลำดับ ปริมาณรังสีสะสมรวม ปริมาณรังสีเฉลี่ย และ ปริมาณรังสีเฉลี่ยต่อจำนวนชุดการตรวจ เมื่อพิจารณาเป็น CTDIvol, DLP และ Effective dose มีค่าเรียงตามลำดับดังนี้ 200.5, 40.8 และ 10.7 มิลลิเกรย์ สำหรับค่า CTDIvol ; 3206.8, 652.6 และ 171.3 มิลลิเกรย์.ซม.และ 6.7, 1.4, และ 0.4 มิลลิซีเวิร์ท

โดยสรุปปริมาณรังสีที่ได้จากการตรวจผู้ป่วยโรคหลอดเลือดสมอง ด้วยเครื่องเอกซเรย์คอมพิวเตอร์ชนิด 320 แถวหัววัด โดยใช้เทคนิค Axial volume mode มีปริมาณรังสีสะสมรวมสูง เนื่องจากการเปิดลำรังสีครอบคลุมส่วนที่ต้องการตรวจได้กว้างขึ้น (large z-coverage) อีกทั้งมีการใช้กระแสไส้หลอดที่สูง และจำนวนชุดของการตรวจที่มาก ข้อมูลที่ได้จากการศึกษาครั้งนี้ได้ถูกนำไปเปรียบเทียบกับระดับปริมาณรังสีอ้างอิงอื่นๆ เพื่อจัดทำโปรโตคอลเพื่อปรับลดปริมาณรังสีให้เหมาะสมกับอายุและขนาดของผู้ป่วยในอนาคต แม้ว่าปริมาณรังสีที่ผู้ป่วยได้รับจะมีค่าสูง แต่ประโยชน์ที่ได้รับจากการตรวจด้วยเทคนิคนี้ สามารถกำจัดข้อจำกัดเรื่องขอบเขตการตรวจ CT Perfusion ของสมอง สามารถลดปริมาณสารทึบรังสีให้กับผู้ป่วย ทั้งยังช่วยลดเวลาในการตรวจให้สั้นลง นอกจากนี้แล้วข้อมูลชุดแรก (Mask image) และชุดสุดท้ายของการตรวจ ยังสามารถนำไปใช้เป็นภาพเนื้อสมองก่อนและหลังการฉีดสารทึบรังสีตามลำดับได้อีกด้วย

ภาควิชา รังสีวิทยา	ลายมือชื่อนิสิต ....
สาขาวิชา ฉายาเวชศาสตร์	ลายมือชื่อ อ.ที่ปรึกษาวิทยานิพนธ์หลัก ....
ปีการศึกษา 2556	ลายมือชื่อ อ.ที่ปรึกษาวิทยานิพนธ์ร่วม ....
	ลายมือชื่อ อ.ที่ปรึกษาวิทยานิพนธ์ร่วม ....

5574172330 : MAJOR MEDICAL IMAGING
KEYWORDS: 320- DETECTOR CT / COMBINED CTA AND CTP / RADIATION DOSE / COMPREHENSIVE STROKE IMAGING

SAIFHON ADMONTREE: RADIATION DOSE IN WHOLE BRAIN COMPUTED TOMOGRAPHY IN COMPREHENSIVE STROKE IMAGING USING AXIAL VOLUMETRIC 320-DETECTOR CT. ADVISOR: ASSOC. PROF. ANCHALI KRISANACHINDA, Ph.D.,ASSOC. PROF. JIRAPORN LAOTHAMATAS, M.D., ASSOC. PROF. PANRUETHAI TRINAVARAT, 93 pp.

The 320- detector row CT scanner enables a larger z-coverage (16 cm), competently entire whole brain imaging to be acquired. Dynamic series of CT Angiography, CT Venography and CT Perfusion in single exam after contrast medium injected with intravenously at a very rapid acquisition time increase the effectiveness of stroke's patient management.

At Advanced Diagnostic Imaging Center (AIMC), Ramathibodi Hospital, the patients have been serviced on the diagnostic in comprehensive stroke imaging by using axial volume mode which produce relatively high patient dose. The purpose of the study is to determine the radiation dose in whole brain Computed Tomography in comprehensive stroke imaging using Axial Volumetric 320-detector MDCT.

The patient data is collected on scan parameters and radiation dose for CT Perfusion of the brain examination in comprehensive stroke imaging using the combo protocol in axial volume mode. The effective dose, E, is determined and compared with others. 21 patients of 11 male and 10 female, age range, 6-77 years; mean age, 45.4 years were studied. Range of cumulative radiation dose for CTDIvol, DLP and E were 142.9-313.4 mGy, 2286.6-5014.2 mGy.cm and 4.80-10.5 mSv respectively. The cumulative dose, average dose, and average dose per volume scan of CTDIvol, DLP and E were 200.5, 40.8 and 10.7 mGy; 3206.8, 652.6 and 171.3 mGy.cm and 6.7, 1.4, and 0.4 mSv consecutively.

In conclusion, the radiation dose in whole brain Computed Tomography in comprehensive stroke imaging using Axial Volumetric 320-detector MDCT in this study is high due to large z-coverage, high tube current and large number of total volume scans. The data had been compared with DRLs and other studies for the setup of the dose reduction protocols at various patient age and size in future study. Although the high radiation dose is one of the main concerns, the advantage can eliminate the brain coverage limitation, reduce volume of contrast media and decrease the acquisition time. Besides, the first and also last volume can be used as with and without contrast enhancement head CT.

Department:	Radiology	Student's Signature	....
Field of Study:	Medical Imaging	Advisor's Signature	....
Academic Year:	2013	Co-Advisor's Signature	....
		Co-Advisor's Signature	....

ACKNOWLEDGEMENTS

I would like to express gratitude and deepest appreciation to Associate Professor Anchali Krisanachinda, Ph.D., Department of Radiology, Faculty of Medicine, Chulalongkorn University, my advisor, for her guidance, helpful suggestion, supervision, constructive comments and polishing of the thesis writing to improve the readability and English expression.

I would like to extremely greatly Associate Professor Jiraporn Laothamatas, M.D., Department of Advanced Diagnostic Imaging Center, Faculty of Medicine, Ramathibodi Hospital, Mahidol University, and Associate Professor Panruethai Trinavarat, M.D., Department of Radiology, Faculty of Medicine, Chulalongkorn University for her advice and comments in the research.

I would like to extremely greatly Associate Professor Sivalee Suriyapee, M.Eng., Division of Radiation Oncology, Department of Radiology, Faculty of Medicine, Chulalongkorn University, my teacher, for her invaluable advices, constructive comments.

I would like to deeply thank Professor Franco Milano, Ph.D. from University of Florence Italy, an external examiner of this thesis defense for his helpful recommendations, constructive comments and teaching in Medical Imaging.

I am extremely thankful to Associate Professor Katsumi Tsujioka, Faculty of Radiological Technology, School of Health Sciences, Fujita Health University, Japan, for his teaching in advanced Computed Tomography and sharing his useful experiences of my research.

I am extremely grateful for all teachers, lecturers and staffs at Master of Science Program in Medical Imaging, Faculty of Medicine, Chulalongkorn University for their help, and unlimited knowledge during the course in Medical Imaging. I would like to thank Mrs. Weeranuch Kitsukjit for her suggestion for the improvement

I would like to deeply thank Assistant Professor Sawwanee Asavaphatiboon. M.Sc., and Ms. Prapa Sodkokkruad M.Sc., Physicists at Department of Radiology, Faculty of Medicine, Ramathibodi Hospital, Mahidol University, for their support and guidance on the quality control of CT system.

I am thankful for all staff at Advanced Diagnostic Imaging Center, Faculty of Medicine, Ramathibodi Hospital, Mahidol University, for their suggestions, facilitating on protocol in this research, useful advices and encouragement.

Finally, I am greatly thankful to my family for their invaluable encouragement, entirely care and understanding during the entire course of the study.

CONTENTS

Page

Page

Page

Page

LIST OF TABLES

Page

LIST OF FIGURES

Page

Page

Page

LIST OF ABBREVIATION

Abbreviation	Terms
3D	Three dimensions
2D	Two dimensions
AAPM	American Association of Physicists in Medicine
AIDR	Adaptive Iterative Dose Reduction
$C_{a,\,100}$	CT air kerma index at 100 millimeter length
Cm	Centimeter
CT	Computed Tomography
CTA	CT Angiography
CTDI	Computed Tomography Dose Index
$CTDI_{vol}$	Volume Computed Tomography Dose Index
$CTDI_w$	Weighted Computed Tomography Dose Index
$_nCTDI_w$	Normalized Weighted Computed Tomography Dose Index
CTP	CT Perfusion
CTV	CT Venography
DRLs	Dose reference levels
DLP	Dose-Length Product
dSVDs	delay-insensitive singular value decomposition
E	Effective Dose
f	Conversion factors DLP to Effective dose
FDA	Food and drug administration
FDK	Feldkampt algorithm
FOV	Field of view
FWHM	Full Width at Half Maximum
g	Gram
GSO	Gadolinium oxysulphide
HU	Hounsfield Unit
HVL	Half value layer
IAEA	International Atomic Energy Agency
ICRP	International Commission on Radiological Protection
IEC	International Electrotechnical Commission
kV	Kilo voltage
kVA	Kilovolt- ampere
kV_p	Kilo voltage peak

Abbreviation	Terms
kW	Kilo watt
kPa	Kilopascal
Lp/cm	Line pairs per centimeter
mA	Milliampere
mAs	Milliampere-second
MDCT	Multi-Detector Computed Tomography
mg	Milligram
mGy	Milligray
mGy.cm	Milligray-centimeter
MHU	Mega heat unit
mm	Millimeter
MSCT	Multi-Slice Computed Tomography
mR	Milliroentgen
MTT	Mean Transit Time
NRPB	National Radiological Protection Board
nT	Nominal beam width
PMMA	Polymethylmethacrylate
QDS	Quantum Denoising Software
rCBF	regional Cerebral Blood Flow
rCBV	regional Cerebral Blood Volume
RF	Radiofrequency
ROI	Region of interest
SD	Standard deviation
TTP	Time To Peak

CHAPTER I
INTRODUCTION

1.1 Background and Rationale

The utility of computed tomography (CT) has increased dramatically since the invention by Sir Godfrey Hounsfield in 1972. Recent developments of the 320-row multi detector CT is based on 16 cm detector coverage and the shortest tube rotation time of 0.35second facilitate volume mode to avoid the over-beaming effect of helical scan.

The characteristics of the 320-MDCT leading to the presumption of axial volumetric mode, provides dynamic volume scanning and enable larger area of coverage. So, the 320-row CT scanner has the ability of scanning entire organs in a single rotation (such as the brain), which can provide the combo protocol (the same dataset of CT Angiography and CT Perfusion in one examination) for visualization of dynamic vascular and perfusion of an entire whole brain after contrast medium administration intravenously at a very short scan time, helping to increase efficiently manage of stroke's patient.

The superior in clinical applications demonstrate the occlusion in arterial blood vessel and extension or location of infarcts at the vertex of the brain. Furthermore, the very rapid procedures help particularly unconscious patient.

At present, CT scans become the major source of human exposure to diagnostic X-rays as they represent the highest share of collective doses from medical exposures. This is the reason to concern about the increasing use of CT. The justification of such a study should be considered. The optimization of image quality and patient dose is a dynamic process that aims to give sufficient diagnostic image quality with minimum dose to the patient, involves input from the radiologist, radiographer and medical physicist. [1]

Regarding the use of radiation has been rising along with the tendency to inappropriate use of CT in patients the cost-risk-benefit must be considered effectively. However, CT doses seem to be lower in updated reports, because of the concerns for radiation and the advances in CT technology. [2] Technologists and radiologists should produce and interpret images of acceptable quality, not of the highest quality from very high dose scans, which would only increase the radiation dose.

Diagnostic Reference Levels (DRLs) are applicable for standard procedures in all areas of diagnostic radiology particularly high reduction in risk examinations and help to the awareness of radiation usage. DRLs were used as practical tool to manage radiation dose to patients, promoted attainment of the optimum use of radiation exposure for a specific medical imaging protocol. [3]

At Advanced Diagnostic Imaging Center (AIMC), Ramathibodi Hospital, the patient has been serviced on the diagnostic of lesion in the brain. In some case the 320-row MDCT (Aquilion ONE, Toshiba Medical Systems Corporation, Japan) scanner has been used, for axial volume mode feasibility to cover whole brain to visualize both of dynamic flow as well as perfusion by combine CT Angiography, CT Venography and CT Perfusion in single procedure, the same data set achieved with one contrast medium administration.

Nevertheless, the axial volume mode 320-detector CT also produce relatively high patient dose. The purpose of the present study is to determine the radiation dose in whole brain Computed Tomography in comprehensive stroke imaging using Axial Volumetric 320-detector MDCT.

1.2 Hypothesis

The radiation dose in whole brain Computed Tomography in comprehensive stroke imaging can be reduced by the use of axial volume mode.

1.3 Objective

To determine the radiation dose in whole brain Computed Tomography in comprehensive stroke imaging using Axial Volumetric 320-detector MDCT.

1.4 Definition

- Axial scan mode (Volume): Data acquisition while the patient table remains stationary; the table position may be incremented between x-ray exposures to collect data over a longer z axis range.

- CT air kerma index (C_a, 100): CT air kerma index measured free-in-air for a single rotation of a CT scanner is the quotient of the integral of the air kerma (K(z)) along a line parallel to the axis of rotation of the scanner over a length of 100 mm and the total collimated beam width, NT, where N is the number of data slices or tomographic sections and T is the nominal detector width.

- Computed Tomography Dose Index (CTDI): Computed Tomography dose index (CTDI) means the integral of the dose profile along a line perpendicular to the tomographic plane divided by the product of the nominal tomographic section thickness and the number of tomograms produced in a single scan.

• $CTDI_{vol}$ (volume CTDI) or C_{vol}: The $CTDI_{vol}$ is defined as $CTDI_w$ divided by the beam pitch factor. It is the most commonly cited index for modern MDCT equipment.

• CT Angiography: A computed tomography technique used to visualize arterial vessels that bring blood to organs such as the brain, commonly used to investigate causes of stroke such as carotid stenosis, arteriovenous malformations and aneurysms, among others.

• CT Perfusion: The method by which perfusion to an organ measured by CT carried out for neuroimaging using dynamic sequential scanning of a pre-selected region of the brain during the injection of a bolus of iodinated contrast material as it travels through the vasculature.

• CT Venography: A computed tomography technique used to visualize venous vessels.

• Diagnostic Reference Levels (DRLs): is defined by the International Commission on Radiological Protection (ICRP) Publication 73(1996) as a form of investigation level, applied to an easily measured quantity, usually the absorbed dose in air, or tissue-equivalent material at the surface of a simple phantom or a representative patient.

• Dose Length Product (DLP): DLP characterizes exposure for a complete examination to linear integration of the dose to standard head and body CT dosimetry phantom on the basic of absorbed dose to air (mGy.cm).

• Dynamic scan mode - single detector widths: Data acquisition at multiple time points over the same anatomic location(s) while the patient table remains stationary; x-ray exposure can be continuous or intermittent.

• Effective Dose (E): Different tissues/organs have different degree of sensitivity to radiation stochastic effect. Effective dose is obtained by multiplying the equivalent dose by tissue weighting factor. The resulting quantity can be used to express detriment to the whole body as a summation of several organ doses (unit Sieverts, Sv).

• Stroke: The World Health Organization defines stroke as a "neurological deficit of cerebrovascular cause that persists beyond 24 hours or is interrupted by death within 24 hours", sometimes referred to by the older term cerebrovascular accident (CVA), is the rapid loss of brain function due to disturbance in the blood supply to the brain. This can be due to ischemia (lack of blood flow) caused by blockage (thrombosis, arterial embolism), or a hemorrhage.

• Wide cone beam CT scanner: The scanner is capable of acquisition of a volume that is 160 mm in length, measured along the axis of rotation, in combination with a field of view of 500 mm (in the axial plane), within one 0.35 second full rotation.

• Wide-detector CT scanner: The development in CT technology to acquire larger scan volumes with high-resolution capability, enabling large-volume scanning in minimal time, a large anatomical area can be covered in less time and larger anatomical regions can be scanned with minimal overlap (i.e. a 320-detector row MDCT scanner has a scan volume of 160 mm defined at scanner iso-center).

CHAPTER II

REVIEW OF RELATED LITERATURE

2.1 Theory

2.1.1 Historical development of Computed Tomography

J.H. Radon, a Bohemian mathematician published the mathematical framework for reconstruction of an object from its line integrals in 1917. A.M. Cormack, a hospital physicist, developed a method for reconstructing the absorption coefficient of a slice of a human body from transmission measurements but was not able to prove the medical significance of this invention. G.N. Hounsfield invented the Computed Tomography independently in 1972, and firstly developed a successful practical implementation. He began his experiments using radioisotope as sources for his transmission measurement, using more powerful X- ray tubes which took about 9 hours to complete a measurement. Nevertheless, Hounsfield was able to install a first prototype of his CT system at Atkinson Morley Hospital (AMH) at Wimbledon, London, UK and, working closely with neuroradiologist J. Ambrose, successfully scanned the first patient as in figure 2.1, to obtain cross-sectional images of the head free of superimposition with dramatically improved low-contrast resolution capabilities. In 1979 Hounsfield and Cormack were awarded the Nobel Prize for their invention. [4]

Figure 2.1 CT image of the head obtained with an early CT scanner. [5]

The growth of the CT in the first ten years, between 1973 and 1983 was increasing dramatically. In the mid-1980s, another high-speed CT scanner was introduced using electron beam technology. In 1990, Dr. Robert Ledley invented the automatic computed transverse axial CT scanner. [6] The spiral/helical CT scanner was developed by Dr. Willi Kalender as single-slice or volume CT scanner. In 1998, the multi-slice CT scanners were introduced at the RSNA meeting in Chicago, USA. Multislice CT scanner is based on the use of multidetector technology to scan more than single slice per gantry rotation, thus increasing the volume coverage speed of single-slice and dual-slice volume CT scanner.

2.1.2 Components of Computed Tomography

The components of MDCT scanner comprise of x-ray generator, a high-powered generator, filtration, collimation, detector and detector electronics, data transmission systems (slip rings) contained within the gantry and the computer system for image reconstruction and manipulation.

The gantry is a mounted framework that surrounds the patient in a vertical plane. Modern gantry cooling systems circulate ambient air from the scanner room throughout the gantry. The stability of both focal spots and the position of detector during rotate the important for mechanical design of CT gantry. Include the mechanical support for x-ray tube, data measurement system and tube collimator must be designed to resist the high gravitational forces associated with gantry rapidly rotate. Two component features of the gantry are the gantry aperture and gantry tilting range to accommodate all patients and clinical examination. The basic components of a modern third-generation CT system as shown in figure 2.2.

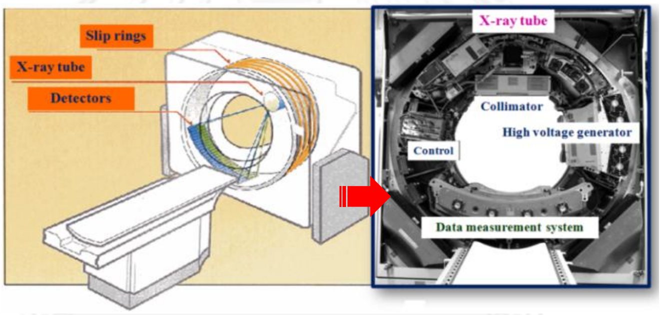

Figure 2.2 The basic component of a modern third-generation CT system. [7]

The couch should be made with a material that will not cause artifacts when scanned, such as carbon fiber material and also strong to support the weight of the patient. Additionally, it should provide for safety and comfortable. [8]

The high-frequency inverter circuit is used in the high-frequency generator, after high-voltage rectification and smoothing, the voltage ripple from a high-frequency generator is less than 1%. The rotating anode tubes produce a heterogeneous beam of radiation from a large diameter anode disk with focal spot sizes to facilitate the special resolution requirements of the scanner. In CT, high speed anode rotation allows the use of higher load ability. The introduction of spiral-helical CT with the x-ray tube rotate continually for a long period of time, the tube must be able to sustain higher power level. The x-ray tube and generator combination give a peak power of 60-100 kW, generally 80-140 kV. The effective energy of the 80 and 140-kV spectrum is approximately 40 and 60 keV consecutively. The different kV setting and clinical requirement of x-ray spectrum are the choice of optimize image quality at the lowest dose.

Mega Cool x-ray tube, specifically designed for Aquilion CT systems incorporate technology minimize focal movement and virtually eliminates off-focal x-rays thereby reducing unnecessary radiation to the patient. This innovation employs a durable copper alloy to absorb recoil electrons that may produce unwanted off-focal x-rays. Bearing supports at both ends of the anode axis also add stability and reduce variation in the beam, permitting high-quality imaging to be performed at faster speeds with minimal additional patient dose from the penumbra.[9]

The filtration, beam shaping filter or a bow tie filter serves a dual purpose in CT; remove long wavelength x-rays because they do not play a role in CT image formation but instead contribute to patient dose, and shapes the energy distribution across the radiation beam to produce uniform beam hardening when x-ray pass through the filter and the object. Three different types of bow tie filters (small, medium and large) are illustrated in figure 2.3, in order to equalize or flatten the x-ray fluence that reaches the detector array, consequences both on patient dose and on image quality. [10]

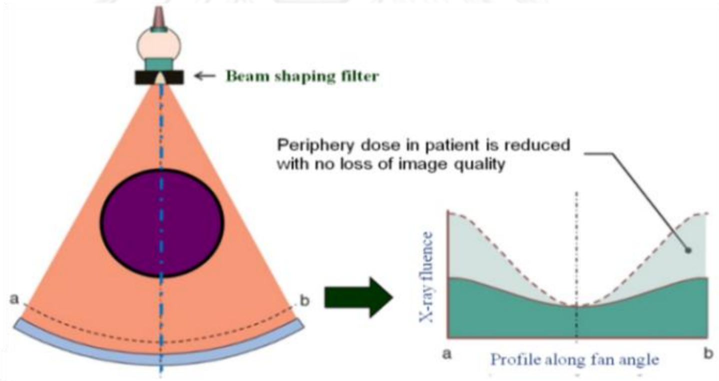

Figure 2.3 The x-ray beam striking the detector array is made more uniform when a beam shaping filter is used.

Two bow tie filters, head (also in pediatric body imaging) and body bow tie are used in commercial CT scanners. Some vendor has more than two bow tie filters tailor the beam profile and beam energy based on the type of examination (Toshiba Aquilion ONE CT systems) as shown in figure 2.4. [9]

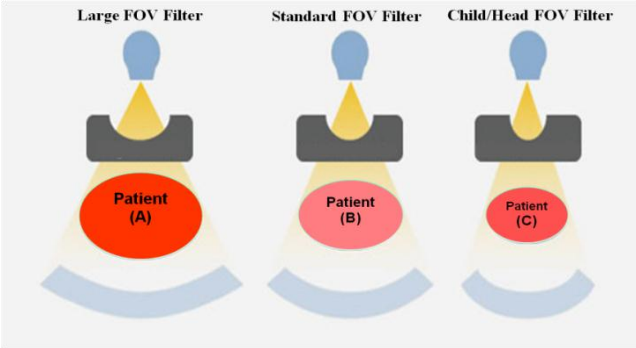

Figure 2.4 The physical filters, available in large (A), medium (B) and small (C) patient sizes.

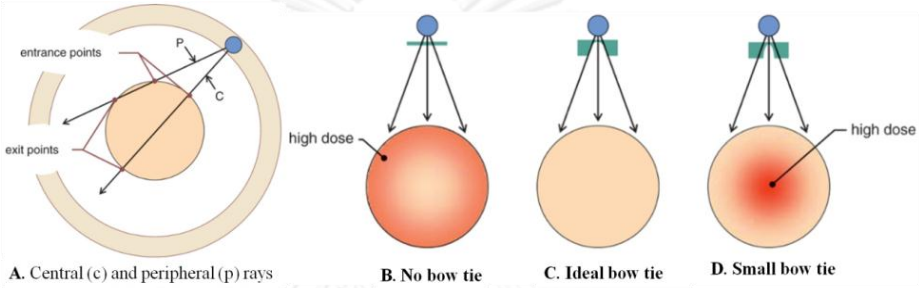

Figure 2.5 (A) The periphery ray (p) and the central ray (c) on circular object.
(B) No bow tie filter. (C) An ideal bow tie filter. (D) Small bow tie filter.

The periphery ray (p) passes through a shorter part of tissue to reach the exit point than the central ray (c) on circular object and the dose at the exit point for ray p is greater than for ray c. (figure 2A). When no bow tie filter is used, the radiation dose is increased at the periphery of the patient as shown in figure 2.5B. Ideal bow ties filter produced a nearly homogeneous dose distribution in the patient, as shown in figure 2.5C. If the bow tie filter has too much peripheral beam attenuation, then it will concentrate the radiation toward the center of the patient and lead to higher central doses as in figure 2.5D. [10]

In CT, the collimation affects patient dose and image quality. The two types of collimation are prepatient collimation and postpatient or predetector collimation. Prepatient collimation design is influenced by the size of the focal of the x-ray tube because of the penumbra effect associated with focal spots; the larger focal spot, the greater penumbra and the more complicated the design of the collimators. Detector collimators also shape the beam and remove scatter. For spiral CT scanning with adaptive beam collimation collimators are used to get rid of the unnecessary x-ray beam at the beginning and end of the scan length, results in patient dose reduction and improve dose efficiency of helical CT acquisition (as shown in figure 2.6B).

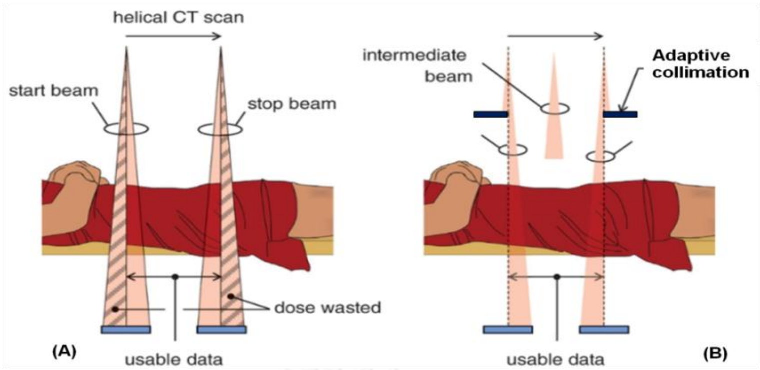

Figure 2.6 (A): No adaptive beam collimation. (B): With adaptive collimation, collimators eliminate the wasted dose both edges of the scan.

2.1.3 Computed Tomography detector technology

The radiation beam from the patient is captured by CT detectors converted to the electrical signals and binary code information respectively. The detector must demonstrate several characteristics essential for CT image production; efficiency, response time, dynamic range, high reproducibility and stability. In modern CT scanners generally use solid-state photodiode multiplier scintillation detectors, consists of a scintillation crystal or a radiation-sensitive solid-state material (such as cadmium tungstate, both of the conversion efficiency and photon capture efficiency are 99 % and the dynamic range about 1,000, 000 to 1).

The electronic module has gain channels for each detector in the module and also contains the analog-to-digital converter, which converts the amplified electronic signal to a digital number. The slice thickness is determined by the detector configuration, and the x-ray beam width is determined by the collimator.

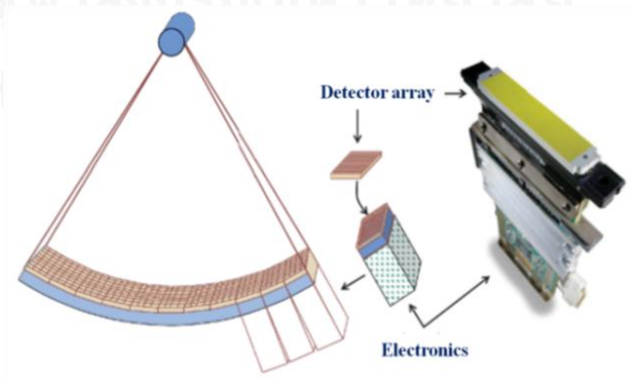

Figure 2.7 Detector arrays of modern CT.

All arrays of detectors of modern CT scanners comprise of groupings of detectors (detector module) sits on top of a larger stack of electronic modules, provide power to the detector array and receive the electronic signals from each photodiode (as in Figure 2.7). [10]

The data transfer in modern CT systems mainly used contactless transmission technology, such either as laser or electro-magnetic transmission with a coupling between rotating transmission ring antenna and a stationary receiving antenna. The stream of data transmission systems of MDCT scanner must be competent of handing significant data rate.

2.1.4 The basic scheme for data acquisition

Data acquisition refers to the method by which the patient is scanned to obtain enough data for image reconstruction. Two elements in a basic scheme for data acquisition; beam geometry refers to the size, shape and motion of the beam and its path, and components refer to those physical devices that shape and defined the beam, measured its transmission through the patient and convert this information into digital data for input into the components. Scanning is defined by the beam geometry, which characterizes the particular CT system and also plays a central role in spatial resolution and artifact reduction.

2.1.4.1 Data acquisition geometries

Three primary types of acquisition geometry are parallel beam, fan beam and the most recently used geometry in modern CT scanner, spiral beam geometry. As a result, simply characterized CT scanner is based on the scanning geometry, scanning motion and number of detectors, as followings;

First-generation scanner, parallel beam geometry was first used by Hounsfield and the EMI scanner also other earlier scanners based on this concept. The data acquisition process is based on a translate-rotate principle in which a single, highly collimated x-ray beam and one or two detector first translate across the patient to collect the transmission reading. The method of scanning is referred to as rectilinear pencil beam scanning.

Second-generation scanner, based on the translate-rotate principle, fan beam geometry translates across the patient to collect a set of transmission reading, after that the tube and detector array rotate and translate repeated for 180 degrees (referred to as rectilinear multiple pencil beam scanning).

Third-generation scanner, based on a fan beam geometry that x-ray tube rotates continuously around the patient for 360 degrees as in Figure 2.8. The projection profiles are collected as the x-ray tube and detectors rotate. Every a fixed point view of the tube and detectors is obtained, this motion referred to as continuously rotating fan beam scanning.

The rotate-rotate geometry of the third-generation CT is still the most widely used geometry on modern scanners.

Fourth-generation scanner, based on the rotate-fixed ring geometry, a ring of fixed detectors completely surrounds the patient. The X-ray tube rotates inside the detector ring through a full 360 degrees with a wide fan beam producing a single image.

Fifth-generation, scanner is classified as high speed CT scanners. Two such scanners are the dynamic spatial reconstructor scanner (DSR) and electron beam CT scanner (EBCT). DSR scanner produces dynamic three-dimensional images of volume of the patient. The data acquisition geometry of EBCT is a fan beam of x-ray produced by a beam of electrons that scans several stationary tungsten target rings.

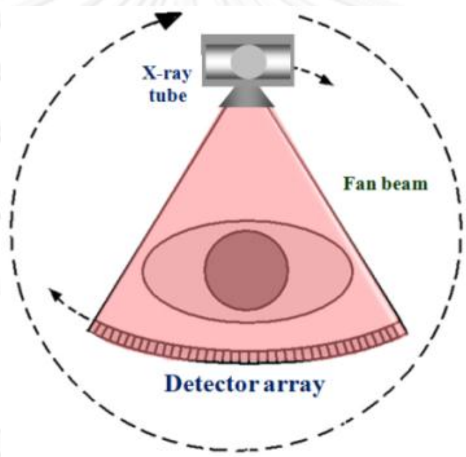

Figure 2.8 The third generation CT scanner, fan beam and rotate-rotate geometry.

Time consuming and mechanically complex translation motion was eliminated by opening x-rays into fan beam.

2.1.4.2 Computed Tomography scanning in Spiral/Helical geometry

The most recent development in CT data acquisition is spiral geometry, faster scan times and data are continuously collected in volumes rather than individual slices. Slip-ring technology is the fundamental used in spiral CT scanning, which shortens the high tension cables to the x-ray tube to allow continuous rotation gantry.

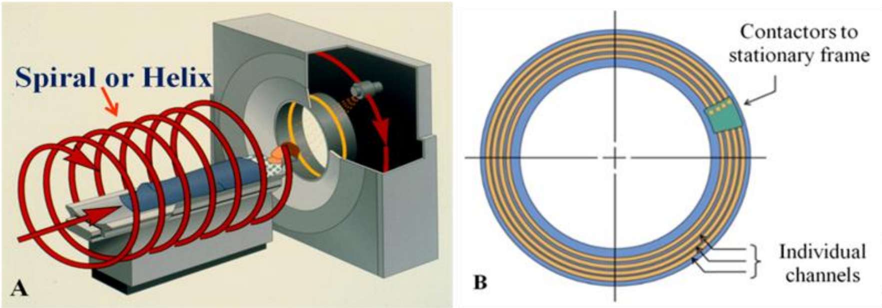

Figure 2.9 (A) The path traced by the x-ray tube in spiral/helical CT scanning.
(B) A slip ring is a component in all modern CT scanners.

All modern CT scanners use slip rings technology, allow for the gantry uninterrupted rotation (for a full rotation of 360 degrees of the x-ray tube around the patient) as in figure 2.9. Slip rings are 'electromechanical devices comprising of circular electrical conductive rings and brushes that transmit electrical energy across a rotating interface'. [11] The advantages of slip ring provide the elimination of the long, high-tension cables to x-ray tube used in conventional start-stop CT scanner, removal of the cable wrap-around process and minimize interscan delays. **The** facility of slip-ring technology permits the tube and detectors rotate freely as the patient is translate continuously through the gantry bore, so the volume data can be acquired rapidly.

2.1.5 Multislice/ Multidetector Computed Tomography

2.1.5.1 Physical principles of Multidetector Computed Tomography

In the 1990s, single-slice volume CT was introduced and successful in many body applications. But, several limitations of single-slice volume CT are; poor geometric efficiency due to only a small percentage x-ray beam is highly collimated to the size of a single row of detectors (1D detector array). Additionally, the volume coverage speed performance is also limited.

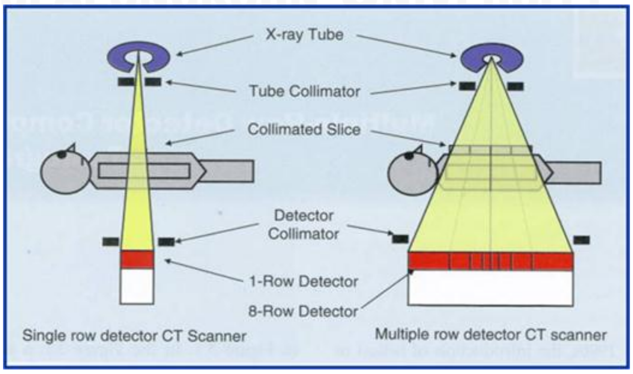

Figure 2.10 Single row detector (left) and Multiple row detector (right) CT scanners.

Multislice/ Multidetector CT technology provides higher speed with higher pitch ratios to increase the acquisition of longer volume of coverage; with finer slice thickness has improved image quality leading to enhancing 3D resolution. The 'multi-detector-row' nature of MDCT scanners refers to the use of multiple detector arrays (rows) in the longitudinal direction utilize CT geometry in which the arc of detectors and the x-ray tube rotate together.

Multi-slice CT is achieved with detector system provide multiple rows of detector elements perpendicular to the detector arc, e.g. arrays with 4 to 16 active detector rows (sections) along the z-axis. In MSCT, solid-state detector elements (scintillators) are used exclusively; such detectors are 20-30% more dose efficient than the gas-filled detectors used in single slice CT. During a helical MSCT acquisition, the patient moves at constant speed through the gantry. The table speed, rotation time and the total width of all simultaneously imaged sections determine whether the transverse slabs of the patient, which are exposed sequentially during data acquisition, are overlapping, contiguous or with interspaces. The acquisition parameters table speed, rotation time, section thickness and number of simultaneous acquired sections determines the CT pitch factor. For an overlapping acquisition, the CT pitch factor is smaller than one, for contiguous acquisition the CT pitch factor equals one and for an acquisition with interspaces the CT pitch factor is larger than one.

The fundamental physics and data flow of MDCT are the same as conventional nonspiral CT scanner, but differ about the data acquisition geometry, multislice image reconstructions algorithm and new concept relates to technology of detector. The beam geometry of MDCT, the widen beam covered the length of detector array is influenced by the fan angle of the beam (larger number of detector row, wider beam in the z-direction). The data acquisition geometry for MDCT is shown in figure. 2.11. The multirow detector array coupled to the x-ray tube describes the third generation geometry. The important features of multislice data acquisition relate to x-ray tube, filters, collimation, beam geometry and pitch. The beam is collimated by precollimator to fall on the entire multirow detector array and beam width (BW) is defined in the z-axis at the center of rotation.

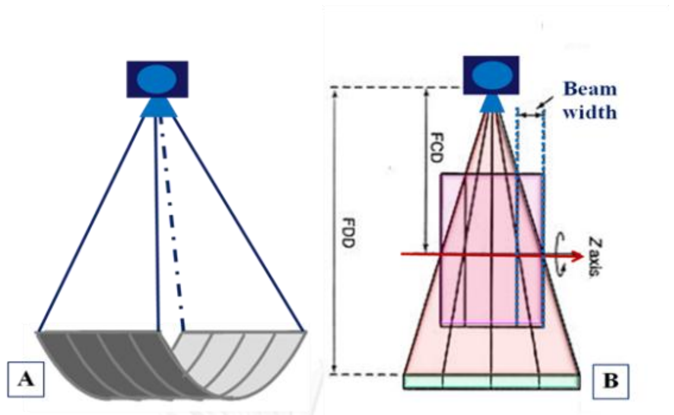

Figure 2.11 (A): Data acquisition geometry for MDCT (4-slice CT scanner) with four active acquisition channels. (B): A cross-section (side view).

The disadvantages of MDCT are occurrence of multislice artifacts and cone-beam artifacts. Moreover contribute to increase in dose-length product due to an additional half rotation is needed over the planned scan range both at the beginning and also the end of a spiral scan required for data interpolation and reconstruct image (overranging). Figure 2.12A shows a more accurate depiction of a modern multislice CT scanner, where the fan angle defines the “fan beam geometry”. For typical 64 to 128 detector array CT scanners, the fan angle is approximately 60 degrees, while the full cone angle is about 2.4 degrees.

Antiscatter collimation was used at the detector array (post collimation) to minimize scatter radiation. While the width of the x-ray beam has increased, scatter suppression must be concerned in large multidetector array CT system (e.g. 40, 80 mm, and larger) as in figure 2.12B.

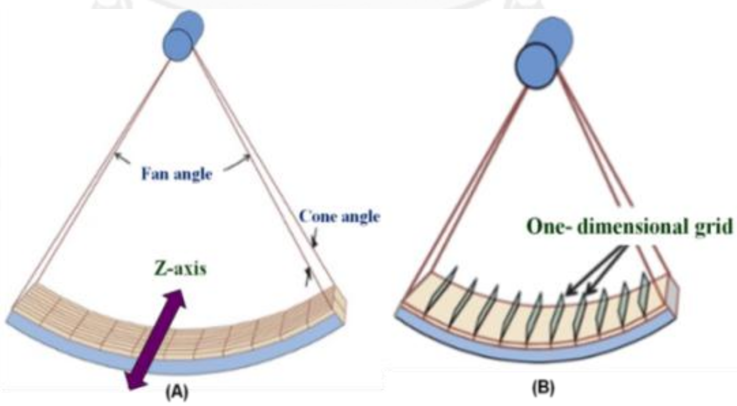

Figure 2.12 (A): The cone beam geometry in modern multislice CT scanner. (B): The septa of antiscatter grid.

The cone beam geometry results in a wider divergence of x-ray beam at the detector array. The septa of antiscatter grid are aligned with the dead space between individual detectors attempt to maintain the detection efficiency of the system.

2.1.5.2. Data acquisition component in Multislice/Multidetector CT

The multidetector CT is generally used in terms of multirow CT or multislice CT scanner, based on the third-generation system design. The isocenter is the center of rotation of the CT gantry, and also the center of the reconstructed CT image. The two basic modes of MDCT data acquisition are helical mode and sequential mode.

Sequential mode or axial mode is known as 'step and shoot' (Figure 2.13), the cough is stationary during the gantry rotate and then step pass through the bore of gantry to the next z-position for acquired another data set. The clinical applications; such as head scanning, high-resolution lung scanning, perfusion CT and interventional applications were used axial 'step and shoot' scanning of MDCT.

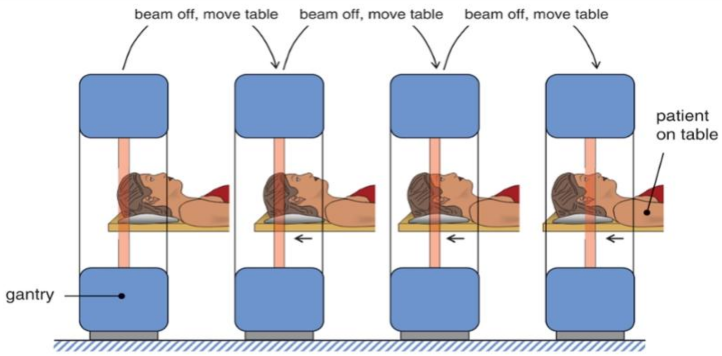

Figure 2.13 The axial or sequential CT scan.

Helical or spiral mode is characterized by continuous gantry rotation while the patient table is moving with constant speed. [10] (Figure 2.14).

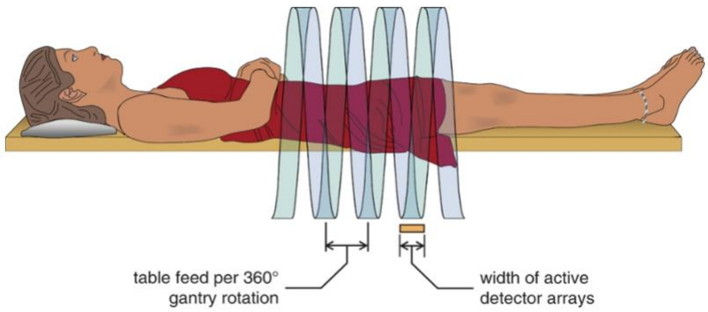

Figure 2.14 The helical or called spiral scanning.

A true cone beam CT scanner has the half cone angle approached 10 degrees, whereas most conventional CT systems still make use of only slight cone angles on the order of 2 degrees (cone half-angle). Technically, the reconstruction algorithm of true cone beam is used to convert the raw data into CT images takes into account the cone angle. Toshiba Aquilion One CT system has a 320-detector array with 0.5-mm thickness; 16 cm along z-axis can be sufficient coverage entire for most organs such a head, heart, kidneys and pediatric patient. The drawbacks of the wide cone beam design are increased x-ray scatter and increased cone beam artifacts. However, the advantage of this design is the entire organ can be captured with stationary table. For CT brain perfusion studies, the whole brain coverage is sufficient with high temporal resolution.

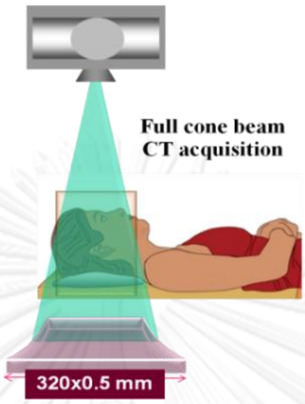

Figure 2.15 The wide cone beam CT acquisition.

2.1.5.3 Image reconstruction in Computed Tomography

The acquirement of actual projection data is applied by the preprocessing procedures prior to CT image reconstruction. The bow tie filter is characterized by performing air scans during routine CT scanner calibration. The air scans also characterize differences in individual detector response, which may be due to differences in photodiode or amplifier gain. The measured projection data for a given CT scan to be reconstructed are normalized by the calibration scans, and this procedure corrects for previously identified inhomogeneities in the field. Scatter correction algorithms generally need to be applied. [10]

The CT image reconstruction is a mathematical process that generates images from X-ray projection data acquired at many different angles around the patient (a large number of projection data 1,000 to 4,000 projections are acquired in clinical CT). Image reconstruction has a fundamental impact both on image quality and radiation dose, improve image quality can be translated into a reduction of radiation dose owing to images of acceptable quality.

Analytical reconstruction and iterative reconstruction are two major categories of exist method. Filtered backprojection (FBP) are one type of analytical reconstruction that is widely used on clinical CT scanners because of their computational efficiency and numerical stability. The reconstruction kernel is referred to as “filter” or “algorithm”. Smooth kernel generates the lower noise images with reduced spatial resolution. In contrary, sharp kernel generates the higher spatial resolution images by increases the noise. The reconstruction kernel is selected based on specific clinical application.

The iterative reconstruction method was implemented in present CT scanners in order to improve image quality by decrease image noise and using low radiation dose.

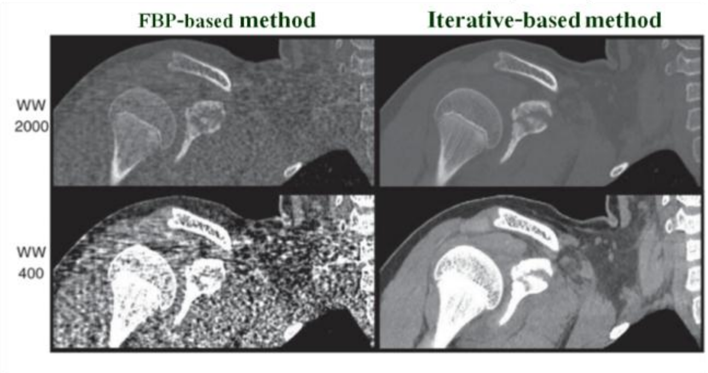

Figure 2.16 The filtered backprojection images in bone window (WW 2000) and standard window (WW 400) (Left), the iteratively reconstructed images (Right). [10]

The distinct advantage of the reconstruction by iteratively reconstructed images over the filtered backprojection images in bone window (WW 2000) and standard window (WW 400) (as in figure 2.16)

Adaptive Iterative Dose Reduction in 3D (AIDR 3D, Toshiba specific name) is the latest evolution of iterative reconstruction technology that has been fully integrated into the imaging chain to ensure automatic dose reduction. Once the scan has been performed with low-dose parameters, automatic reconstruction with AIDR 3D is performed. This advanced iterative reconstruction algorithm works in two parts. The first part adaptively removes photon noise in the 3D raw data domain. This is followed by the second part, model-based iterative noise reduction in the reconstruction process. AIDR is able to eliminate up to 50% of image noise, resulting in a dose reduction of up to 75%. Quantum Denoising Software (QDS) is an adaptive noise reduction algorithm that selectively smoothest out areas of uniform density while preserving the edge information within the image, thus reducing noise while increasing the signal to noise ratio and improving image quality. [12]

2.1.5.4 Cone Beam Reconstruction [10]

Cone beam reconstruction algorithms are similar to standard fan beam reconstruction algorithms, but they keep track of the beam divergence in the z-direction. The basic cone beam reconstruction process, often referred to as the Feldkampt algorithm or FDK, reconstructs the entire volume data set (a series of CT images of a given thickness) simultaneously. Cone beam reconstruction violates mathematical requirements for sampling Fourier space, and for extreme cone beam geometries used in flat panel detectors or other very wide cone beam CT systems, this can lead to cone beam artifacts.

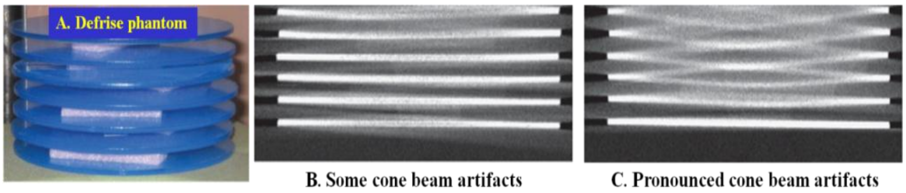

Figure 2.17 A. Defrise phantom B. and C. Cone beam artifacts.

Cone beam acquisition strategies can lead to under-sampling in the cone angle dimension, and this can cause a well-known cone beam artifact (Fig. 2.17). The Defrise phantom, which is a stack of attenuating disks separated by low density material (Fig. 2.17A), can be used to evaluate cone beam artifacts. In a well-sampled environment, cone beam artifacts can be kept to a minimum (Fig. 2.17B); however, the use of large cone angles can lead to considerable artifacts (Fig. 2.17C). Cone beam artifacts are a result of fundamental deficits in the acquired data, and the most obvious solution for these artifacts is to acquire a more complete data set.

2.1.6 The dosimetry in Multidetector Computed Tomography [13]

Currently three dosimetric quantities, the volume Computed Tomography dose index ($CTDI_{vol}$,mGy), the dose-length product (DLP, mGy.cm) and the effective dose (E, mSv) provide an indication of the average dose in the scanned region, the exposure from the complete CT examination and the radiation risk of the entire CT scan. The technical acquisition parameters such as tube current (mA), rotation time, tube voltage (kV_p), beam filtration and geometric efficiency are the primary factors affect the $CTDI_{vol}$. These parameters should be optimized to yield the required image quality at a dose level that is as low as reasonably achievable (ALARA) principle. The $CTDI_{vol}$ is derived from measurements in two cylindrical PMMA CT dosimetry phantoms representing the attenuation of respectively the adult head (16 cm diameter PMMA) and body (32 cm diameter PMMA), two positions the central axis and a peripheral axis 1 cm below the surface are measured. The $CTDI_{vol}$ is parameter for comparison between different protocols and different MSCT scanners. Under the same exposure conditions, the quantitative value of the $CTDI_{vol}$ in the relatively small head phantom is higher than the larger body phantom. Nowadays, $CTDI_w$ divided by the pitch factor is current practice to use the $CTDI_{vol}$. In addition to considerations of local absorbed dose, the dose-length product should take into account the extent of the exposed during all sequences of the examination. DLP is the result of the $CTDI_{vol}$ multiplied by the exposed length for each sequence and is influenced by the length of the scanned range and the number of sequences. Most MDCT scanners enable display the radiation dose information, $CTDI_{vol}$ and DLP are basically dose descriptor displayed on the CT monitor for each examination. For cone beam CT scanning or perfusion studies without patient motion, the CTDI paradigm does not apply and the reported value of $CTDI_{vol}$ will significantly overestimate the dose. [14]

2.1.7 The Computed Tomography brain perfusion principle [15]

Computed Tomography (CT) perfusion is a technique in neuroradiology to assess tissue level perfusion and delivery of blood to the brain and/or tissues of the head and neck. The linear relationship between CT numbers or Hounsfield units (HU) and the amount of iodinated contrast material in an image pixel, together with the high spatial and temporal resolution characteristics of the scanning paradigm, make CT perfusion a valuable tool for evaluating blood supply to neoplastic and non-neoplastic tissue (including normal and ischemic tissue). In particular, the evaluation of cerebral ischemia or the angiogenesis state of a tumor is readily performed with CT perfusion imaging. CT perfusion should be performed only for a valid medical reason and with the minimum radiation dose necessary to achieve an optimal study. [16], [17]

2.1.7.1 Computed Tomography perfusion protocol [18]

The Neuro ONE protocol (Toshiba Aquilion One CT system) allows acquisition of multiple low-dose volume scans of the entire brain during contrast infusion to provide whole brain perfusion and whole brain dynamic vascular analysis in one examination. The dynamic series of CT perfusion scan are performed for 60 seconds, 50 cc of nonionic iodinated 300 mg/cc concentration contrast media injected at 5cc/sec followed by 40 cc saline intravenously. Perfusion computations are performed on an image-processing workstation after scan completion. Each green bar in figure 2.18 shows the tube current at different phases employing a 320-detector row CT in the same data set. The mA increases for the arterial portion of the scan to provide improved image quality for the digitally subtracted angiogram (DSA) image.

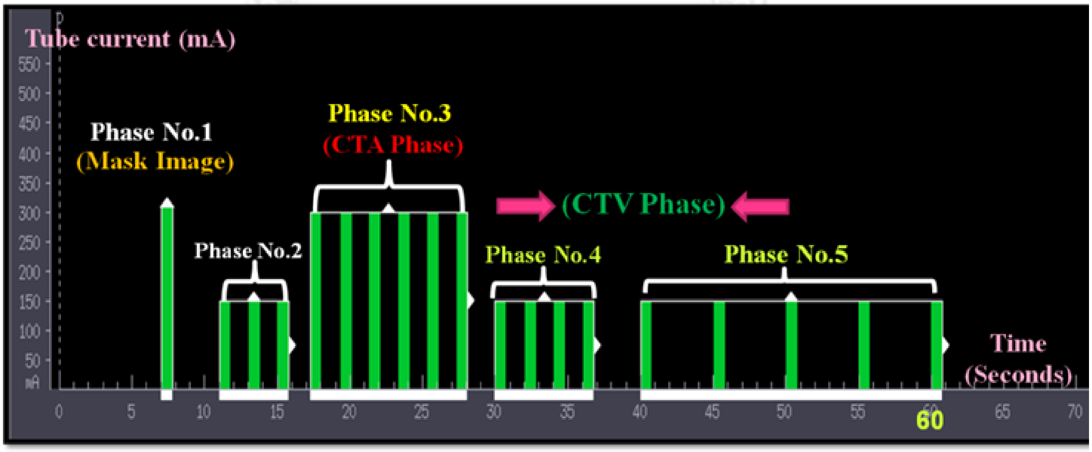

Figure 2.18 The dynamic volume of CT Angiography, CT Venography and CT Perfusion.

The CT scan starts prior to the intravenous injection of contrast, and hence the scanner produces a number of CT images prior to the arrival of the contrast bolus to the organ of interest. This is necessary because the mathematical models that are used to compute the parametric maps require an input function (HU versus time), typically the artery supplying blood to the organ of interest. From this data set of temporal CT scans, and with physician demarcation of the location of the input function, parametric maps are computed with high resolution. Parametric images are the physiologic metrics such as (A) vascular perfusion, (B) time to peak enhancement, and (C) blood volume computed using software designed for this purpose. (Figure 2.19)

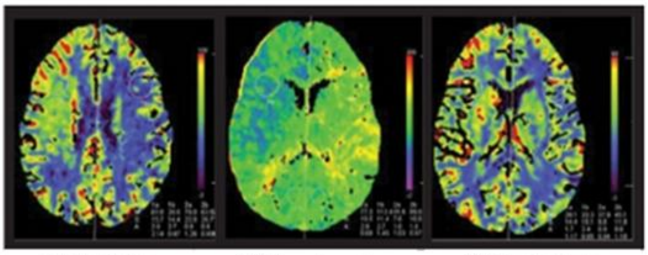

Figure 2.19 Computed parametric mages (A) vascular perfusion, (B) time to peak enhancement, (C) blood volume.

2.1.7.2 The Computed Tomography brain perfusion analysis [19]

Post-processing algorithms, based on mathematical modeling of the changes in signal intensity over time accompanying the intravenous administration of contrast, are used to estimate quantitative results related to regional cerebral blood volume (rCBV), mean transit time (MTT), regional cerebral blood flow (rCBF) and tissue time to peak (TTP). The rCBV is defind as the area under the computed residue function, adjusted by the brain concentration of contrast and the hematocrit constant in unit cc/100g of tissue. The mean transit time (MTT) is defind as the ratio of the area under the computed residue function to the maximum value of the computed residue function, regional cerebral blood flow (rCBF), time to peak of tissue (TTP) is defined as the time at which the intensity reaches a maximum value, and delay of tissue response (Delay) is the time when the computed residue function reaches the maximum. The color-coded maps can be generated to show the variations in these measures. The presence of a matched CBF/CBV perfusion deficit suggests irreversibly ischemic infarct "core", and not a target for reperfusion therapies.

Because of the long duration of repetitive ("cine") imaging over a single brain region associated with CTP scanning, there is a risk of excessive radiation exposure if the X-ray energy settings for CTP image acquisition are inappropriately high. In 2009, the FDA issued a notification regarding an investigation of a single facility where a number of patients received excessive radiation exposure from CTP exams up to eight times the maximum FDA recommended dose.

Subsequently, this problem was also discovered at a small number of other stroke centers, where the standard scan parameters for CTP acquisition, as suggested in the literature and accepted by the stroke imaging community for over a decade, were similarly not followed. A substantial proportion of those patients experienced transient hair loss a few weeks after admission, an effect that has been associated with cumulative exposure to 3-5 Gray (Gy) absorbed dose of ionizing radiation to the skin.

The dose management should be as followings;

(1) Tube voltage 80 kV_p should be used to increase iodine signal brightness, because the conspicuity of the iodine contrast agent is much greater at 80 kV_p, resulting in improved CTP map image quality at a markedly lower radiation dose,

(2) Low dose per single scan (i.e. one tube rotation) is critical, since repeated scanning will result in a relatively high cumulative dose,

(3) Time interval between scans, and hence the total number of scans over the exam duration, should be set carefully, taking into account the analysis algorithm (some approaches require relatively dense data points), and

(4) Dose (tube current) modulation *should not be used*, as it may interfere with the calculation of the BV and BF parameters.

2.2 Review of Related Literature

Several researchers have studied on radiation dose in comprehensive stroke imaging by means of Computed Tomography Perfusion in various CT scanner vendors.

Shankar J.J., and Lum C. [20] studied the whole brain CT perfusion on a 320-slice CT scanner. Computed tomography perfusion (CTP) has been criticized for limited brain coverage. This may result in inadequate coverage of the lesion, inadequate arterial input function, or omission of the lesion within the target perfusion volume. The availability of 320-slice CT scanner offers whole brain coverage which minimizes the chances of misregistration of lesions regardless of location, and makes the selection of the arterial input function easy. They presented different clinical scenarios in which whole brain CTP was especially useful.

Imaging protocol: CT perfusion was performed using 40 cc of nonionic iodinated contrast media (300 mg/cc of iodine), injected intravenously at the rate of 4 cc/s. A total of 19 volumes covering the whole brain were acquired, with each volume consisting of 320 images of 0.5 mm thickness covering a total of 16 cm of the head in the z direction. The first volume was acquired with an acquisition delay of 7 s after the injection of contrast media. The time delay allowed the acquisition of baseline images without contrast enhancement, which were used as a mask for obtaining bone subtraction for subsequent computed tomographic angiogram (CTA).

The acquisition parameters for the first volume were 80 kV_p and 300 mA. Next, 13 volumes of the brain were acquired starting at 11 s after the injection of contrast media at a sampling interval of one volume every 2 s. These volumes were acquired during the arterial and the capillary phase. Then, five volumes were acquired at a sampling interval of one volume every 5 s. The acquisition parameters for all volumes after the first volume were 80 kVp and 100 mA. The total duration of the acquisition was 60 s.

Data processing was performed on a Vitrea fx, version 1.0 workstation. Color maps of the hemodynamic parameters such as blood flow (BF), blood volume (BV), mean transit time (MTT), and time to peak (TTP) were calculated. A higher radiation dose has been one of the major concerns in whole brain CTP. However, this has to be seen in the light of the fact that both CTA and CTP information can be obtained from the same whole brain CTP study. The average effective dose for whole brain CTP on a 320-slice scanner is 4.002 mSv. With a modified algorithm, it can be further reduced up to 2.1 mSv.

They had highlighted the advantages and new implications of whole brain CTP compared to the limited-slice CT perfusion. Other avenues to harness the potential of whole brain CTP will open up with further experiences in this field. Using different protocols, the radiation dose can also be reduced for whole brain CTP.

Salomon E.J., et al. [21] studied the dynamic CT Angiography and CT Perfusion employing a 320-detector row CT (Protocol and current clinical applications) for the aim to report the initial clinical experience of a 320-detector row computed tomography (CT) scanner in cerebrovascular disorders. Volumetric CT using the full 160-mm width of the 320 detector rows enables full brain coverage in a single rotation that allows for combined time-resolved whole-brain perfusion and four-dimensional CT angiography (CTA). The protocol for the combined dynamic CTA and CT perfusion (CTP) is presented, and its potential applications in stroke, stenoocclusive disease, arteriovenous malformations and dural shunts are reviewed based on clinical examples.

The combined CTA/CTP data can provide visualization of dynamic flow and perfusion as well as motion of an entire volume at very short time intervals which is of importance in a variety of pathologies with altered cerebral hemodynamics. The 320 detector rows offer z-axis coverage allowing for whole-brain perfusion and subtracted dynamic angiography of the entire intracranial circulation. The most important caveat relates to radiation dose. The calculated effective dose of 5.129–5.635 mSv is in the same range as that reported previously for a similar protocol at the same scanner by a different group (5 mSv). The radiation exposure in a comprehensive CT protocol of the head in acute stroke is in the same range or more with effective doses of 1.7 mSv for CT, 1.9 mSv for CTA of intracranial vessels, and, depending on examination parameters, effective doses of 1.1 to 9.0 mSv for cerebral CTP. Since the radiation dose of cerebral angiography for four vessels, the bilateral carotid and vertebral arteries, is approximately 300–400 mGy, the radiation dose with fluoroscopy is somewhat greater than that and therefore in the same range as the described protocol.

Diekmann S, et al. [22] studied the dose exposure of patients undergoing comprehensive stroke imaging by multidetector-row CT compared between 320 and 64-detector row CT scanners, the protocol consisting of standard CT of the head, CTA of cerebral and cervical vessels, and CTP.

Organ doses were measured by using LiF-TLDs located at several organ sites in an Alderson-Rando phantom and the effective doses were derived from adding the measured organ doses multiplied by tissue weighting factor (ICRP 103). The effective doses was measured for the different scanning protocols ranged between 1.61 and 4.56 mSv, resulting in an effective dose for complete stroke imaging in m/f of 7.52/7.54 mSv for 64-detector row CT and 10.56/10.6 mSv for 320-detector row CT. The highest organ doses within the area of the primary beam were measured in the skin (92 mGy) and cerebral hemispheres (69.91 mGy). Use of an eye-protection device resulted in a 54% decrease of the lens dose measured for the combo protocol for whole-brain perfusion with the 320-detector row CT scanner. The dose differences are due to the approximately 4 times larger z-coverage of the 320-detector row CT (14 cm in the protocol investigated here) compared with 64-detector row CT (3.2 cm).

They concluded that, the new 320-detector row CT scanner generation enables perfusion imaging of the entire neurocranium and dynamic CTA of the intracranial vessels. Their experimental results suggest that perfusion imaging on the new CT scanner is associated with a higher effective dose while z-coverage is also larger. Here, the physician has to weigh the expected diagnostic benefits against the risks of a higher radiation dose.

Siebert E, et al. [23] studied 320-slice CT neuroimaging: initial clinical experience and image quality evaluation. 26 patients with presumptive cerebrovascular pathology underwent 320-slice CT. Single-rotation CT of the head, incremental CT angiography (three-dimensional (3D) CTA) as well as four-dimensional whole-brain CTA (4D CTA) and whole-brain CT perfusion (CTP) were performed and the resulting images were assessed for quality and compared with those obtained with 64- slice CT protocols. 320-slice CT neuroimaging could be performed in all cases.

The image quality of 320-slice CT of the head and 3D CTA was inferior to that of the 64-slice protocols. The image quality of 4D 320-slice CTA was rated as inferior to both 320- and 64-slice 3D CTA. 4D CTA-CTP imaging added information with pivotal clinical implications.

Parameters for combined 4D CTA-CTP protocol consisted of three sets of scans: (1) a set of three intermittent scans for acquisition of a bone subtraction mask during a total scan time of 3 s (11.2 mGy; DLP 179.3 mGy cm); (2) a continuous scan with a total scan time of 15 s (56.0 mGy; DLP 896.3 mGy cm) during which arrival of a bolus of contrast medium occurred as calculated beforehand by a test bolus protocol at the level of the circle of Willis; and (3) five intermittent scans, rotation time 0.5 s each, performed every 5 s (18.7 mGy; DLP 298.8 mGy cm). According to the manufacturer's phantom measurements, radiation exposure during the dynamic whole brain 4D CTA-CTP combined protocol amounts to 5– 6 mSv.

The calculated effective dose, the product of DLP and the ICRP factor for the head (2355.4 mGy cm, k = 0.0023 mSv mGy^{-1} cm^{-1}), is 5.4 mSv, which is in line with the exposure of conventional CTP published in the literature. Comprehensive neuroimaging of cerebrovascular pathology using 320-slice CT is a feasible and robust method. For the first time dynamic whole-brain imaging can be performed by CT, increasing the potential to delineate pathologies that alter cerebral haemodynamics.

Cohnen M, et al. [24] studies radiation exposure of patients in comprehensive Computed Tomography of the head in acute stroke. The purpose of the phantom study was to assess patient radiation exposure in comprehensive stroke imaging using multidetector row CT (MDCT) combining standard CT of the head, cerebral perfusion (CTP), and CT angiography (CTA) studies. Dose measurements were performed at a 64-detector-row CT scanner. They examined 4 different protocols, including a standard CT of the head and CTA of intracranial and cervical vessels. Furthermore, CTP was performed as implemented by the vendor (protocol I). Because different technical parameters are specified in literature, this protocol (270 mAs, 80 kV) was changed, and protocols II (200 mAs, 80 kV) and III (200 mAs, 120 kV) were assessed.

An Alderson-Rando anthropomorphic phantom with lithium-fluoride thermoluminescent dosimeter (LiF-TLD-) rods (1x6 mm) was used to assess radiation exposure. Radiation doses were assessed by reading out LiF-TLD using a Glowcurve analyzer Harshaw filtrol 2000D within 24 hours after exposure. The total radiation dose of the brain was 22.2 mGy, whereas for the eye lenses and the thyroid, particularly sensitive organs, 5.4 and 1.1 mGy were noted. Both for the CTA of the intracranial as well as the cervical vessels these doses did not exceed 20 mGy.

In a review on cerebral CTP, the estimations of local doses based on Monte Carlo methods; the effective doses between 2.0 and 3.4 mSv for the perfusion study and between 1.5 and 2.5 mSv for the routine brain study were estimated. The actual dose to the irradiated volume was discussed to range between 110 and 300 mGy. For cerebral CTP, few data exist on direct measurements both on local organ doses that have to be expected in the area of the primary beam as well as on the effective dose as an indicator of the general radiation exposure of the patient. A dedicated analysis on central and peripheral dose values showed the direct dependence of doses on the chosen examination parameters. This study demonstrated local doses between 90 and 1600 mGy in the center as well as a range from 160 to 2260 mGy on the surface of the head phantom. Comprehensive stroke imaging using CT may lead to effective doses in the range of 5–10 mSv, depending on the chosen scan parameters. Local doses do not reach thresholds for the development of cataract formation, induction of thyroid malignancy, or hair loss.

Arandjic D, et al. [25] studied the radiation dose in cerebral perfusion Computed Tomography: patient and phantom study. As a part of routine patient monitoring, data were collected on patients in terms of the skin dose, CT dose index ($CTDI_{vol}$) and dose-length product (DLP) values. For the estimation of the dose to the lens a phantom study was performed. Dose values for skin and lens were below the threshold for deterministic effects. The values collected on patients were in the ranges 230–680 mGy for $CTDI_{vol}$ and 2120–2740 mGy cm for DLP, while the skin dose and estimated effective dose were 340–800 mGy and 4.9–6.3 mSv, respectively. The values measured in the phantom were similar, while the doses estimated to the lens were 53 and 51 mGy for the right and left lens, respectively.

A cerebral perfusion study is very important for the diagnosis and decision for further treatment of patients with cerebrovascular diseases. However, the exposure level of patients may be very high and therefore very special attention must be paid to patient protection.

Murayama K, et al [26] studied whole-brain perfusion CT performed with a prototype 256 –detector row CT system: initial experience. In purpose to preliminarily evaluate the feasibility and potential diagnostic utility of whole-brain perfusion computed tomography (CT) performed with a prototype 256–detector row CT system over an extended range covering the entire brain to assess ischemic cerebrovascular disease.

The dose-length product was calculated by multiplying the weighted CT dose index (measured in milligrays) by the scanning range (12.8 cm). The effective radiation dose was obtained by multiplying the dose-length product by a conversion coefficient (0.0023 mSv/ [mGy cm] for the head) and the effective dose of perfusion CT was compared with the effective dose of conventional multi– detector row CT. The maximum effective radiation dose was 4.6 mSv for 25 scans performed with 80 kV, 80 mA, and 1 second per rotation, and the minimum effective dose was 3.5 mSv for 19 scans performed with the same parameters. In head examinations performed with 64–detector row CT at their hospital, the radiation dose is 60 mGy for routine unenhanced CT, 214 mGy for perfusion CT, and 53.2 mGy for 3D CT angiography. The total dose-length products for these three examinations were calculated with the assumption that the width of the entire brain was 12.8 cm, and the effective dose (5.0 mSv) was converted.

Mnyusiwalla A, et al. [27] studied the radiation dose from multidetector row CT imaging for acute stroke to determine the radiation dose delivered during comprehensive computed tomography (CT) imaging for acute stroke.

CT protocol performed an unenhanced CT head, CT angiography from the arch to vertex, CT perfusion/permeability, and an enhanced CT head. All imaging was acquired with a 64-MDCT which ninety-five examinations were included. Mean DLP was 6,790 mGy•cm.

Effective doses ranged from 11.8 to 27.3 mSv, mean effective dose of 16.4 mSv. Mean effective dose for acquisition of the unenhanced head was 2.7 mSv. Largest contribution to effective dose was the CTA with a mean effective dose of 5.4 mSv. Mean effective dose for the CT perfusion was 4.9 mSv.

In conclusion, the comprehensive CT acute stroke protocol delivered a mean effective dose of 16.4 mSv, which is approximately six times the dose of an unenhanced CT head. These high-dose results must be balanced with the benefits of the detailed anatomic and physiologic data obtained. Centers should implement aggressive dose reduction strategies and freely use MR as a substitute.

Kroft L J. M, et al [28] studied the scan time and patient dose for thoracic imaging in neonates and small children using Axial Volumetric 320-detector row CT compared to Helical 64-, 32-, and 16- detector row CT acquisitions. The purpose is to evaluate by means of a phantom study, scan time and patient dose for thoracic imaging in neonates and small children by using axial cone-beam and helical fan beam MDCT acquisitions. Scan time was 0.35 s for 320-MDCT axial volumetric acquisitions and varied between 1.9 s and 8.3 s for helical acquisitions.

Dose savings varying between 18% and 40% were achieved with axial volumetric scanning as compared to helical scanning (for 320- versus 64-MDCT at 160 mm and 80 kVp, and for 320- versus 16-MDCT at 80 mm and 100 kVp, respectively). Statistically significant reduction in radiation dose was found for axial 320-MDCT volumetric scanning compared to helical 64-, 32-, and 16-MDCT scanning.

Mahadevappa M. [29] studied 'The advances in CT technology and application to pediatric imaging'. The use of imaging in both hospital and nonhospital settings has expanded to more than 70 million CT procedures in the United States per year, with nearly 10% of procedures performed on children. The availability of multiple-row detector CT (MDCT) systems has played a large part in the wider usage of CT. This rapid increase in CT utilization combined with an increasing concern with regard to radiation exposure and associated risk demands the need for optimization of MDCT protocols.

Optimization of MDCT requires thorough understanding of all technical aspects of CT, including relevant scan parameters, available radiation dose reduction techniques, and technological advances. In addition, one needs to tailor the scan and technical parameters according to child size, body regions and, most important, clinical questions. With all the efforts to reduce radiation dose in CT imaging one underlying principle should be that considerable attention is required to maintain image quality. A number of technological advances are being made to reduce CT dose, including improved tube current modulation techniques, improved detector efficiency, wide-detector CT scanners (256–320 row MDCT), dual-source CT scanners, dynamic collimation, iterative reconstruction and lower tube voltage techniques.

Currently, CT imaging appears to be a high-dose procedure, sometimes performed inappropriately. As long as the CT examination is justified, the benefits far outweigh the associated radiation risks. Technological advances, along with increased scrutiny and review of CT protocols, with optimization as the ultimate goal, are paving the way for better and safer CT imaging. Many of the newer technological advances are specifically aimed at decreasing radiation doses. It is imperative that these methods be rapidly disseminated to users and that the methods are clearly understood and optimally utilized.

Trinavarat P. et al [30] studied the method to reduce the radiation dose from CT scanning. They have undertaken a systematic review of the literatures to document the radiation dose from CT, the lifetime cancer risk from CT exposure, CT dose parameters, the international CT diagnostic reference levels, the use and limitation of the CT effective dose.

In addition, a brief survey had been conducted on the use of CT scan in some university hospitals in Thailand and estimated current CT doses at these hospitals. From the review and survey, it had been the suggested that CT scanning provides a great benefit in medicine but it also becomes the major source of X-ray exposure. Radiation doses from a CT scan are much higher than most conventional radiographic procedures. This raises concerns about the carcinogenic potentials. We encourage every CT unit to adhere to the International Guidelines of CT dose parameter references. Preliminary survey revealed that CT radiation doses are within acceptable standard ranges. The data show a wide range of CT doses between hospitals in Thailand for each type of CT scan. The effective dose of CT brain ranges from 2.5-5.0 mSv, CT chest from 5.1-10.1 mSv, CT upper abdomen from 15.2-19.4 mSv, and CT whole abdomen from 14.7-26.1 mSv.

Kritsaneepaiboon S., Trinavarat P. and Visrutaratna P. [31] studied the survey of pediatric MDCT radiation dose from university hospitals in Thailand: a preliminary for national dose survey. They found that the increasing pediatric CT usage worldwide needs the optimization of CT protocol examination.

Although there are previous published dose reference level (DRL) values, the local DRLs should be established to guide for clinical practice and monitor the pediatric CT radiation dose. A retrospective review of CT dosimetry in pediatric patients (< 15 years of age) who had undergone head, chest, and abdominal MDCT in three major university hospitals in Thailand was performed. Volume CTDI ($CTDI_{vol}$) and DLP were recorded, categorized into four age groups: <1 year, 1– < 5 years, 5–<10 years, and 10–<15 years in each scanner. Range, mean, and third quartile values were compared with the national reference dose levels for CT in pediatric patients from the UK and Switzerland according to International Commission on Radiological Protection (ICRP) recommendations.

The third quartile values per age group, for brain, chest, and abdominal CTs were, in terms of $CTDI_{vol}$: 25, 30, 40, and 45 mGy; 4.5, 5.7, 10, and 15.6 mGy; 8.5, 9, 14, and 17 mGy; and in terms of DLP: 400, 570, 610, and 800 mGy cm; 80, 140, 305, and 470 mGy cm; and 190, 275, 560,765 mGy cm respectively.

CHAPTER III

Research Methodology

3.1 Research Design

This study is an observational descriptive design.

3.1.1 Conceptual framework

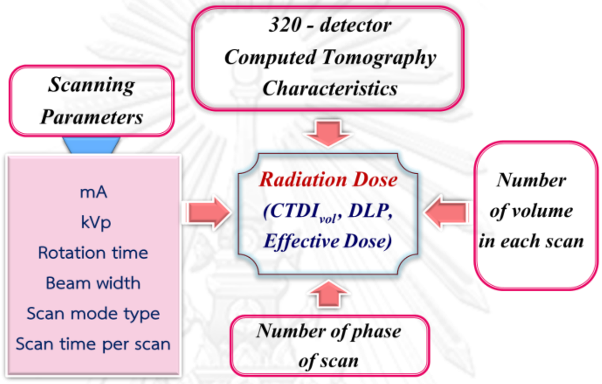

Figure 3.1 Conceptual framework.

3.1.2 Research Design Model

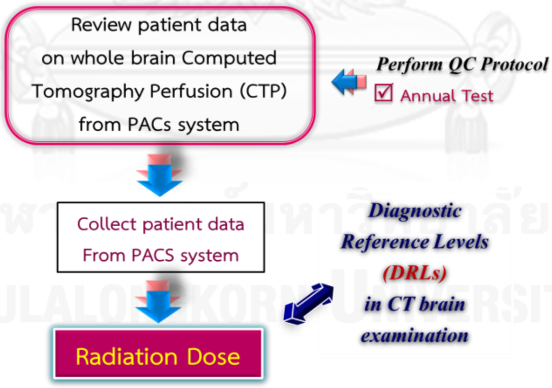

Figure 3.2 Research design model.

The data collected from Aquilion ONE 320-detector Computed Tomography scanner at AIMC Center, Sirikit Building, 2nd floor, Ramathibodi Hospital, Bangkok Thailand.

3.2 Research Question

What is the radiation dose in whole brain Computed Tomography in comprehensive stroke imaging using axial 320-row MDCT volumetric mode?

3.3 The sample

3.3.1 Target population: All patients who were requested for whole brain Computed Tomography in comprehensive stroke imaging using axial volume mode at AIMC Center, Ramathibodi Hospital from 2010 to 2012.

3.3.2 Sample population: In-Out patients who were requested for whole brain Computed Tomography in comprehensive stroke imaging using axial volume mode.

3.3.3 Eligible criteria:

3.3.3.1 Inclusion criteria: The patients

- Are both male and female.
- Are scanned by Aquilion ONE Toshiba 320-detector Computed Tomography scanner with axial volume mode.
- Are examined in comprehensive stroke imaging.

3.3.3.2 Exclusion criteria: Patients who underwent routine CT brain imaging using helical mode.

3.3.4 Sample size estimation:

(1) The data is consecutive collection.

(2) The sample population is independent, retrospective data.

This is a pilot study providing preliminary descriptive statistics that will be used to design a larger, adequately powered study, so all of patient data which met the inclusion criteria is collected in this study.

3.4 Materials

3.4.1 Equipment: Computed Tomography scanner

In this study, Toshiba Aquilion ONE 320-detector CT scanner at AIMC Center, Sirikit Building, 2nd floor, Ramathibodi Hospital, Faculty of Medicine, Mahidol University was used. CT scanner had been installed since 2010.

Computer software operates with Window NT system. The reconstructed CT images in axial volumetric mode were obtained by using volumeXact reconstruction method. The Vitrea workstation (Vitrea® fx version 1.0-3.0, Vital Images) was used in perfusion analysis. The perfusion map was generated by using delay-insensitive singular value decomposition or dSVDs , ViTAL's algorithm (co-developed by Toshiba Medical Systems, Japan). The technical specifications of CT scanner show in table 3.1.

Table 3.1 The technical specifications of Toshiba Aquilion ONE 320-detector CT scanner. (Comparative specifications 128-320 slice CT scanners. CEP08028.March 2009). [32]

Technical specifications		Details
Gantry	Scan type	3^{rd} generation
	Aperture	72 cm
	Focus- isocenter distance	600 mm
	Focus- detector distance	1072 mm
	Slip ring for power supply	Lower voltage
	Slip ring for data transmission	RF
	Power supply requirements (gantry)	3 phase 380-480V, 125kVA
X-ray generator	Type	High frequency
	Method of generator cooling	Air
	Power rating	70 kW
	kV setting	80, 100, 120, 135
	mA range (and step size)	10-50 (5 mA steps), 50-580 (10 mA step)
X-ray tube	Pattern and type of X- rays	Fan beam, continuous X-rays
	Focal spot size(s), quoted to IEC 336/93 standard	0.9x0.8 mm 1.6x1.4 mm
	Total filtration at maximum kV(inherent +beam sharping filter on center axis, mm Al equivalent @ 120 kV)	4.8 (L wedge filter) 4.8 (M wedge filter) 3.9 (S wedge filter)
	X-ray beam shielding lead equivalent	2.4 mm Pb or more
	X-ray tube unit inherent filtration	1.0 mm Al equivalent or more
	Inherent filtration on other than the X-ray tube unit	Minimum 1.5 mm Al equivalent
	Total filtration of the system	Minimum 2.5 mm Al equivalent
	Anode heat capacities	7.5 MHU
	Maximum anode cooling rate	1386 kHU/min
	Method of tube cooling	Liquid
	Expected tube life (amp-hours)	300000 rotations

Technical specifications		Details
Classification	According to the type of protection against electrical shock	CLASS I Equipment
Couch	Couch top material	Carbon fiber
Data processing	Reconstruction algorithm-sequential scanning	ConeXact
	Reconstruction approach- sequential scanning	Volume
Detector system	Detector type	Solid state array
	Detector material	Gadolinium oxysulphide (GOS)
	Maximum number of simultaneously acquire data set (number of 'slices')	320
	Number of detector elements along z-axis	320
	Effective length of detector elements along z-axis (at isocenter)	320x0.5 mm
	Total effective length of detector array at iso-center	160 mm
Acquisition parameters and image reconstruction	kV steps	80, 100, 120, 135
	Maximum mA (for each kV)	80 kV: 580 mA 100 kV: 580 mA 120 kV: 580 mA 135 kV: 510 mA
	Automatic mA control (AEC/ mA modulation) software	SUREExposure3D
	Scan field of view	18, 24, 32, 40, 50 cm
	Rotation times for sequential scanning	0.35, 0.375, 0.4, 0.45, 0.5, 0.6, 0.75, 1, 1.5, 2, 3 s
	Reconstruction matrices	512x512
Advanced scanning facilities	CT perfusion capability	Cerebral Brain Perfusion
	Maximum scan coverage for perfusion scans-sequential scanning	160 mm
	CT perfusion analysis	Cerebral Brain Perfusion

Figure 3.3 The 320-row MDCT (Aquilion ONE, Toshiba Medical Systems Corporation, Japan) scanner.

3.4.2 QC Materials

3.4.2.1 The cylindrical PMMA 16 and 32 cm diameter CT dosimetry phantoms

The CT phantom is in compliance with the FDA's performance standard. The standard cylindrical head and body CT dosimetry phantoms are constructed of Polymethyl Methacrylate (PMMA) having cylindrical holes (at 1 cm from the edge, and one at the center) and 14 cm in length. All of the unused holes are plugged with acrylic rods, individually handled to facilitate measurements. Two sizes of standard cylindrical PMMA head (16 cm in diameter) and body (32 cm in diameter) CT dosimetry phantoms can be separate or combined (the head phantom is the innermost cylinder in body phantom) as in Figure3.4.

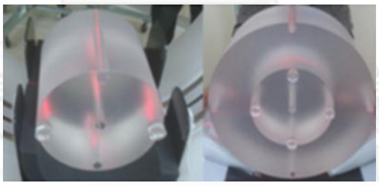

Figure 3.4 Two sizes of standard cylindrical PMMA head (16 cm in diameter) and body (32 cm in diameter) CT dosimetry phantoms with holes for acrylic rods insertion at various location of the hole.

3.4.2.2 The pencil type ionization chamber

The pencil type ionization chamber (10X6-3CT) is a Computed Tomography Dose Index (CTDI) designed specifically for CT X-ray beam measurements, 3.0 cm^3 active volume, 1.5m low noise triax cable, 0.11 kg weight, the chambers excellent energy and partial volume response as well as uniformity along its entire 10 cm active length as show in Figure 3.5. The pencil type ionization chamber was connected to the measuring assembly and electrometer, positioned at the isocenter of the CT bore. The chamber was calibrated by SSDL (Secondary Standard Dosimetry Laboratory), both temperature and pressures were available to correct the measured dose.

3.4.2.3 Radcal model Accu-ProTM dosemeter

Radcal model Accu-ProTM dosemeter built-in digital display and computer display with optional XLPRO software are shown in table 3.2 and 3.3, the dosemeter is displayed in figure 3.6.

Figure 3.5 Pencil ionization chamber manufacture Radcal used for dosimetry of CT. The active volume of the chamber is 3 cm^3 and the active length is 10 cm. (Copyright © 2012 RADCAL CORPORATION)

Table 3.2 Characteristics of Radcal model Accu-ProTM dosemeter.

Characteristics	Display
Min rate	2 μR/s
Max rate	40 R/s
Min dose	20 μR
Max dose	118 kR
Cine specifications	n/a
Calibration accuracy	±4% using X-rays @ 150kV_p and 10.2 mm Al HVL
Exposure rate dependence	±2%, 2mR/s to 40 R/s
Energy dependence	±5%, 3 to 20 mm Al HVL
Construction	air-equivalent walls and electrode: polyacetal exterior cap; 3 cm^3 active volume; 1.5m, low noise triax cable; 0.11kg

Table 3.3 Digital display of the dosemeter.

Dose	Time
R (Roentgens) Gy (Grays) C (Coulombs) Auto Dose Dose Accumulate/Hold Last Dose Dose Rate	Seconds Minutes Hours

Figure 3.6 Radcal model Accu-ProTM dosemeter.

3.4.2.4 Catphan® 600 CT quality assurance phantom

Catphan® 600 phantom was used to test the performance of CT scanner. Place the phantom case on the table end and the box is adequately counterweighed to prevent tipping, use the level and adjusting thumb screws to level the Catphan® as shown in figure 3.7.

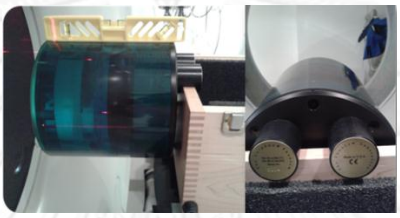

Figure 3.7 Catphan® 600 CT quality assurance phantom.

The Catphan® 600 phantom is all test sections located by precisely indexing the table from center of section 1 (CTP404) to the center of each subsequence test module. The indexing distances from section 1 are listed below. Catphan® 600 test module locations:

Module	Distance from section 1 center (CTP 404)
CTP404, slice width, sensitometry and pixel size	
CTP591, Bead geometry	32.5 mm
CTP528, 21 line pair high resolution	70 mm
CTP528, Point source	80 mm
CTP515, Subslice and supra-slice low contrast	110 mm
CTP486, Solid image uniformity module	150 mm

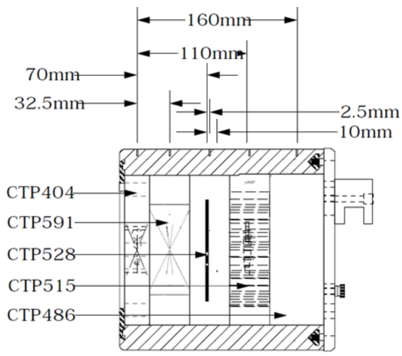

Figure 3.8 Illustration of Catphan® 600models (Catphan® 500 and 600 Manual Copyright © 2012).

3.4.3 Patients

All patients underwent whole brain Computed Tomography in comprehensive stroke imaging using axial volume mode at AIMC Center, Ramathibodi Hospital from 2010 to 2012. Patients who underwent helical scan mode of CT head region were excluded in this study.

3.5 Methods

The study had been carried out as in the following sequence.

(1) The quality control of CT scanner was performed according to IAEA Human Health Series No.19 protocol as following details: Mechanical accuracy, imaging performance and dosimetry for $CTDI_{vol}$ (to verify the values on the CT monitor console).

(2) The patient data for CT Perfusion of the brain examination in comprehensive stroke imaging were collected; such as gender and age.

(3) The scanning parameters and radiation dose were recorded; such as kV_p, mA, rotation time (second), total number of volumes scan, scan mode type, scan time in each volume, beam width (mm), scan length (mm), $CTDI_{vol}$ and Dose Length Product (DLP).

DLP (units: mGy cm) is an indicator of the mean absorbed dose to the patient of each series in CT exam and defined as the product of $CTDI_{vol}$ multiplied with scan length.

The effective dose (E) is calculated approximately from the DLP (Dose Length Product) and the conversion coefficient, f, [mSv/(mGy•cm)] in head region by the formula;

$$E = DLP \times f$$

Table 3.4 Published conversion factors for standard head CT scans.

Region	Conversion factor from DLP to Effective dose in [mSv/(mGy.cm)] by age				
	0 year	1 year	5 year	10 year	Adult
Head	0.011	0.0067	0.0040	0.0032	0.0021

Effective dose estimation based on published conversion factors for standard CT scans.(All data normalized to $CTDI_w$ measured in the 16-cm diameter CT dosimetry phantom) [33]

3.6 Statistical and data analysis

3.6.1 Summarization of Data

(1) Mean is used to calculate the radiation dose.

(2) Maximum and minimum are used to represent the highest and lowest values.

The data were analyzed by using Microsoft Excel for evaluation.

3.6.2 Data Presentation

The table, graph and bar chart were used to present the radiation dose of whole brain Computed Tomography in comprehensive stroke imaging.

3.7 Ethical Consideration

This research will be retrospective study. The data will be recorded from the PACs system of the hospital, not directly contacts to collect data from patients.

The research proposal had been approved by the Ethical Committee of Faculty of Medicine, Chulalongkorn University and had received permission from the Director of Faculty of Medicine, Ramathibodi Hospital, Mahidol University to get patient information from the PACs system.

3.8 Limitations

The patient who underwent whole brain computed Tomography in comprehensive stroke imaging using helical scan mode is excluded.

3.9 Expected benefits

(1) Radiation doses in the scan area underwent whole brain Computed Tomography in comprehensive stroke imaging using Axial Volumetric MDCT examination.

(2) The awareness of the radiation dose from whole brain CT Computed Tomography in comprehensive stroke imaging using Axial Volumetric MDCT examination.

CHAPTER IV
RESULT

4.1 Quality control of the Multidetector Computed Tomography scanner: TOSHIBA Aquilion ONE

The quality control of the MDCT scanner was performed following IAEA Human Health Series No.19 [34] and Technical Report Series no. 457.[35] It includes the test of electromechanical component, image quality and radiation dose. Quality control of MDCT scanner is shown in Appendix B, with the summarized report of CT system performance test.

4.1.1 Report of Computed Tomography system performance

Location:	2nd floor Sirikit Building, AIMC, Ramathibodi Hospital (Since 2010).
Manufacturer:	Toshiba
Model:	Aquilion One
Serial number:	2CA08X2062
Date:	February 20, 2013
Pass	Scan Localization Light Accuracy
Pass	Alignment of Table to Gantry
Pass	Table Increments Accuracy
Pass	Slice Increment Accuracy
Pass	Gantry Tilt
Pass	Beam Alignment
Pass	Reproducibility of C.T. Numbers
Pass	mAs Linearity
Pass	Linearity of C.T. Numbers
Pass	High Contrast Resolution
Pass	Low Contrast Resolution
Pass	Accuracy of distance measurement
Pass	Image Uniformity

4.2 Verification of Computed Tomography Dose Index (CTDI)

4.2.1 Measurement of $C_{a,100}$ free in air (C_{air} or $CTDI_{air}$)

Purpose: To measure the C_{air} ($CTDI_{air}$) values for all X-ray beam collimations and kV_p.

Method: The procedure is as followings:

1. Set the gantry tilt to 0°

2. Position the chamber support stand on the couch.

3. Fix the 100 mm pencil chamber in position at the isocenter of the CT bore and ensure the ion chamber is not tilted or twisted. Alignment to within 5° is acceptable.

3. Adjust the position of the support so that all of the active volume of the chamber extends beyond the end of the couch.

4. Use the optical alignment aids provided with the scanner to position and align the chamber so that its axis is coincided with the axis of the scanner and the centre of the chamber volume lies on the scan plane.

5. The scan parameter is 100 mA tube current, 1 sec scan time and small focal spot size setting for all measurements at kilovoltage setting of 80, 100, 120 and 135.

6. Select a single axial rotation.

7. Measure the $CTDI_{100}$ in air using head and body protocols.

8. Record the dosimeter reading for a single rotation of the scanner.

9. Calculate $C_{a,100}$ free in air from the dosimeter readings for each X ray beam collimations and kV used.

Technique: 100 mA, 1.0 Second, FOV 240 (S)

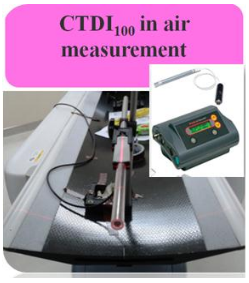

Figure 4.1 $CTDI_{100}$ in air (C_{air} or $CTDI_{air}$) measurement using pencil ion chamber set in air, at isocenter of CT gantry bore.

Results:

Table 4.1 The measured $CTDI_{100}$ in air for head protocols for each kV_p.

kV_p	$C_{a,100}$ (mGy) in air, Head protocol 8 Slice Collimations in mm (NT)							
	1 (1x1)	2 (0.5x4)	4 (1x4)	8 (2x4)	12 (3x4)	16 (4x4)	20 (5x4)	32 (8x4)
80	6.29	3.84	2.52	1.87	1.65	1.54	1.47	1.36
100	10.38	6.33	4.18	3.08	2.74	2.53	2.42	2.23
120	15.70	9.55	6.22	4.54	3.99	3.71	3.54	3.25
135	21.13	12.66	8.16	5.88	5.11	4.73	4.51	4.13

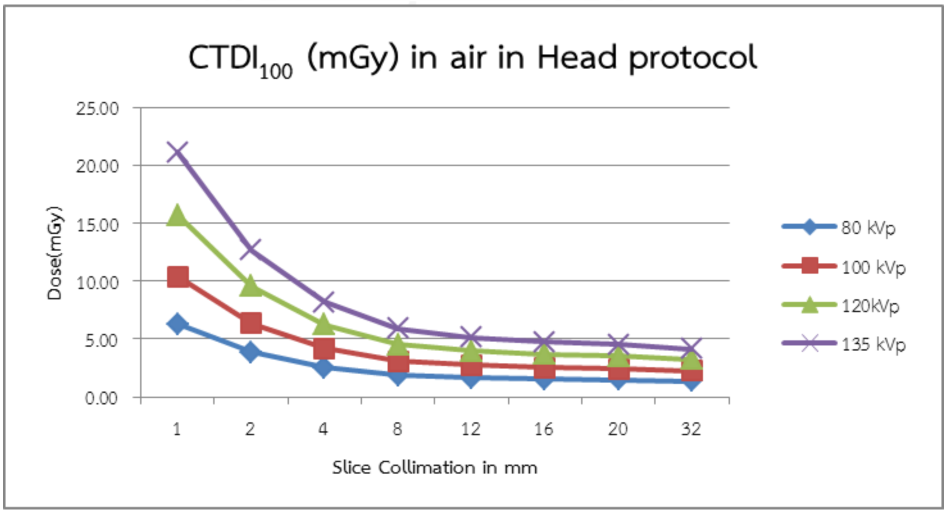

Figure 4.2 $CTDI_{100}$ (mGy) in air in head protocol

Tolerance: The acceptance of $CTDI_{100}$ measurements for each X-ray beam collimation should be less than ± 20% of manufacturer's specifications.

$CTDI_{a,\ 100}$ was calculated from the equation;

$$CTDI_{a,\ 100} = (1/nT) \times \text{Dosimeter reading} \times \text{Chamber length (mm)}$$

Technique: 100 mA, 1.0 Second, 400mm FOV (L)

Table 4.2 The measured $CTDI_{100}$ in air for body protocols for each kV_p with small focal spot, 400 mm FOV (L).

kV_p	$C_{a,100}$ (mGy) in air, body protocol 8 Slice Collimations in mm (NT)							
	1 (1x1)	2 (0.5x4)	4 (1x4)	8 (2x4)	12 (3x4)	16 (4x4)	20 (5x4)	32 (8x4)
80	6.71	3.92	2.45	1.71	1.44	1.33	1.25	1.14
100	8.74	5.34	3.51	2.59	2.28	2.13	2.03	1.88
120	13.74	8.31	5.40	3.95	3.47	3.22	3.08	2.82
135	18.96	11.27	7.24	5.22	4.54	4.20	3.99	3.65

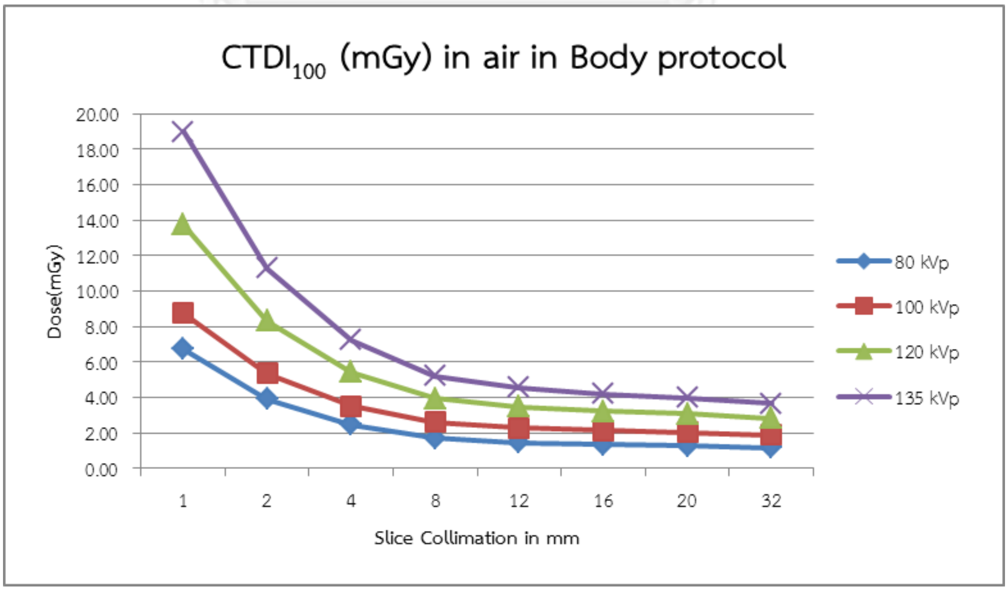

Figure 4.3 $CTDI_{100}$ (mGy) in air in body protocol with small focal spot, 400mm FOV (L).

Table 4.3 The measured $CTDI_{100}$ in air for body protocols for each kV_p with large focal spot, 500 mm FOV (LL).

kV_p	$C_{a,100}$ (mGy) in air, body protocol							
	8 Slice Collimations in mm (NT)							
	1 (1x1)	2 (0.5x4)	4 (1x4)	8 (2x4)	12 (3x4)	16 (4x4)	20 (5x4)	32 (8x4)
80	6.72	3.93	2.45	1.71	1.44	1.32	1.25	1.14
100	11.67	6.79	4.22	2.96	2.48	2.28	2.16	1.97
120	18.10	10.46	6.49	4.50	3.77	3.45	3.26	2.96
135	24.44	14.05	8.63	5.91	4.92	4.49	4.23	3.82

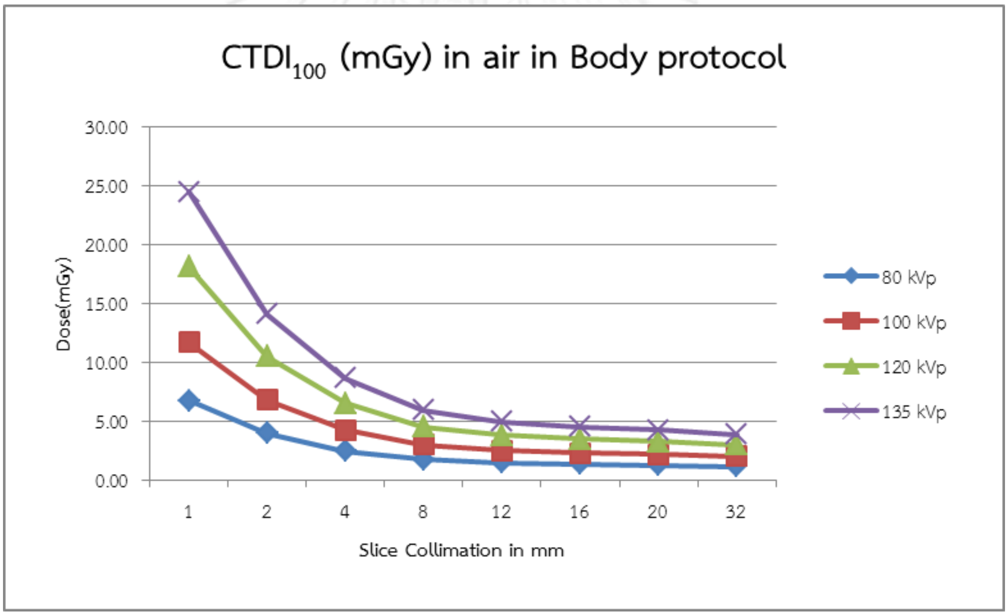

Figure 4.4 $CTDI_{100}$ (mGy) in air in body protocol with large focal spot, 500mm FOV (LL)

4.2.2 Measurement of $CTDI_{100}$ in head phantom

Purpose: To measure $CTDI_{100}$ at each hole of head phantom for each kV_p, $CTDI_w$ and ${}_nCTDI_w$ in unit of mGy/100mAs.

Method:

1. The $CTDI_{100}$ in head phantom was measured using a 100 mm pencil ionization chamber (Radcal dosimeter) place in each hole of 16 cm diameter PMMA phantom at the isocenter of the CT bore.

2. The scan parameters were 100 mA, 1 sec scan time, 240mm FOV and 4x4 mm collimation setting for all measurements at kV_p setting of 80, 100, 120 and 135 respectively.

Technique: 100 mA, 1.0 second, FOV 240, slice collimation 4x4 mm, detector width (nT) 16mm.

Result:

Table 4.4 The measured $CTDI_{100}$ at each hole of head phantom for each kVp, $CTDI_w$ and ${}_nCTDI_w$ in unit of mGy/100mAs.

kV_p	$CTDI_{100}$ in *head* phantom (mGy)						$CTDI_c$	$CTDI_p$	$CTDI_w$ or C_w (mGy at 100mAs)	${}_nCTDI_w$ or ${}_nC_w$ (mGy/mAs)
	At center	At peripheral								
		3 o'clock	6 o'clock	9 o'clock	12 o'clock	Average				
80	1.189	1.348	1.465	1.465	1.403	1.42	7.431	8.877	8.39	0.08
100	2.215	2.342	2.623	2.544	2.477	2.497	13.844	15.603	15.02	0.15
120	3.536	4.018	3.764	3.937	4.272	3.998	22.100	24.986	24.02	0.24
135	4.662	5.287	5.15	5.157	4.98	5.144	29.138	32.147	31.14	0.31

Note:

$CTDI_{center}$, $CTDI_{periphery}$, $CTDI_w$, and ${}_nCTDI_w$ were calculated from the equation;

$CTDI_{center}$ = (1/nT) x Center reading x Chamber length (mm)

$CTDI_{periphery}$ = (1/nT) x Average periphery reading x Chamber length (mm)

$CTDI_w = 1/3(CTDI_{center}) + 2/3\,(CTDI_{periphery})$

${}_nCTDI_w = CTDI_w/mAs$

4.2.3 Measurement of $CTDI_{100}$ in body phantom

Purpose: To measure $CTDI_{100}$ at each hole of body phantom, $CTDI_w$ and ${}_nCTDI_w$ in unit of mGy/100mAs for each kV_p.

Technique: 100 mA, 1.0 second, 400mm FOV (L), slice collimation 4x4 mm, detector width (nT) 16mm.

Result:

Table 4.5 The measured $CTDI_{100}$ at each hole of body phantom, $CTDI_w$ and ${}_nCTDI_w$ in unit of mGy/100mAs at each kV_p, 400 mm FOV.

kV_p	$CTDI_{100}$ in *body* phantom (mGy)								$CTDI_w$ or C_w (mGy at 100mAs)	${}_nCTDI_w$ or ${}_nC_w$ (mGy/mAs)
	At center	At peripheral					$CTDI_c$	$CTDI_p$		
		3 o'clock	6 o'clock	9 o'clock	12 o'clock	Average				
80	0.263	0.653	0.585	0.661	0.692	0.648	1.644	4.048	3.25	0.03
100	0.579	1.504	1.063	1.264	1.375	1.302	3.619	8.134	6.63	0.07
120	1.025	2.522	1.788	2.317	2.162	2.197	6.406	13.733	11.29	0.11
135	1.43	3.338	2.425	2.831	3.329	2.981	8.938	18.630	15.40	0.15

4.2.4 Comparison of the $CTDI_{vol}$ on monitor and calculated $CTDI_w$

Purpose: To compare the $CTDI_{vol}$ displayed on the CT monitor with the calculated $CTDI_w$ for the same acquisition parameters**.**

Method:

1. Determine the $CTDI_w$ by using the results in Table 4.4 and 4.5.
2. The $CTDI_{vol}$ displayed on CT monitor were recorded to compare percentage difference with the calculated values as shown in table 4.6 for $CTDI_{vol}$ in head phantom and table 4.7 for $CTDI_{vol}$ in body phantom.

Result:

Table 4.6 $CTDI_{vol}$ displayed on monitor and calculated $CTDI_w$ using head techniques mAs 100 and 240 mm FOV (S).

kV_p	$CTDI_{vol}$ (mGy) in *head* phantom		% difference
	Calculated $CTDI_w$, 16cm PMMA head phantom	Displayed $CTDI_w$, 16cm PMMA head phantom	
80	8.39	8.0	4.9
100	15.02	14.7	2.2
120	24.02	22.6	6.3
135	31.14	29.9	4.1

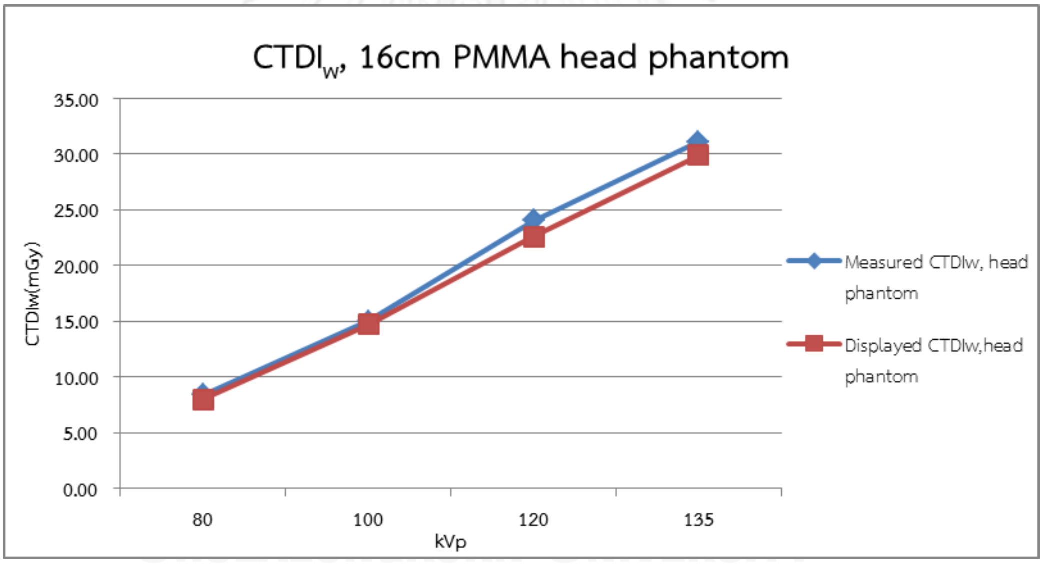

Figure 4.5 Calculated and displayed $CTDI_w$ (mGy) in 16cm PMMA head phantom.

Tolerance: The difference between measured $CTDI_w$ and displayed should be less than±10%

Comment: ☑ Pass

Table 4.7 $CTDI_{vol}$ displayed on monitor and calculated $CTDI_w$ using body techniques mAs 100 and 400 mm FOV (L).

kVp	$CTDI_{vol}$ (mGy) in *body* phantom		% difference
	Calculated $CTDI_w$, 32 cm PMMA head phantom	Displayed $CTDI_w$, 32 cm PMMA head phantom	
80	3.25	3.4	-4.4
100	6.63	7.0	-5.3
120	11.29	11.4	-1.0
135	15.4	15.8	-2.5

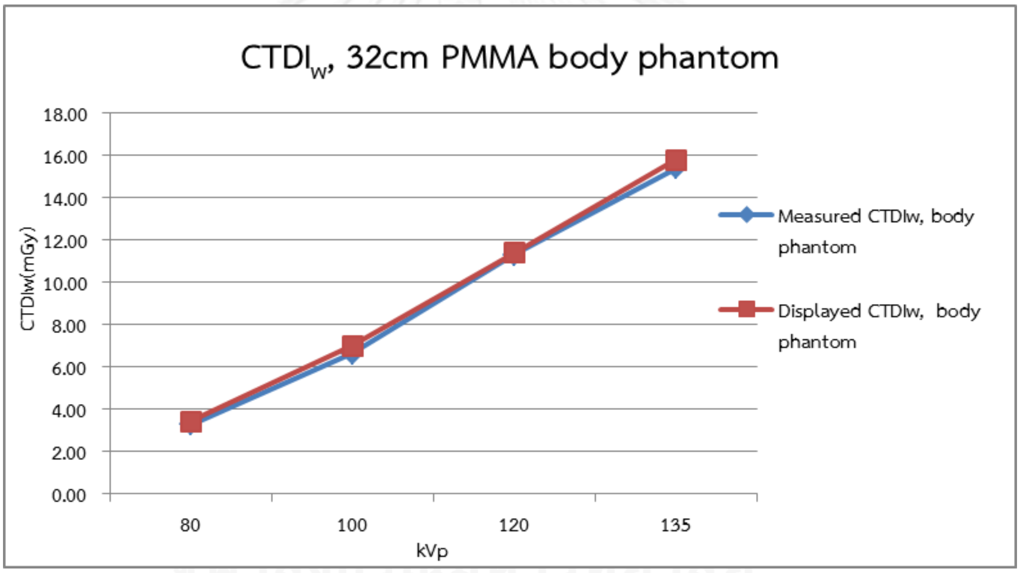

Figure 4.6 Calculated and displayed $CTDI_w$ (mGy) in 32cm PMMA body phantom.

Tolerance: The difference between calculated and $CTDI_w$ displayed should be less than±10%

Comment: ☑ Pass

4.2.5 Comparison of calculated $CTDI_{vol}$ with manufacturer's specifications

Purpose: To verify the calculated $CTDI_{vol}$ with manufacturer's specification.

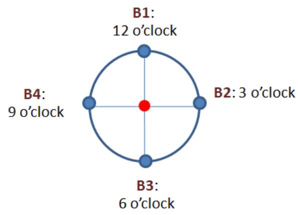

Figure 4.7 Five positions for calculated $CTDI_w$ following the IEC.

Table 4.8 $CTDI_{100}$ (mGy) and $CTDI_w$ under typical scan conditions.

Position	Head mode • 120 kV, 100mA, 1-s scan • Scan field: S (240mm) • 4 mm x 4mm slice thickness • 160-mm-diameter phantom (150 mm in length)			Body mode • 120 kV, 100mA, 1-s scan • Scan field: L (400mm) • 4 mmx 4 mm slice thickness • 320-mm-diameter phantom (150 mm in length)		
	IEC	Calculated	% difference	IEC	Calculated	% difference
Center	22.60	22.1	-2.2	7.22	6.4	-11.4
Periphery (Mean value)	24.16	25	3.5	13.93	13.7	-1.7
Periphery (Max value)	25.46 (B1)	26.7 (B1)	4.9	14.34 (B2)	15.8 (B2)	10.2
Periphery;						
B1: 12 o'clock	25.46	26.7	4.9	14.34	13.5	-5.9
B2: 3 o'clock	24.03	25.1	4.5	14.15	15.8	11.7
B3: 6 o'clock	23.10	23.5	1.7	12.90	11.2	-13.2
B4: 9 o'clock	24.03	24.6	2.4	14.31	14.5	1.3
$CTDI_{vol}$	**24.51**	**24.03**	**-1.96**	**12.94**	**11.27**	**-12.91**

Tolerance: The difference between calculated $CTDI_{vol}$ and manufacturer's should be less than ±20%

Comment: ☑ Pass

4.2.6 Comparison of $CTDI_{vol}$ among calculated, displayed on monitor and IEC CT individual standard (IEC 60601-2-44)

Result:

Table 4.9 The comparison of $CTDI_{vol}$ among calculated, displayed on monitor and IEC CT individual standard (IEC 60601-2-44) in head phantom.

kV_p	$CTDI_{vol}$ (mGy) in *head* phantom			% difference between *calculated* and *displayed* $CTDI_{vol}$	% difference between *displayed* and *IEC* $CTDI_{vol}$	% difference between *calculated* and *IEC* $CTDI_{vol}$
	Calculated $CTDI_{vol}$	Displayed $CTDI_{vol}$ on monitor consol	$CTDI_{vol}$ following the IEC CT Individual standard (Manufacturer's specification)			
120	**24.02**	**22.6**	**24.51**	**6.30**	**-7.79**	**-1.96**

Table 4.10 The comparison of $CTDI_{vol}$ among calculated, displayed on monitor and IEC CT individual standard (IEC 60601-2-44) in body phantom.

kV_p	$CTDI_{vol}$ (mGy) in *body* phantom			% difference between *calculated* and *displayed* $CTDI_{vol}$	% difference between *displayed* and *IEC* $CTDI_{vol}$	% difference between *calculated* and *IEC* $CTDI_{vol}$
	Calculated $CTDI_{vol}$	Displayed $CTDI_{vol}$ on monitor consol	$CTDI_{vol}$ following the IEC CT Individual standard (Manufacturer's specification)			
120	**11.29**	**11.4**	**12.94**	**-0.97**	**-11.90**	**-12.91**

Tolerance: The difference between calculated $CTDI_{vol}$ and manufacturer's should be less than ±20%

Comment: ☑ Pass

4.2.7 The measured $CTDI_{100}$ in air for head protocols for each kV_p (in Axial volume mode)

Purpose: To measure the C_{air} ($CTDI_{air}$) values for all X-ray beam collimations and kV_p.

Method: The same method is used in section *4.2.1* but change scan mode type from a single axial rotation (conventional mode) to axial volume mode.

Technique: 100 mA, 1.0 second, FOV 240 (S), Volume mode selection.

Result:

Table 4.11 The measured $CTDI_{100}$ in air for head protocols in axial volume mode for each kV_p

kV_p	$C_{a,100}$ (mGy) in air, *head* protocol 6 Slice collimations in mm (NT)					
	40 (0.5x80)	60 (0.5x120)	80 (0.5x160)	120 (0.5x240)	140 (0.5x280)	160 (0.5x320)
80	1.24	1.2	1.18	0.93	0.8	0.7
100	2.07	1.97	1.94	1.53	1.32	1.15
120	3.04	2.88	2.84	2.21	1.92	1.68
135	3.85	3.64	3.54	2.77	2.42	2.12

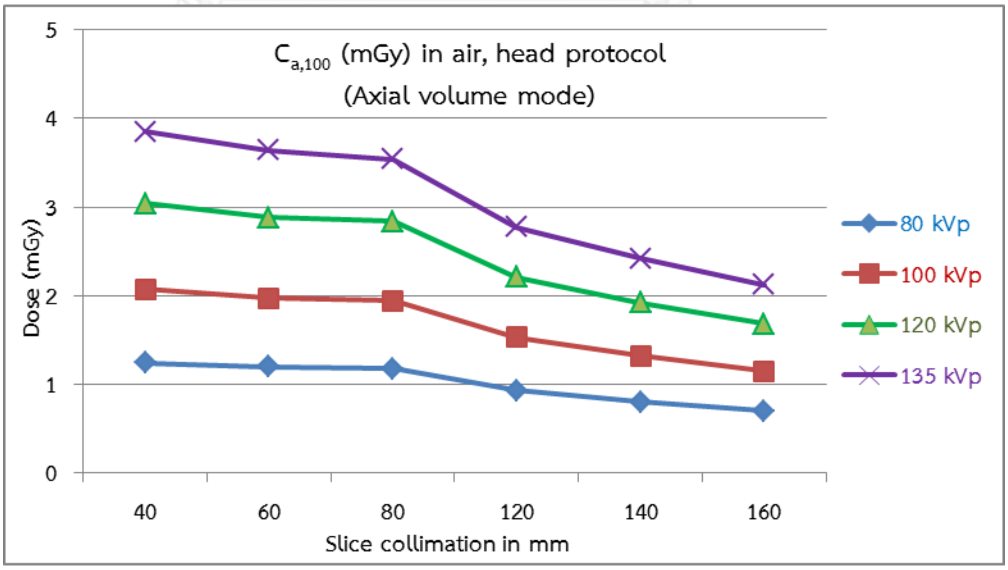

Figure 4.8 $CTDI_{100}$ (mGy) in air in head protocol with axial volume mode scan.

4.2.8 The measurement of $CTDI_{100}$ in head phantom (in Axial Volume Mode)

Purpose: To measure $CTDI_{100}$ at each hole of head phantom, $CTDI_w$ and ${}_nCTDI_w$ in unit of mGy/100mAs for each kV_p.

Method: The same method is used in section 4.2.2 but change scan mode type from a single axial rotation (conventional mode) to axial volume mode.

Technique: 100 mA, 1.0 second, FOV 240, slice collimation 0.5x320 mm, detector width (nT) 160mm.

Result:

Table 4.12 The measured $CTDI_{100}$ at each hole of head phantom in axial volume mode for each kV_p, $CTDI_w$ and ${}_nCTDI_w$ in unit of mGy/100mAs.

kV_p	$CTDI_{100}$ in *head* phantom (mGy)						$CTDI_w$ or C_w (mGy at 100mAs)	${}_nCTDI_w$ or ${}_nC_w$ (mGy/mAs)
	At center	At peripheral						
		3 o'clock	6 o'clock	9 o'clock	12 o'clock	Average		
80	6.442	7.526	7.291	7.738	8.681	7.809	7.35	0.07
100	12.13	12.9	12.91	13.37	15.03	13.553	13.08	0.13
120	18.89	19.95	19.67	20.28	20.61	20.128	19.72	0.20
135	24.74	25.93	26.72	26.62	26.8	26.518	25.93	0.26

Note:

When the nominal beam width (nT) take as 160 mm, exceeds the sensitive length of 100 mm long pencil ionization chamber, the average dose was defined for wide cone beam CT scanner; [36]

$$CTDI_{100} = \text{average dose} = (1/100) \times \text{reading} \times \text{Chamber length (mm)}$$

4.2.9 Comparison the calculated $CTDI_w$ and $CTDI_{vol}$ displayed on monitor (Axial Volume Mode)

Purpose: To compare the calculated $CTDI_w$ with the $CTDI_{vol}$ displayed on the CT monitor for the same acquisition parameters in axial volume mode.

Method: The same method is used in section 4.2.4 but change scan mode type from a single axial rotation (conventional mode) to axial volume mode.

Result:

Table 4.13 $CTDI_{vol}$ displayed on monitor and calculated $CTDI_w$ using head techniques mAs 100 and 240 mm FOV (S).

kV_p	$CTDI_{vol}$ (mGy) in *head* phantom		% difference
	Calculated $CTDI_w$, 16cm PMMA head phantom	Displayed $CTDI_{vol}$, 16cm PMMA head phantom	
80	7.35	7.1	3.52
100	13.08	13	0.62
120	19.72	19.9	-0.90
135	25.93	26.2	-1.03

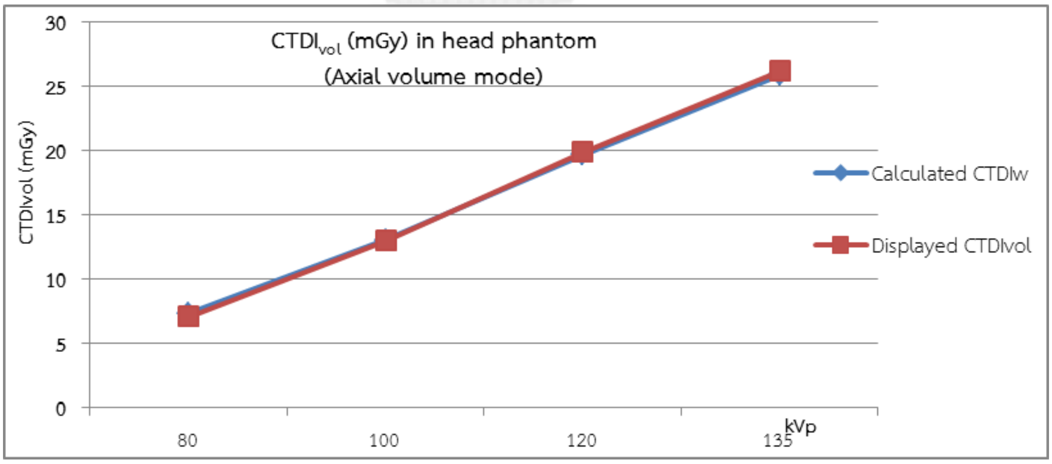

Figure 4.9 Calculated $CTDI_w$ and displayed $CTDI_{vol}$ (mGy) in 16cm PMMA head phantom with axial volume mode.

Tolerance: The difference between calculated $CTDI_w$ and displayed $CTDI_{vol}$ should be less than±10%

Comment: ☑ Pass

4.3 The data of patient studies

4.3.1 The patient data and radiation dose

The parameters of twenty one patients who underwent in whole brain Computed Tomography in comprehensive stroke imaging using axial volumetric 320-detector MDCT were shown in table 4.14. Tube voltage 80 kV_p, beam width 320x0.5mm, coverage 16 cm and rotation time 0.75 second per rotation are the same for all of cases but tube current and number of volume scan are varying. Among 21 patients there were 11 males and 10 females, age range, 6-77 years; mean age, 45.4 years.

Table 4.14 The patient parameters from 21 patients who underwent Comprehensive stroke imaging using axial volume mode.

Case No/ Age (year)/Gender (M/F)	Number of volume scan	Total mAs
1/6/F	19	n/a
2/7/F	19	1875
3/20/M	19	1987
4/21/F	19	2025
5/21/F	19	2813
6/22/F	19	2025
7/39/M	24	3383
8/42/F	19	2821
9/42/M	19	2821
10/44/M	19	2821
11/49/M	19	1987
12/49/F	19	2821
13/51/M	19	2821
14/51/M	19	2821
15/64/F	10	2600
16/66/M	19	2821
17/66/M	19	4271
18/70/F	19	2821
19/73/M	19	n/a
20/73/M	19	2821
21/77/F	24	2814

The patient parameters were collected from Picture Archiving and Communication System (PACS) of Ramathibodi Hospital, from the year 2010 to 2012. The software version of PACS was changed during the period of patient data collection, so the tube current was not displayed on screen in some case.

4.3.2 Radiation dose

$CTDI_{vol}$ and DLP were recorded from PACS system of the hospital. The effective dose was calculated from DLP multiplied conversion coefficient for head region, 0.004 mSv/mGy.cm in case number 1 and 2, and 0.0021 in the other case. The $CTDI_{vol}$, DLP and effective dose considered in terms of cumulative dose, average dose and average dose per a volume are shown in table 4.15, 4.16 and 4.17 respectively.

Table 4.15 The mean $CTDI_{vol}$, DLP and effective dose considered in terms of ***cumulative dose.***

Case No/ Age (year)/ Gender (M/F)	**$CTDI_{vol}$ (mGy) (*Cumulative*)**	**DLP (mGy.cm) (*Cumulative*)**	**Effective Dose (mSv) (*Cumulative*)**
1/6/F	154.02	2157.0	8.63
2/7/F	134.84	2156.9	8.63
3/20/M	142.94	2286.6	4.82
4/21/F	200.00	3192.9	6.71
5/21/F	145.64	2329.7	4.89
6/22/F	145.64	2329.7	4.89
7/39/M	240.00	3829.9	8.04
8/42/F	202.72	3243.6	6.81
9/42/M	202.72	3243.6	6.81
10/44/M	202.72	3243.6	6.81
11/49/M	142.94	2286.6	4.80
12/49/F	202.72	3243.6	6.81
13/51/M	202.72	3243.6	6.81
14/51/M	202.72	3243.6	6.81
15/64/F	184.10	2943.6	6.18
16/66/M	202.72	3243.6	6.81
17/66/M	313.42	5014.2	10.53
18/70/F	202.72	3243.6	6.81
19/73/M	185.40	2965.9	6.23
20/73/M	202.72	3243.6	6.81
21/77/F	285.40	4557.0	9.57

The $CTDI_{vol}$, DLP and effective dose considered in terms of cumulative dose, average dose and average dose per a volume are shown in figure 4.10-4.12, 4.13-4.15 and 4.16-4.18 respectively.

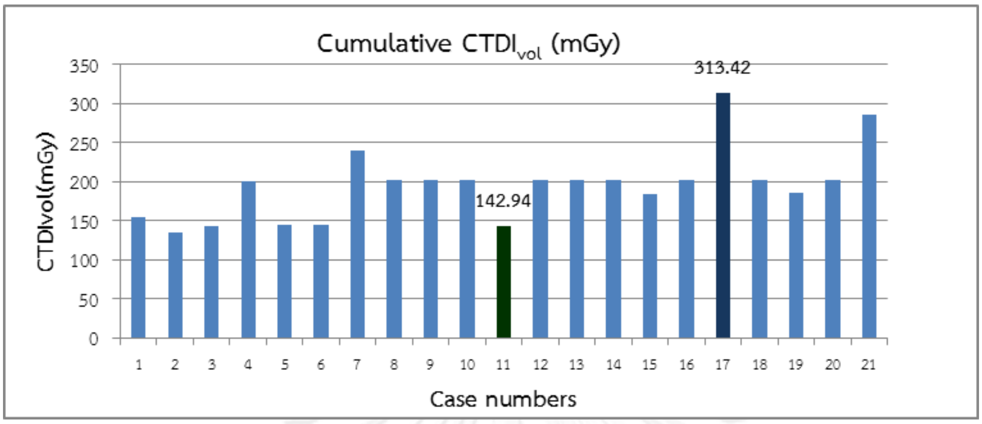

Figure 4. 10 The $CTDI_{vol}$ considered in terms of cumulative dose.

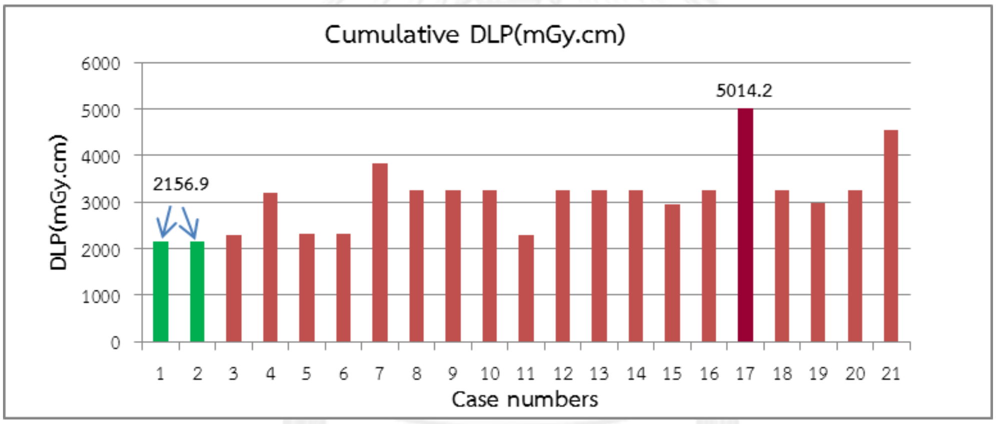

Figure 4.11 The dose-length product (DLP) considered in terms of cumulative dose.

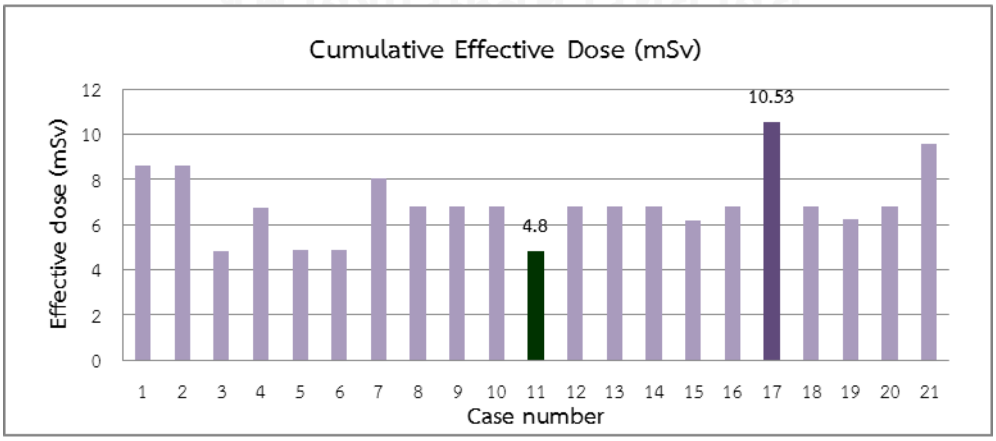

Figure 4.12 The effective dose considered in terms of cumulative dose.

Table 4.16 The mean $CTDI_{vol}$, DLP and effective dose considered in terms of ***average dose***

Case No/ Age (year)/ Gender (M/F)	$CTDI_{vol}$ (mGy) (*Average*)	DLP(mGy.cm) (*Average*)	Effective Dose (mSv) (*Average*)
1/6/F	30.80	431.40	1.73
2/7/F	26.97	431.38	1.73
3/20/M	28.59	457.32	0.96
4/21/F	28.59	457.32	0.96
5/21/F	40.00	638.60	1.34
6/22/F	29.13	465.90	0.98
7/39/M	40.00	638.32	1.34
8/42/F	40.54	648.70	1.36
9/42/M	40.54	648.72	1.36
10/44/M	40.54	648.72	1.36
11/49/M	28.59	457.32	0.96
12/49/F	40.54	648.70	1.36
13/51/M	40.54	648.70	1.36
14/51/M	40.54	648.70	1.36
15/64/F	46.03	735.90	1.55
16/66/M	62.68	1002.80	2.11
17/66/M	62.68	1002.80	2.11
18/70/F	40.54	648.70	1.36
19/73/M	37.08	593.20	1.25
20/73/M	40.54	648.72	1.36
21/77/F	47.57	759.47	1.59

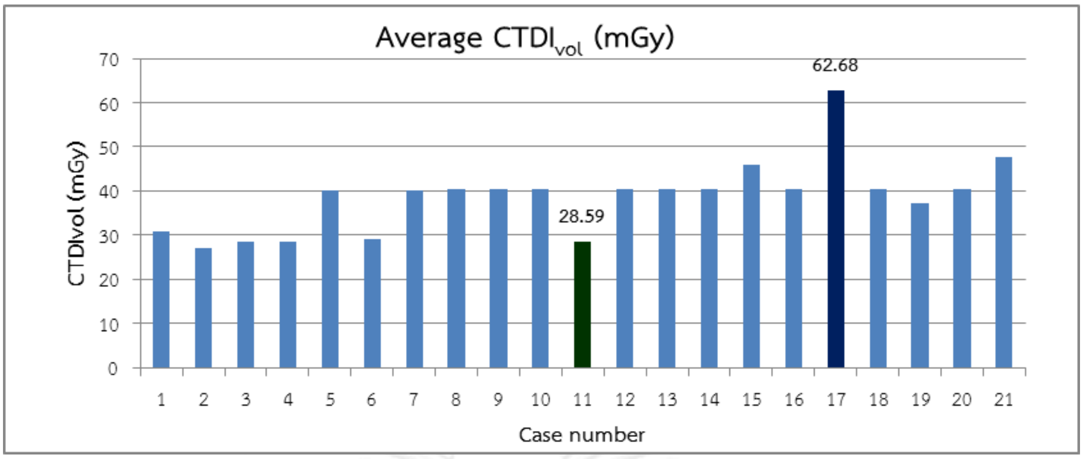

Figure 4.13 The CTDI$_{vol}$ considered in terms of average dose.

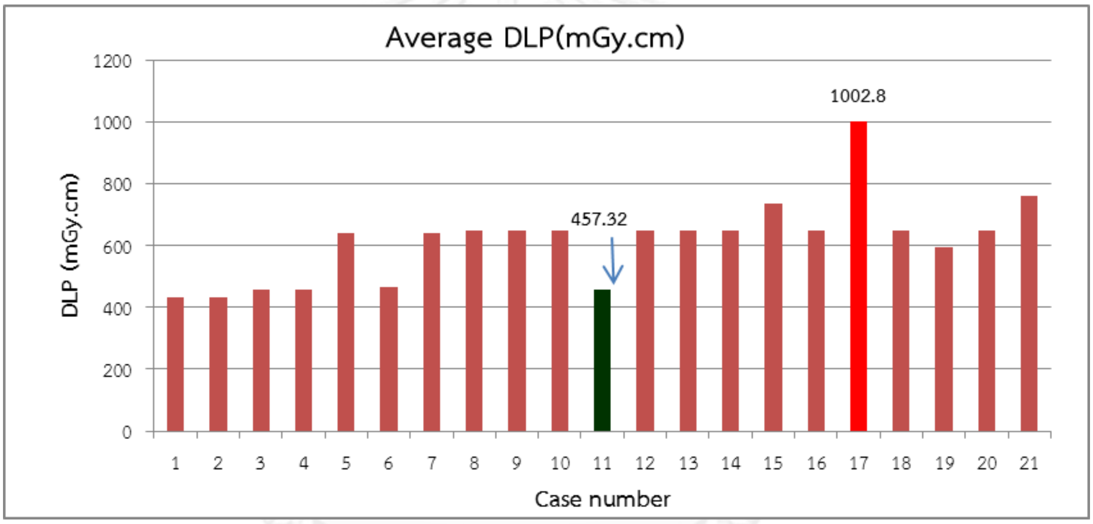

Figure 4.14 The dose-length product (DLP) considered in terms of average dose.

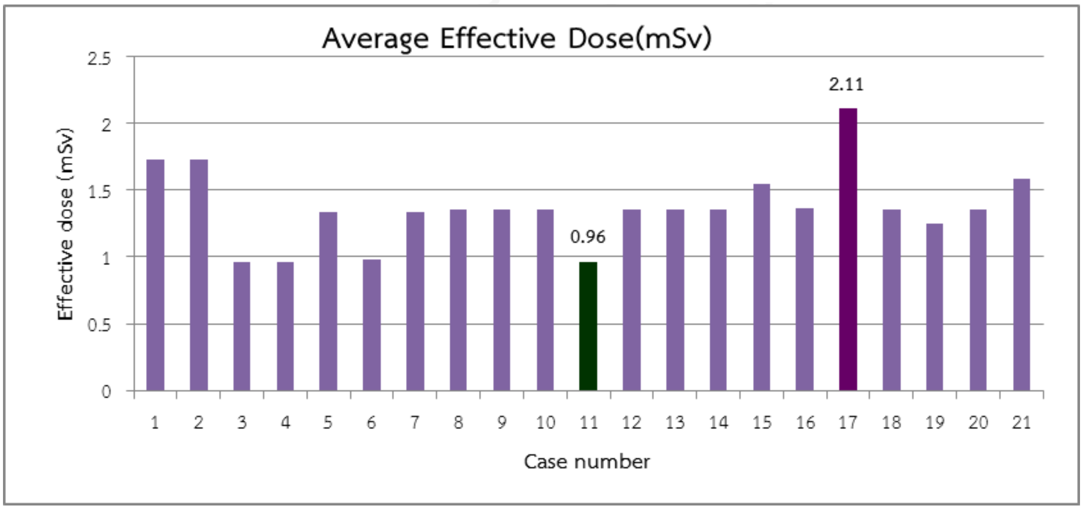

Figure 4.15 The effective dose considered in terms of average dose.

Table 4.17 The mean $CTDI_{vol}$, DLP and effective dose considered in terms of average dose per volume scan.

Case No/ Age (year)/ Gender (M/F)	$CTDI_{vol}$ (mGy) (*Average dose per volume*)	DLP(mGy.cm) (*Average dose per volume*)	Effective Dose (mSv) (*Average dose per volume*)
1/6/F	8.11	113.53	0.45
2/7/F	7.10	113.52	0.45
3/20/M	7.52	120.35	0.25
4/21/F	7.67	122.62	0.26
5/21/F	10.53	168.05	0.35
6/22/F	7.67	122.62	0.26
7/39/M	10.00	159.58	0.34
8/42/F	10.67	170.72	0.36
9/42/M	10.67	170.72	0.36
10/44/M	10.67	170.72	0.36
11/49/M	7.52	120.35	0.25
12/49/F	10.67	170.72	0.36
13/51/M	10.67	170.72	0.36
14/51/M	10.67	170.72	0.36
15/64/F	18.41	294.36	0.62
16/66/M	10.67	170.72	0.36
17/66/M	16.50	263.91	0.55
18/70/F	10.67	170.72	0.36
19/73/M	9.76	156.10	0.33
20/73/M	10.67	170.72	0.36
21/77/F	11.89	189.87	0.40

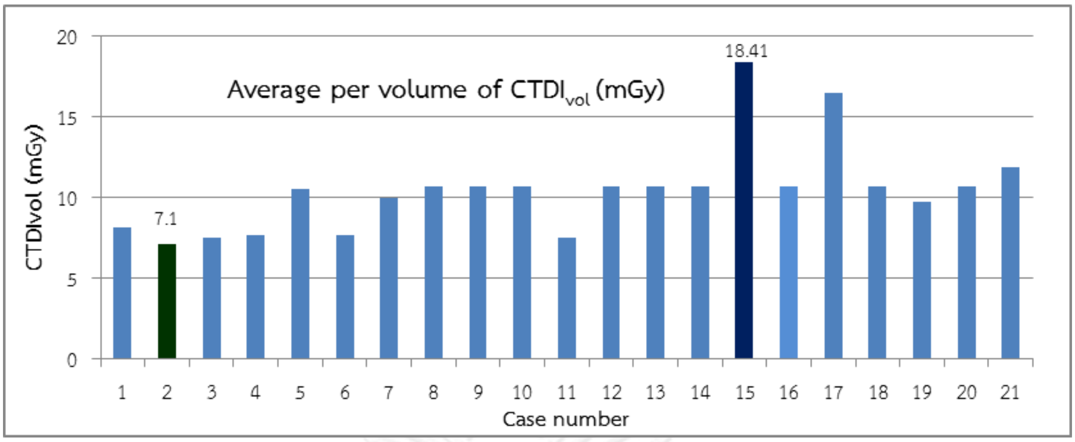

Figure 4.16 The $CTDI_{vol}$ considered in terms of average dose per volume scan.

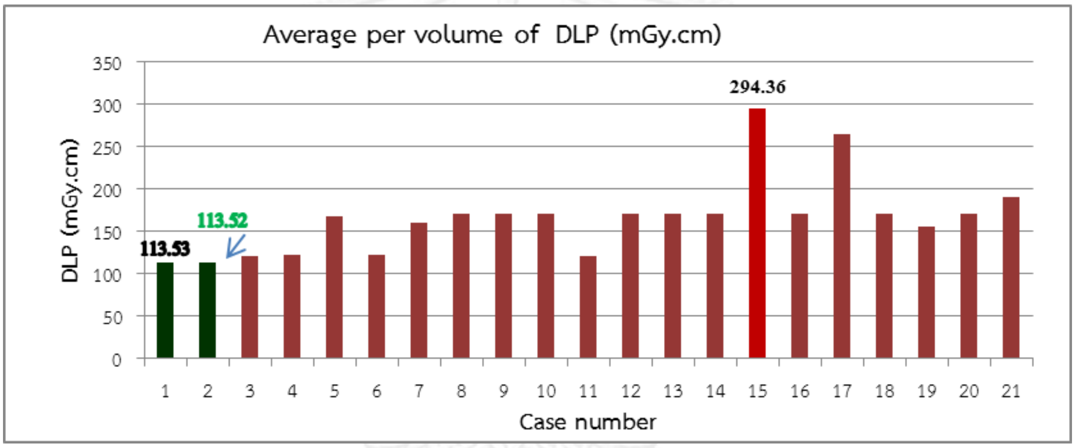

Figure 4.17 The dose-length product (DLP) considered in terms of average dose per volume scan.

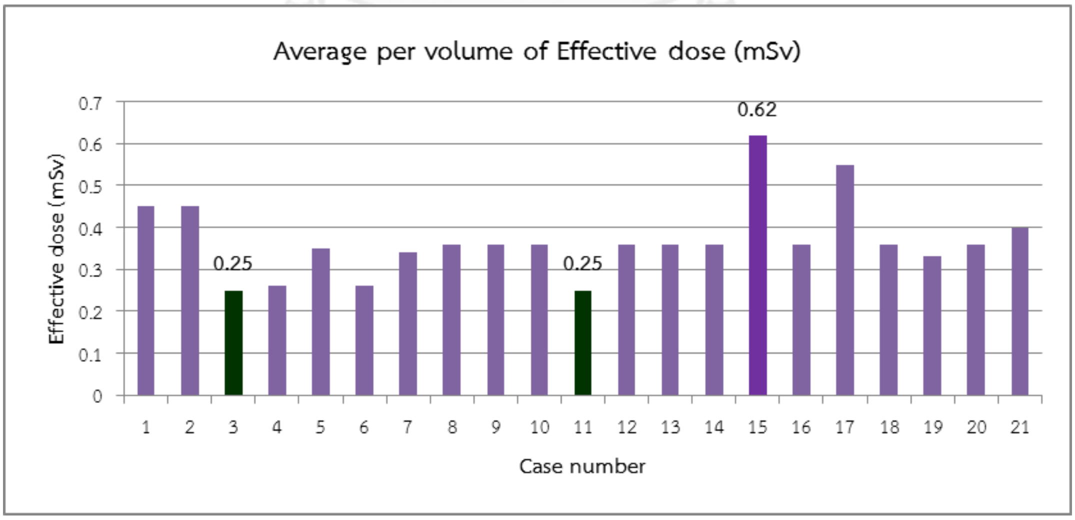

Figure 4.18 The effective dose considered in terms of average dose per volume scan.

The conclusion of $CTDI_{vol}$, DLP and effective dose using axial volume mode are shown in table 4.18

Table 4.18 The conclusion of $CTDI_{vol}$, DLP and effective dose using axial volume mode.

Radiation dose	$CTDI_{vol}$ (mGy)		DLP (mGy.cm)		Effective Dose (mSv)	
	Mean	Range	Mean	Range	Mean	Range
Cumulative dose	200.5	142.9-313.4	3206.8	2286.6-5014.2	6.7	4.8-10.5
Average dose	40.8	28.6-62.7	652.6	457.3-1002.8	1.4	1.0-2.1
Average dose per volume scan	10.7	7.5-18.4	171.3	120.4-294.4	0.4	0.3-0.6

Table 4.19 The summary of $CTDI_{vol}$, DLP and effective dose using axial volume mode in terms of cumulative dose, average dose and average dose per volume scan consecutively.

Case No/ Age(y)/ Gender (M/F)	$CTDI_{vol}$ (mGy)			DLP(mGy.cm)			Effective Dose (mSv)		
	Cumulative dose	Average dose	Average dose per volume	Cumulative dose	Average dose	Average dose per volume	Cumulative dose	Average dose	Average dose per volume
1/6/F	154.02	30.80	8.11	2157.0	431.40	113.53	8.63	1.73	0.45
2/7/F	134.84	26.97	7.10	2156.9	431.38	113.52	8.63	1.73	0.45
3/20/M	142.94	28.59	7.52	2286.6	457.32	120.35	4.82	0.96	0.25
4/21/F	200.00	28.59	7.67	3192.9	457.32	122.62	6.71	0.96	0.26
5/21/F	145.64	40.00	10.53	2329.7	638.6	168.05	4.89	1.34	0.35
6/22/F	145.64	29.13	7.67	2329.7	465.90	122.62	4.89	0.98	0.26
7/39/M	240.00	40.00	10.00	3829.9	638.32	159.58	8.04	1.34	0.34
8/42/F	202.72	40.54	10.67	3243.6	648.70	170.72	6.81	1.36	0.36
9/42/M	202.72	40.54	10.67	3243.6	648.72	170.72	6.81	1.36	0.36
10/44M	202.72	40.54	10.67	3243.6	648.72	170.72	6.81	1.36	0.36
11/49M	142.94	28.59	7.52	2286.6	457.32	120.35	4.80	0.96	0.25
12/49/F	202.72	40.54	10.67	3243.6	648.70	170.72	6.81	1.36	0.36
13/51M	202.72	40.54	10.67	3243.6	648.70	170.72	6.81	1.36	0.36
14/51M	202.72	40.54	10.67	3243.6	648.70	170.72	6.81	1.36	0.36
15/64/F	184.10	46.03	18.41	2943.6	735.90	294.36	6.18	1.55	0.62
16/66M	202.72	62.68	10.67	3243.6	1002.8	170.72	6.81	2.11	0.36
17/66M	313.42	62.68	16.50	5014.2	1002.8	263.91	10.53	2.11	0.55
18/70/F	202.72	40.54	10.67	3243.6	648.70	170.72	6.81	1.36	0.36
19/73M	185.40	37.08	9.76	2965.9	593.20	156.10	6.23	1.25	0.33
20/73M	202.72	40.54	10.67	3243.6	648.72	170.72	6.81	1.36	0.36
21/77/F	285.40	47.57	11.89	4557.0	759.47	189.87	9.57	1.59	0.40

CHAPTER V
Discussion and Conclusion

5.1 Discussion

5.1.1 Quality Control

The quality control of MDCT scanner is an important procedure to perform before research data collection, following IAEA Human Health Series No.19 and Technical Report Series (TRS) no.457. It includes the test of electromechanical component, image quality and radiation dose. The test results are verified whether they fall within the acceptable limit or not. The difference between the measurement and the displayed values came from the measurement uncertainty. [35] The factors affecting the measurement uncertainty to estimate the CT Dose Index were the characteristics of ionization chamber and electrometer, the measurement scenario, the precision of reading, tube loading, chamber positioning, the phantom construction, the chamber response in phantoms and the inaccuracy on laser beam alignment.

The $C_{a,100}$ measured in air, integrated over 100 mm pencil ion chamber was measured using head and body protocols in all kV_p setting and for each slice collimation. The $C_{a,100}$ in air value decreases when slice collimation increases but increases when kV_p increases from 80 kV_p to 135 kV_p in head protocol. Similarly results were obtained for the $C_{a,100}$ in air values in body protocol.

The $CTDI_{vol}$ are determined by using a 100 mm pencil ion chamber with a cylindrical PMMA head and body dosimetry phantom. The calculated $CTDI_{vol}$ was higher than the displayed $CTDI_{vol}$ values in all kV_p setting for head protocol, the percentage differences of calculated $CTDI_{vol}$ values ranged from 2.2 to 4.9. The calculated $CTDI_{vol}$ for body protocol were lower than the displayed $CTDI_{vol}$ values in all kVp setting, the percentage differences of calculated $CTDI_{vol}$ values ranged from -1 to -5.3.

The comparison of $CTDI_{vol}$ among calculated, displayed on monitor and IEC standard are in the range of tolerance at 120 kV_p both in PMMA head and body phantom. The percentage differences between calculated $CTDI_{vol}$ values versus displayed on monitor and IEC standard were; 6.3, -1.96 and -0.97, -12.91 in PMMA head and body phantom respectively. The $C_{a,100}$ measured in air for head protocols in axial volume mode decreases when slice collimation increases, but increases when kV_p increases. The calculated $CTDI_{vol}$ was higher than the displayed $CTDI_{vol}$ values ranging from 3.52, 0.62, -0.9 and -1.03 in 80-135 kV_p setting for head protocol.

5.1.2 The patient data and radiation dose

The twenty one patient data were 11 male and 10 female, age range, 6-77 years; mean age, 45.4 years.

5.1.3 Radiation dose

The effective dose of case number 1 and 2 are rapidly high even though the $CTDI_{vol}$ and DLP are low, because they are the pediatric patients, and the conversion factor (0.004 mSv/mGy.cm) is greater than twice of adult (0.0021 mSv/mGy.cm). As the small numbers of pediatric patient data of 2 cases, so they were separated. Only adult patient (case number 3 to 21) were analyzed and compared with radiation dose reference values.

In terms of cumulative radiation dose, $CTDI_{vol}$ and DLP are in range of 142.9-313.4 mGy and 2,286.6-5,014.2 mGy.cm; the maximum effective dose was 10.5 mSv for 19 scans performed with 80 kV_p, 4,271 total mAs and 0.75 second per rotation, each volume consists of 320 detector rows of 0.5 mm thickness nominal beam width covering a total of 16 cm of the head in the z-direction (case number 17), and the minimum effective dose was 4.80 mSv for 19 scans performed with 1,987 total mAs, the same kV_p, rotation time, nominal beam width and coverage area parameters (case number11).

In terms of cumulative dose, average dose, and average dose per volume scan, the mean values of $CTDI_{vol}$, DLP and effective dose using axial volume mode were, respectively; 200.5, 40.8 and 10.7 mGy; 3,206.8, 652.6 and 171.3 mGy.cm; 6.7, 1.4 and 0.4 mSv consecutively.

In this study, the radiation dose for comprehensive stroke imaging using axial volume mode combining CTA, CTV of the intracranial vessels and CTP in the same procedure (called the combo protocol) on the 320-detector row CT scanner with a 16-cm scanning length and covering the entire the brain was performed without gantry angulation, unenhanced CT of the brain and helical scan of neck CTA was excluded.

5.1.3.1 Compare the radiation dose among this study (axial volume mode, combo protocol) and references dose data in Computed Tomography perfusion of the brain

Table 5.1 The mean value of $CTDI_{vol}$, DLP and effective dose in this study (axial volume mode, combo protocol) and published data in CT perfusion of the brain.

CT Perfusion study	Number of detector row/ coverage in z- direction	$CTDI_{vol}$ (mGy)	DLP (mGy.cm)	Effective Dose (mSv)
This study	Aquilion ONE /16 cm	**200.5**	**3206.8**	**6.7**
Diekmann S, et al. [22]	Aquilion ONE/16 cm	n/a	n/a	3.6
	Toshiba 64/3.2 cm	n/a	n/a	5.8
Siebert E, et al. [23]	Aquilion ONE/16 cm	n/a	2355.4	5.4
Shankar JJ, et al. [20]	Aquilion ONE/16 cm	n/a	1000	n/a
Murayama K, et al. [26]	Toshiba 256/12.8cm	n/a	n/a	3.5
Arandjic D, et al. [25]	GE VCT 64/4 cm	590	2360	5.4
	GE HD 750/4 cm	680	2740	6.3
	GE HD 750/8 cm	230	2120	4.9
Mnyusiwalla A, et al. [27]	GE VCT 64/4cm	n/a	n/a	4.9
Cohnen M, et al. [24]	Siemens 64/3.84 cm	n/a	n/a	5.0

The mean $CTDI_{vol}$ in the combo protocol for whole-brain perfusion with the 320-detector row CT scanner in this study is the lowest, but the mean DLP and effective dose are the highest. The dose discrepancies are due to the larger z-coverage of the 320-detector row CT (16 cm in this protocol) compared with 64, 256 -detector row CT (3.2 cm-12.8 cm).

At the same 16 cm scan length, the DLP of 3,206.8 mGy.cm in this study was approximately threefold of Shankar et al. (1,000 mGy.cm). As the result, the increasing sampling interval, the radiation dose can be reduced, the lower mA results in decreasing the radiation dose.

The mean effective dose resulted at 6.7 mSv was twice greater than the same modality (Aquilion ONE) because in this study the total scan time was 60 seconds and tube current varying, in contrast, scan time 29.8 seconds and mA 100 were used in Diekmann et al. whereas the tube voltage, 80 kV_p, beam width (collimation) 320x0.5mm and area of coverage 16 cm were the same. Similarly, the effective dose in 4D CTA-CTP combined protocol was 5.4 mSv, due to the constant 100 mA, the rotation time between 0.5 and 1 second were used in Siebert et al, contribute to the lower effective dose slightly lower than our study.

The figures 5.1, 5.2 and 5.3 show the comparison of the mean $CTDI_{vol}$, DLP and effective dose among this study (axial volume mode, combo protocol) and other references in CT perfusion of the brain.

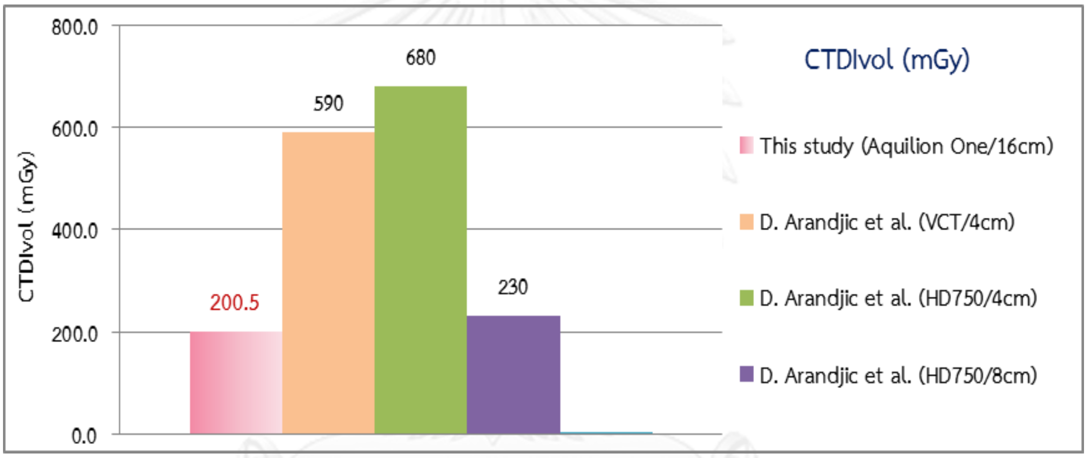

Figure 5.1 The comparison of the mean value $CTDI_{vol}$ among this study (axial volume mode, combo protocol) and other references in CT perfusion of the brain.

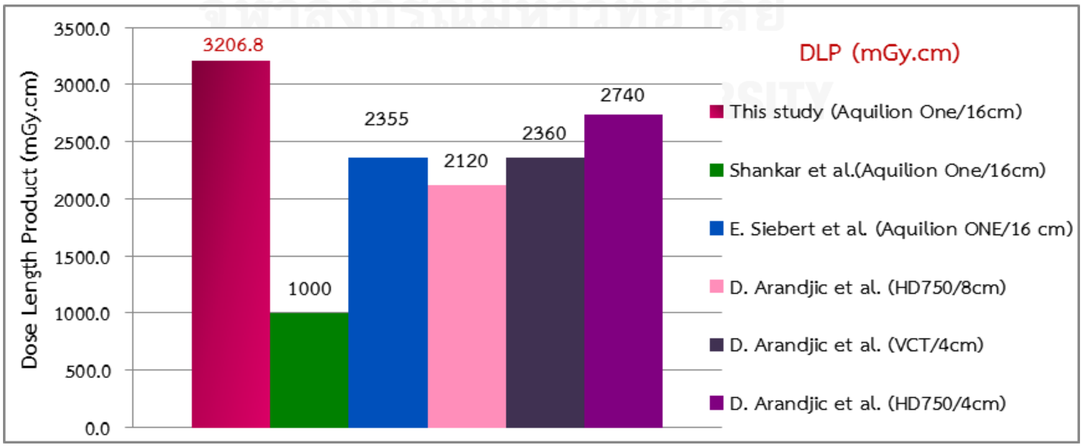

Figure 5.2 The comparison of the dose-length product among this study (axial volume mode, combo protocol) and other references in CT perfusion of the brain.

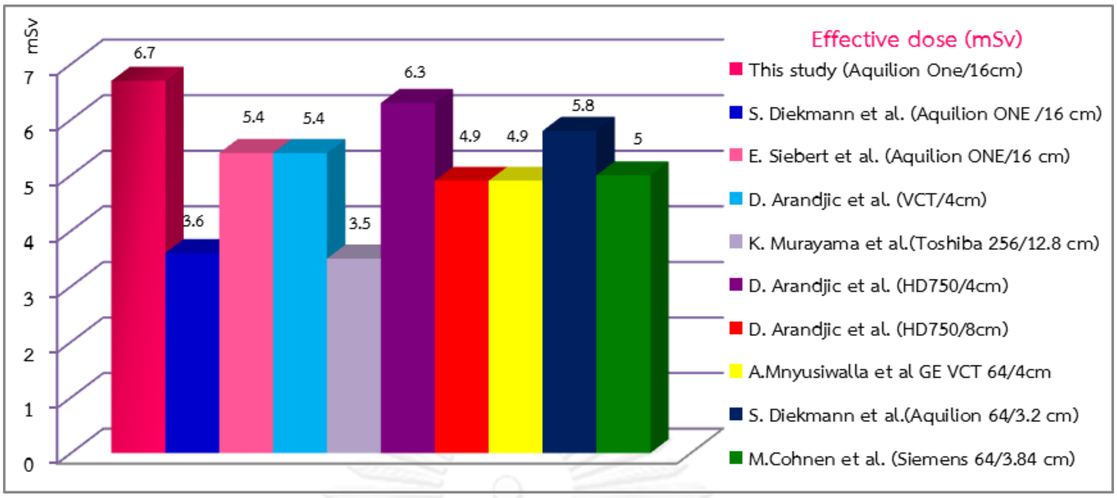

Figure 5.3 The comparison of the effective dose among this study (axial volume mode, combo protocol) and other references in CT perfusion of the brain.

5.1.3.2 The comparison of the mean value $CTDI_{vol}$, DLP and effective dose among this study (average dose per axial volume scan) and published data in CT head

Table 5.2 The mean $CTDI_{vol}$, DLP and effective dose from this study (average dose per axial volume scan) compared with the DRLs of published data in CT head.

Reference DRL	$CTDI_{vol}$ (mGy)	DLP (mGy.cm)	Effective Dose (mSv)
This study	10.7	171.3	0.4
King Chulalongkorn Memorial Hospital [31]	N/A	N/A	2.5
United Kingdom [UK] 2003 [37]	65-100	930	N/A
European Commission [EC] 2004 [38]	60	N/A	N/A
Australian [39]	60	1000	N/A
ICRP Publication 87 [40]	N/A	N/A	2
American College of Radiology [ACR] 2008 [41]	75	N/A	N/A
Germany 2003 [42]	60	1050	N/A
Switzerland 2004 [43]	60	800	N/A
Sweden 2002 [44]	75	1200	N/A
Taiwan 2007 [45]	72	850	N/A

All of the mean $CTDI_{vol}$, DLP and effective dose in average dose per axial volume scan in this study are the lowest because of the tube voltage 80 kV_p was used, whereas tube voltage 120 kV_p usually performed in routine head CT examinations.

Axial volume scan could offer substantial dose reduction with no loss of diagnostic information, especially the use of lower kV_p and may be compromised by increasing tube current for improve the acceptable image quality.

5.2 Conclusion

The radiation dose in whole brain Computed Tomography in comprehensive stroke imaging using axial 320-row MDCT volumetric mode is higher than reference data in terms of mean DLP and effective dose due to the large z-coverage, high tube current and several number of total volume scan.

Although the higher radiation dose is one of the main concerns, but the notably advantage of whole brain Computed Tomography in comprehensive stroke imaging using axial 320-row MDCT volumetric mode can eliminate the limitation of brain coverage. Even though the high cumulative $CTDI_{vol}$ in this study (142.9-313.4 mGy), but they are less than the FDA recommendation for maximum dose of 500 mGy. [46]

Furthermore, CTA, CTV and CTP information can be obtained from the same procedure, reduce volume of contrast media, decrease the acquisition time compared with standard routine (CTA, CTV and CTP) alone. Besides, the first volume of scan can be used as the non-contrast enhancement head CT, similarly to the last volume scan can be used as the contrast enhancement head CT. The image quality can be improved by increase the tube current.

5.3 Recommendations

According to the hypothesis, the radiation dose in whole brain Computed Tomography in comprehensive stroke imaging can be reduced by the use of axial volume mode.

The patient dose reduction should be considered by means of;

1) Reduce the scan coverage of less than 16 cm according to the clinical consideration.
2) Reduce tube current (mA) per volume, especially in mask and CTA volume.
3) Reduce total exposure time by increasing time interval.
4) Reduce number of total volume scan, such as decrease one of the last volume.

Although the optimization of CT Perfusion protocol is excluded for this study, these recommendations should be applied for high value in comprehensive stroke imaging in the future. Otherwise, the qualitative image quality by means of radiologist blinding score should be performed.

REFERENCES

[1] International Atomic Energy Agency. Optimization in clinical practice. IAEA/RCA Regional training Course on Medical Physics in Diagnostic Radiology (2008).

[2] Rehani, M. M. Radiation Protection in newer imaging technologies. Radiat Prot Dosimetry 139(2010):357-62.

[3] European Commission. Guidance on Diagnostic Reference Level (DRLs). Radiation Protection 109(1999).

[4] Schaller, S., Flohr, T. Computed Tomography, Present and Future. In: Reiser M., (ed.). Multislice CT: A practical guid, pp. 4-17. Geramany: Springer, 2004.

[5] Mahesh, M. Search for isotropic resolution in CT from conventional through multiple-row detector. Radiographics : a review publication of the Radiological Society of North America, Inc 22(2002):949-62.

[6] Seeram, E. Computed Tomography: Physical Principles, Clinical Applications, and Quality Control. 2nd ed. Philadelphia, USA: W.B. Suanders, 2001.

[7] The ImPACT Group. Multi-slice CT scanners CEP 08007: Centre for Evidence-based Purchasing (2009).

[8] Reddinger, W. L. CT Instrumentation & Physics. 1997.

[9] Products/ Low Dose/ Low Dose Solution of CT/ Hardware [Internet]. [cited December, 2012]. Available from: http://www.toshibamedical.co.jp/tmd/english/products/dose/lowdose/hardware.html.

[10] Jerrold T, B., J. Anthony Seibert., Edwin M. Leidholdt, Jr., and John M, Boone. Computed Tomography. In: Charles W M., (ed.). The Essential Physics of Medical Imaging, pp. 312-70. Philadephia, USA: Lippincott Williams & Wilkins, 2012.

[11] Brunnett, C. CT design considerations and specifications. Cleveland, Ohio: Picker international, 1990.

[12] Angel, E. AIDR 3D Iterative reconstruction. Toshiba Medical System (2012).

[13] International Commission on Radiological Protection. Managing Patient Dose in Multi-Detector Computed Tomography (MDCT) ICRP Publication 102(2007).

[14] Dixon, R. L., Boone, J. The CTDI Paradigm: A Practical Explanation for Medical Physicists. American College of Radiology (2010.).

[15] American College of Radiology. ACR–SPR Practice Guideline for the performance of Computed Tomography (CT) Perfusion in neurologic imaging. ACR (2012).

[16] Latchaw, R. E., Alberts M. J., Lev M. H., Connors J. J., Harbaugh R. E., Higashida R. T., et al. Recommendations for imaging of acute ischemic stroke: a scientific

statement from the American Heart Association. Stroke; a journal of cerebral circulation 40(2009):3646-78.

[17] Wintermark, M., Albers G. W., Alexandrov A. V., Alger J. R., Bammer R., Baron J. C., et al. Acute stroke imaging research roadmap. AJNR American journal of neuroradiology 29(2008):23-30.

[18] American Ascociation of Physicist in Medicine. Adult Brain Perfusion CT Protocols. AAPM (2012).

[19] Vital Images Inc. CT Brain Perfusion User Guide VPMC-9283A Vitrea® version 4.1. 2008.

[20] Shankar, J. J., Lum C., Sharma M. Whole-brain perfusion imaging with 320-MDCT scanner: Reducing radiation dose by increasing sampling interval. AJR American journal of roentgenology 195(2010):1183-6.

[21] Salomon, E. J., Barfett J., Willems P. W., Geibprasert S., Bacigaluppi S., Krings T. Dynamic CT angiography and CT perfusion employing a 320-detector row CT: protocol and current clinical applications. Klinische Neuroradiologie 19(2009):187-96.

[22] Diekmann, S., Siebert E., Juran R., Roll M., Deeg W., Bauknecht H.-C., et al. Dose exposure of patients undergoing comprehensive stroke imaging by multidetector-row CT: comparison of 320-detector row and 64-detector row CT scanners. AJNR American journal of neuroradiology 31(2010):1003-9.

[23] Siebert, E., Bohner, G.,Dewey, M., et al. 320-slice CT neuroimaging: initial clinical experience and image quality evaluation. The British journal of radiology 82(2009):561-70.

[24] Cohnen, M., Wittsack H. J., Assadi S., Muskalla K., Ringelstein A., Poll L. W., et al. Radiation exposure of patients in comprehensive computed tomography of the head in acute stroke. AJNR American journal of neuroradiology 27(2006):1741-5.

[25] Arandjic, D., Bonutti F., Biasizzo E., Ciraj-Bjelac O., Floreani M., Giustizieri M., et al. Radiation doses in cerebral perfusion computed tomography: patient and phantom study. Radiat Prot Dosimetry 154(2013):459-64.

[26] Murayama, K., Katada K., Nakane M., Toyama H., Anno H., Hayakawa M., et al. Whole-brain perfusion CT performed with a prototype 256-detector row CT system: initial experience. Radiology 250(2009):202-11.

[27] Mnyusiwalla, A. A., R. I. Symons, S. P. Radiation dose from multidetector row CT imaging for acute stroke. Neuroradiology 51(2009):635-40.

[28] Kroft, L. J. M., Roelofs, J.J.H.,Geleijns, J. Scan time and patient dose for thoracic imaging in neonates and small children using axial volumetric 320-detector

row CT compared to helical 64-, 32-, and 16- detector row CT acquisitions. Pediatr Radiol 40(2010):294–300.

[29] Mahesh, M. Advances in CT technology and application to pediatric imaging. Pediatric radiology 41(2011):493-7.

[30] Trinavarat, P., Kritsaneepaiboon, S.,Rongviriyapanich, C.,Visrutaratna, P.,Srinakarin, J. Radiation dose from CT scanning: can it be reduced. Asian Biomedicine 5(2011):13-21.

[31] Kritsaneepaiboon, S., Trinavarat P., Visrutaratna P. Survey of pediatric MDCT radiation dose from university hospitals in Thailand: a preliminary for national dose survey. Acta radiologica (Stockholm, Sweden : 1987) 53(2012):820-6.

[32] The ImPACT Group. Comparative specifications 128-320 slice CT scanners CEP 08028: The Centre for Evidence-based Purchasing; (2009).

[33] Shrimpton, P. C., Hillier M. C., Lewis M. A., Dunn M. National survey of doses from CT in the UK: 2003. The British journal of radiology 79(2006):968-80.

[34] International Atomic Energy Agency. Quality assurance programme for Computed Tomography: Diagnostic and therapy application. 2012. Available from: http://www.iaea.org/books.

[35] International Atomic Energy Agency. Dosimetry in diagnostic radiology : an international code of practice .Technical reports series No.457. Vienna, Austria2007.

[36] Geleijns, J., et al. Computed tomography dose assessment for a 160 mm wide, 320 detector row, cone beam CT scanner. Phys Med Biol 54(2009):3141–59.

[37] Shrimpton, P. “Assessment of Patient Dose in CT” in Bongart G.Z., Golding S.J., Jurik A.G., et al. European Guidelines for Multislice Computed Tomography (2004).

[38] Bongartz, G., Golding, S.J., Jurik, A.G., et al. European Guidelines for Multislice Computed Tomography,” Funded by the European Commission. (2004).

[39] Australian National Adult Diagnostic Reference Levels for MDCT. [Internet]. National Diagnostic Reference Level Survey. [cited October, 2012.]. Available from: http://www.arpansa.gov.au/services/ndrl/adult.cfm.

[40] International Commission on Radiological Protection. Managing Patient Dose in Computed Tomography (ICRP Publication 87): Ann. ICRP 2000.

[41] Cynthia H., M. Diagnostic Reference Levels. American College of Radiology (2010).

[42] Brix, G. Notice of Diagnostic Reference Values for Radiology and Nuclear Medicine Studies. Federal Office for Radiation Protection, Germany (2003).

[43] Aroua A., B. A., Buchillier-Decka I., et al. "Adult Reference Levels in Diagnostic and Interventional Radiology for Temporary Use in Switzerland," . Radiation Protection Dosimetry (2004).

[44] Authority, S. R. P. Regulations and General Advice on Diagnostic Standard Doses and Reference Levels Within Medical X-ray Diagnostics. Swedish Radiation Protection Authority (2002).

[45] Tsai, H. Y., Tung ,C.J., Yu, C.C., Tyan, Y.S. "Survey of Computed Tomography Scanners in Taiwan: Dose Descriptors, Dose Guidance Levels, and Effective Doses," Medical Physics (2007).

[46] Wintermark, M., Lev, M.H. FDA investigates the safety of brain perfusion CT. AJNR American journal of neuroradiology 31(2010).

APPENDICES

APPENDIX A: Case Record Form

Table A 1 Case record form.

Case number: Patient data: Age......years

Date of examination: Gender ☐ Male

☐ Female

Phase of scan	Number of volume scan	Delay time after start scan (s)	Scan mode type	Exposure parameters					Beam width (mm)	Scan length (mm)	Radiation dose		
				kV_p	mA	mAs	Rotation time(s)	Scan time(s)			$CTDI_{vol}$ (mGy)	DLP (mGy.cm)	Effective Dose (mSv)
1 (Mask)		7	Volume	80			0.75		0.5x320	160			
2		3.2	Volume	80			0.75		0.5x320	160			
3		1.8	Volume	80			0.75		0.5x320	160			
4		1.8	Volume	80			0.75		0.5x320	160			
5		3.2	Volume	80			0.75		0.5x320	160			

APPENDIX B: Quality Control of Multidetector Computed Tomography system

1. Scan Localization Light Accuracy

Purpose: To test congruency of scan localization light and scan plane.

Method:

1. Tape localization film to the backing plate making sure that the edges of the film are parallel to the plate edges.
2. Place the film vertically along the midline of the couch aligned with its longitudinal axis. Raise the table to the head position.
3. Make both internal and external light with unique pin pricks along the midline of the light.
4. Expose the internal light localization using the narrowest slice setting at 120-135 kV_p, 50-100 mAs.
5. For external light, increment table to light position under software control and expose the film.

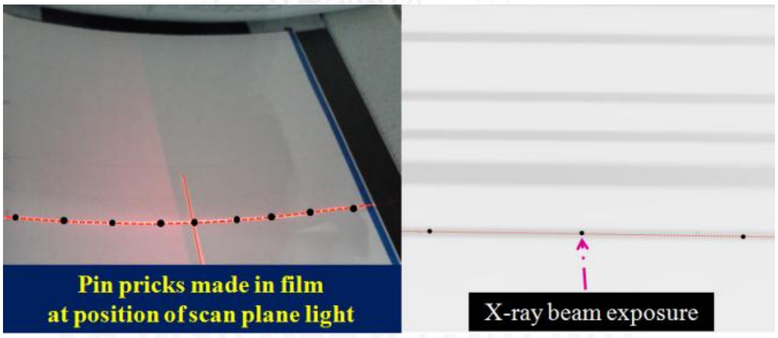

Figure B 1 Pin pricks on localization film.

Results: Measured deviation of beam exposure and laser beam

- External 0 mm.
- Internal 0 mm.

Tolerance: The center of the radiation field from the pin pricks should be less than 2 mm.

Comment: ☑ Pass

2. **Alignment of table to gantry**

Purpose: To ensure that long axis of the table is horizontally aligned with a vertical line passing through the rotational axis of the scanner.

Method:

1. Locate the table midline using a ruler and mark it on a tape affixed to the table.
2. The horizontal deviation between the gantry aperture center and the table midline.

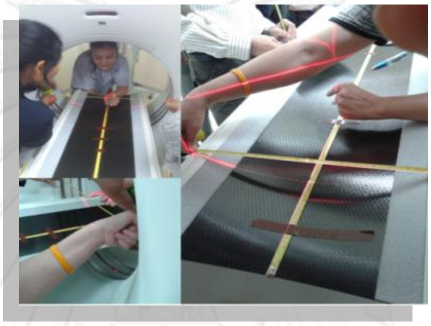

Figure B 2 The gantry bore and couch/table measurement.

Result:

Table B 1 Alignment of table and bore

	Table	Bore
Distance from Right to Centre (mm)	236	358
Distance from Centre to Left (mm)	236	360
Measured Deviation (mm)	0	1

**Measured deviation = (Distance from right to center – Distance from center to Left)/2*

Tolerance: The deviation should be within 5 mm.

Comment: ☑ Pass

This test was not exceed tolerance but the error can occur from the measurement.

3. Table increment accuracy

Purpose: To determine the accuracy and reproducibility of table in longitudinal motion.

Method:

1. Tape a measuring tape at the foot end of the table.

2. Place a paper clip at the center of the tape to function as an indicator.

3. Load the table uniformly with 150 lbs. From the initial position move the table 300, 400 and 500 mm into the gantry under software control (+ ve).

4. Record the relative displacement of the pointer on the ruler. Reverse the direction of motion (-ve) and repeat.

5. Repeat the measurements four times.

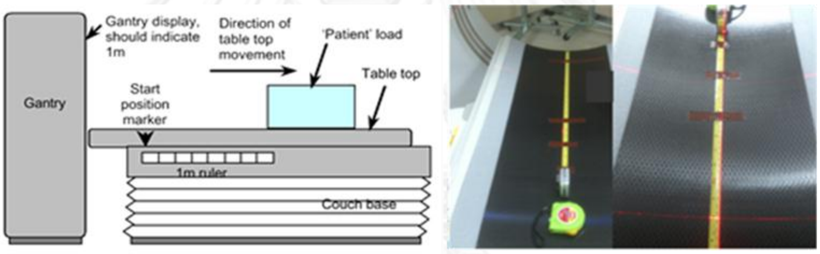

Figure B 3 Tape a measuring tape at the foot end of the table.

Result:

Table B 2 Table increment accuracy

Indicated (mm)	Measured (mm)	Deviation
300	300	0
400	400	0
500	500	0
-300	-300	0
-400	-400	0
-500	-500	0

**Deviation = | Indicated – Measured|*

Tolerance: Positional errors should be within ± 2mm. (NCRP No.99: Quality control test for CT scanner (Section 14)

Comment: ☑ Pass

4. Slice increment accuracy

Purpose: To determine the accuracy of the slice increment.

Method:

1. Set up as you would for beam profile measurement.
2. Select 120 kV_p, 100 mAs and smallest slit width.
3. Perform several scans with different programmed slice separations under auto control.
4. Scan the film (verification film) with a film scanner (OmniPro RT Scanner) and measure the distance between the peaks.

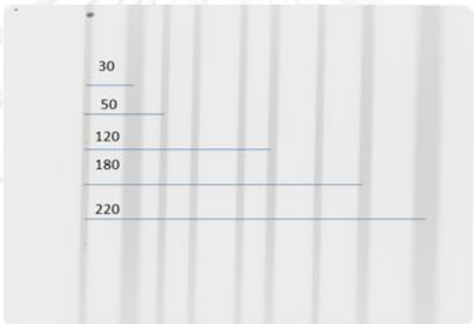

Figure B 4 Slice increment was set and measurement on verification film.

**Deviation = |Slice increment – Measured increment|*

Result:

Table B 3 The accuracy of slice separation

Slice increment in mm	Measured increment in mm	Deviation
20	20	0
30	30	0
50	50	0
120	120	0
180	180	0
220	220	0

Tolerance: The deviation should be within ± 0.5 mm for each measurement. (NCRP No.99: Quality control test for CT scanner, Section 14)

Comment: ☑ Pass

5. Gantry angle tilt

Purpose: To determine the limit of gantry tilt and the accuracy of tilt angle indicator.

Method:

1. Tape a localization film to the backing plate making sure that the edges of the film are parallel to the edges of the backing plate.

2. Place the film vertically along the midline of the couch aligned with its longitudinal axis. Raise the table to the head position. Move the table into the gantry.

3. Center plate to the laser alignment light.

4. Expose the film at inner light location using narrowest slit, 120-135 kV_p, 50-100 mAs.

5. Tilt the gantry to one extreme from the console.

6. Record the indicated gantry angle. Expose the film using the above technique.

7. Measure the clearance from the closest point of gantry to midline of the table.

8. Tilt the gantry to its extreme in the opposite direction.

9. Record clearance and repeat the exposure.

10. Measure the tilt angles from the images on the film.

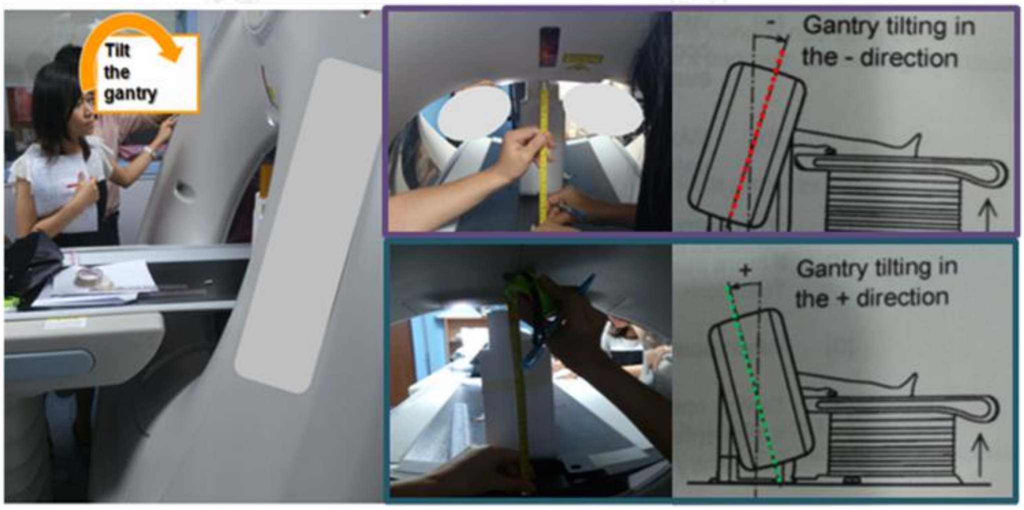

Figure B 5 Toward (+)/away(-) gantry tilted angle and measured the clearance.

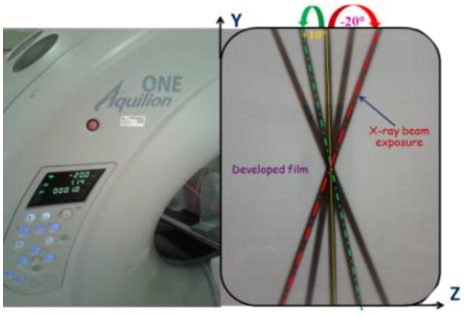

Figure B 6 Measure the tilt angles from the images on the film.

Result:

Table B 4 The accuracy of indicated and measured angle of gantry tilted.

	Away (-)			Towards (+)		
Indicated Angle	0	10	20	0	10	20
Measured Angle	0	10	20	0	10	20
Deviation	0	0	0	0	0	0
Clearance (cm)		33			33	

**Deviation = |Indicated angle – Measured angle|*

Tolerance:

- Deviation between indicated and measured tilt angles should be within ± 3 °
- Gantry clearance should be ≥ 30 cm

Comment: ☑ Pass

6. Reproducibility of C.T. numbers

Method:

1. Using the same set up and technique as position dependence, obtain three scans.
2. Using the same ROI as position dependence in location 5, which is the center of the phantom, obtain mean C.T. numbers for each of the four scans.

Figure B 7 The center position for measured the reproducibility of CT Number.

Result:

Table B 5 The reproducibility of CT Number.

Run Number	1	2	3	4
Mean C.T. (HU)	116.93	116.86	116.92	116.95

Mean global C.T. number	116.9200
Standard deviation	0.0335
Coefficient of variation	0.0003

Tolerance: The coefficient of variation of mean C.T. numbers of the four scans should be less than 0.002.

Comment: ☑ Pass (at slice thickness 3mm in routine head protocol)

7. mAs linearity

Method:

1. Set up the same as position dependence and insert 10 cm long pencil chamber in the center slot of the C.T. dose head phantom.

2. Select the same kV_p and time as used for head scan.

3. Obtain four scans in each of the mA stations normally use in the clinic.

4. For each mA station record the exposure in mGy for each scan.

5. Scans should be performed in the increasing order of mA.

6. Compute mGy/mAs for each mA setting.

Technique: 120 kV_p, 1.0 sec, varying mA, FOV 240 (S)

Result:

Table B 6 The linearity of mGy and mAs.

mA	Exposure in mGy				mGy/mAs	C.V.
	Run 1	Run 2	Run 3	Run 4		
50	1.348	1.361	1.361	1.359	0.03	-
100	2.728	2.713	2.713	2.714	0.03	-0.001
200	5.426	5.424	5.451	5.426	0.03	0
250	6.810	6.770	6.823	6.810	0.03	-0.001
300	8.850	8.853	8.908	8.905	0.03	-0.042
400	11.81	11.81	11.81	11.80	0.03	0.001
500	14.76	14.85	14.72	14.71	0.03	0
550	16.2	16.2	16.22	16.26	0.03	0.001

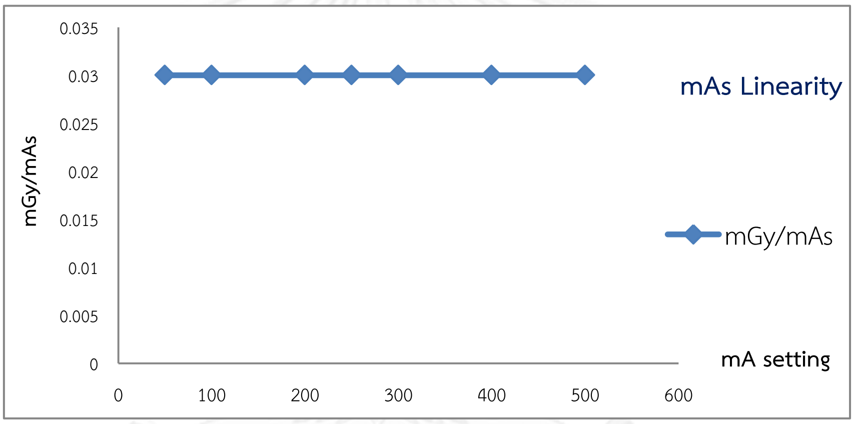

Figure B 8 The mAs linearity curve.

Comment: ☑ Pass

8. Linearity of C.T. numbers

Method:

1. Set up the Catphan phantom as described in beam alignment.
2. Select the section containing the test objects of different C.T. numbers (CTP404 sensitometry and pixel size module).

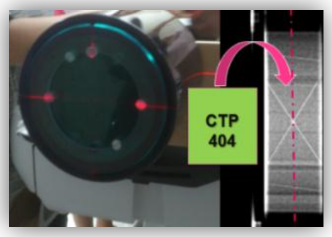

Figure B 9 Catphan phantom setting and reference line of CTP 404 section. (Slice width, sensitometry and pixel size module).

3. Select the head technique and perform a single transverse scan.
4. Select a region of interest (ROI) of sufficient size to cover the test objects.
5. Place the ROI in the middle of each test object and record the mean C.T. number.

Technique: 120 kV_p, 300 mA, 1.0 sec, 240mm FOV, 10mm slice thickness.

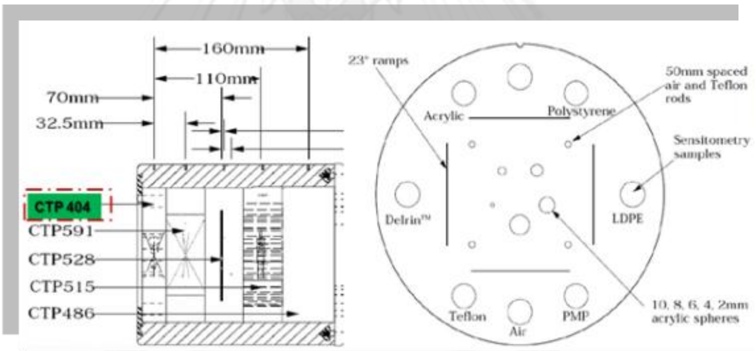

Figure B 10 The section containing the test objects of different CT numbers.

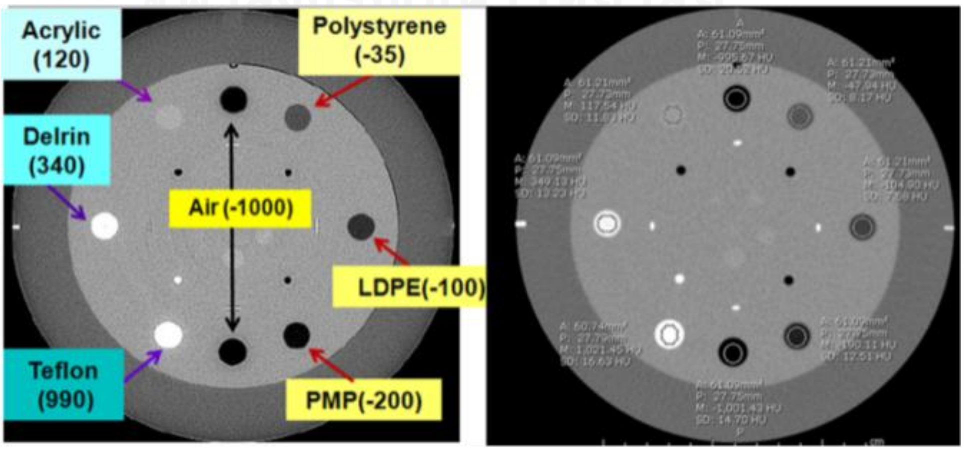

Figure B 11 Seven materials for CT number measurement.

Results:

Table B 7 Linear attenuation coefficient μ [unit cm^{-1}] at 40 KeV

Material	Expected CT Number	Measure CT Number	μ (cm^{-1})
Air (Upper)	-1000	-995.67	0
Air (Lower)	-1000	-1001.43	0
PMP	-200	-190.11	0.189
LDPE	-100	-104.9	0.209
Polystyrene	-35	-47.94	0.229
Water	0	0.1	0.24
Acrylic	120	117.54	0.277
Delrin™	340	349.13	0.327
Teflon	990	1021.45	0.556

Tolerance: R-square between measured CT number and linear attenuation coefficient (μ) more than 0.9

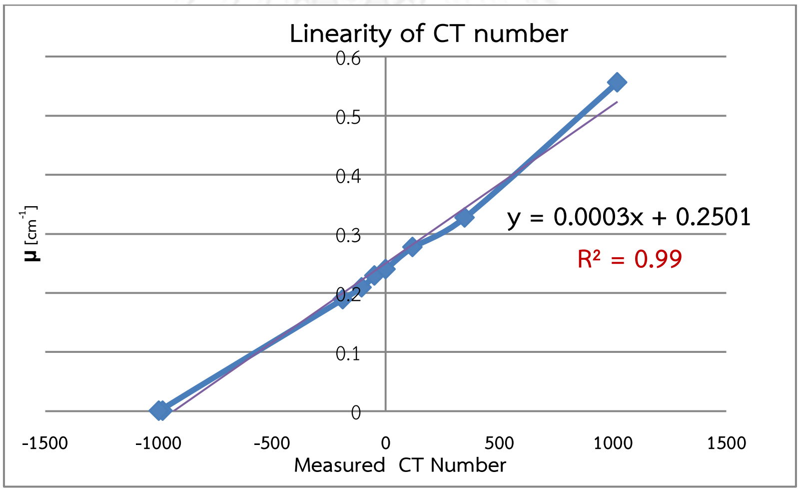

Figure B 12 Linearity of CT number.

Comment: ☑ Pass

9. High contrast resolution

Purpose:

To test resolution sections ranging from 1 to 21 lines pairs per cm. This radial design pattern eliminates the possibility of streaking artifacts from other test objects.

Method:

1. Set up the Catphan phantom as described in beam alignment.

2. Select the section containing the high contrast resolution test objects (CTP528, 21 line pair high resolution Module).

3. Select the head technique and perform a single transverse scan.

4. Select the area containing the high resolution test objects and zoom as necessary.

5. Select appropriate window and level for the best visualization of the test objects.

6. Record the smallest test object visualized on the monitor.

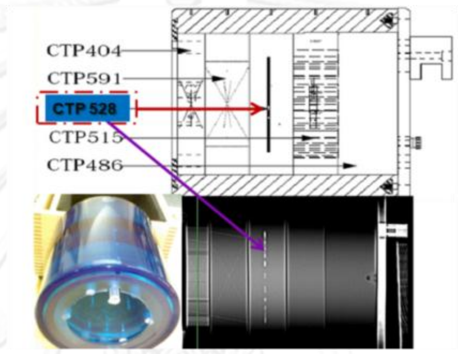

Figure B 13 Catphan phantom setting and reference line of CTP 528 section.

Technique: 120 kV_p, 300mAs, 1.0sec, 240mm FOV

Results:

Table B 8 High contrast resolution.

Slice Thickness in mm	Resolution (Line Pair/cm)	Gap size (cm)	Criteria	Conclude
1	7	0.071		Pass
2	7	0.071	≥ 5 lp/cm	Pass
5	7	0.071		Pass

Tolerance: Should be ≥ 5 lp/cm

Comment: ☑ Pass

Line Pair/cm	Gap Size
1	0.500 cm
2	0.250 cm
3	0.167 cm
4	0.125 cm
5	0.100 cm
6	0.083 cm
7	0.071 cm
8	0.063 cm
9	0.056 cm
10	0.050 cm

Line Pair/cm	Gap Size
11	0.045 cm
12	0.042 cm
13	0.038 cm
14	0.036 cm
15	0.033 cm
16	0.031 cm
17	0.029 cm
18	0.028 cm
19	0.026 cm
20	0.025 cm
21	0.024 cm

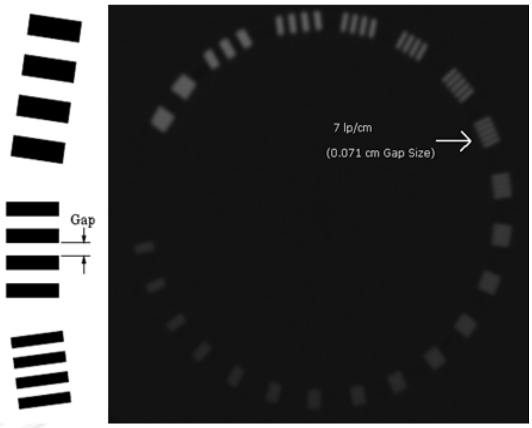

Figure B 14 The number of line pair per centimeter (1 to 21 line pairs per cm) visible from the high contrast resolution measurement.

10. Low contrast resolution

Purpose: To determine the actual target contrasts before testing specific contrast performance specification.

Method:

1. Set up the Catphan phantom as described in beam alignment.
2. Select the section containing the low resolution test objects (CTP515 Sub-slice and supra-slice low contrast module).
3. Select the head technique.
4. Perform a single transverse scan.
5. Select the area containing the high resolution test objects and zoom as necessary. Select appropriate window and level for the best visualization of the test objects.
6. Record the smallest test object visualized.

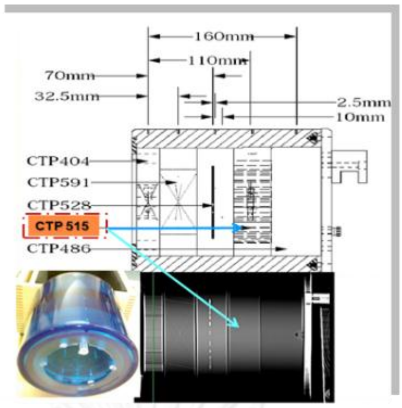

Figure B 15 Catphan phantom setting and reference line of CTP 515 section.

Technique: 120 kV_p, 250 mA, 2.0 sec, 240 mm(S) FOV, slice thickness 10mm.

Results:

Table B 9 Low contrast detectability.

Slice thickness in mm	Smallest target(spokes) diameter (mm) should been seen					
	Contrast level of supra - slice			Length of sub-slice 1.0 %		
	1.00%	0.50%	0.30%	7mm	5mm	3mm
10	9	7	7	3	2.5	1

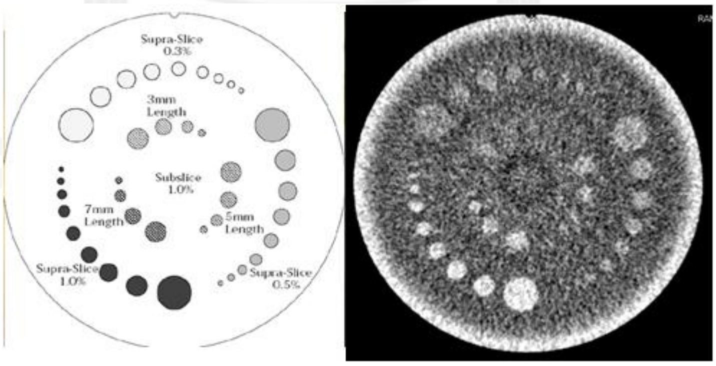

Figure B 16 The low contrast resolution measurement.

Tolerance: At slice thickness 10 mm: The smallest target diameter at 0.5% contrast level of supra - slice should be seen 4 spokes.

Comment: ☑ Pass

11. Slice thickness accuracy

Purpose: To determine the accuracy of the slice thickness.

Method:

1. Set up the Catphan phantom as described in beam alignment set up as you would for beam profile measurement.
2. Select the section containing the accuracy of the slice thickness test objects (CTP404 slice width module).
3. Select the head technique.
4. Select 120 kV_p, 300 mAs, smallest slit width.
5. Perform axial scan with programmed slice thicknesses under auto control.
6. Perform scan following Catphan manual in each slice collimation.
7. Calculate the real slice thickness.

Technique: 120 kV_p, 300mA, 1.0sec, 240mm FOV, slice thickness 1, 3, 5 and 8 mm.

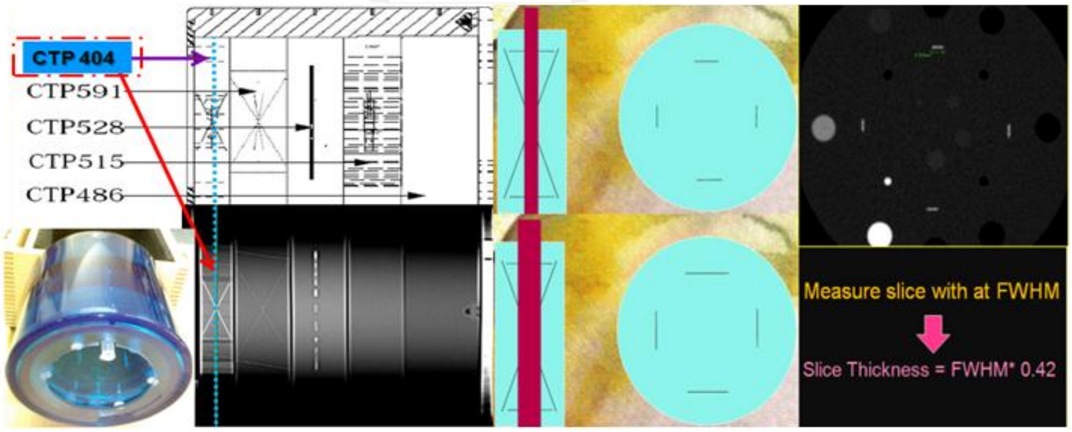

Figure B 17 (Left) Catphan phantom setting and reference line of CTP 404 section (Slice width, sensitometry and pixel size module) and slice thickness calculation from Full Width at Half Maximum (FWHM) by using CTP 404. (Right)

Result:

Table B 10 Slice thickness measurement.

Slice Thickness (mm)	1	3	5	8
Peak	734	337	236	180
BG	92	90.71	88	89.5
Net peak (NP)	642	246.3	148	90.5
50% NP	321	123.15	74	45.25
HM (50% NP + BG)	413	213.86	162	134.75
FWHM L1	2.86	7.51	12.09	18.51
FWHM L2	2.84	7.35	11.92	18.14
FWHM L3	2.86	7.18	11.57	18.86
FWHM L4	2.98	7.18	12.10	18.87
Average FWHM	2.89	7.31	11.92	18.60
Measured Slice Thickness = Average FWHM x 0.42	**1.21**	**3.07**	**5.01**	**7.81**

*Calculate level for measured wire length from

Level setting = (Peak of signal + Background)/2 + Background

*Calculate slice thickness from

Slice width = Length of the ramp x tan 23° = Length of the ramp x 0.42

Table B 11 Slice thickness accuracy.

Slice Thickness in mm	Measured Slice Thickness in mm	Deviation
1.0	1.21	0.21
3.0	3.07	0.07
5.0	5.01	0.01
8.0	7.81	0.19

Tolerance: Slice thickness deviation within 0.5 mm of nominal (NCRP No.99: Quality control test for CT scanner, Section 14).

Comment: ☑ Pass

Note: Radiation Profile width measure from film.

Method:

1. Setting slice thickness in 1, 2, 4, 8 and 12 mm with slice collimation that show in table below with routine head technique ($120kV_p$, 300mA, 1.0sec, 240mm FOV).
2. Scan the film (verification film) with a film scanner (OmniPro RT Scanner) and measure the slice thickness on the film.

Table B 12 Slice thickness accuracy (Measured radiation profile width).

Profile Width (mm)			Deviation	Criteria	Conclusion
Setting (Slice Collimation)		Measured			
1	(0.5x2)	3	2		Fail
2	(0.5x4)	4	2		Fail
4	(1x4)	5	1	± 1	Pass
8	(2x4)	10	2		Fail
12	(3x4)	13	1		Pass

Tolerance: Measured radiation profile width should be within ± 1mm of scan prescription.

Comment: The lack of calibration on scanner can make the measurement over the tolerance level.

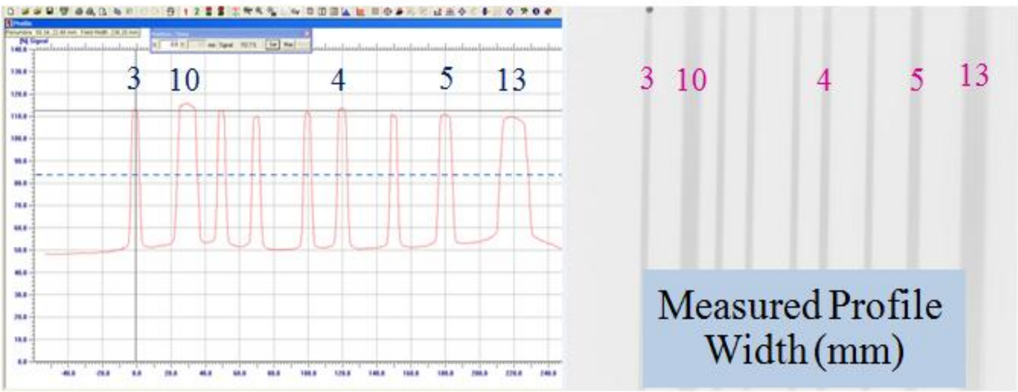

Figure B 18 Slice thickness measurement from radiotherapy film by film scan method.

12. Accuracy of distance measurement

Purpose: To test accuracy of distance measurement and for circular symmetry of the CT image.

Method:

1. Set up the Catphan phantom as described in beam alignment.
2. Select the section containing the test accuracy of distance measurement.
3. Select the head technique and perform a single transverse scan.
4. Measured object in x and y axes.

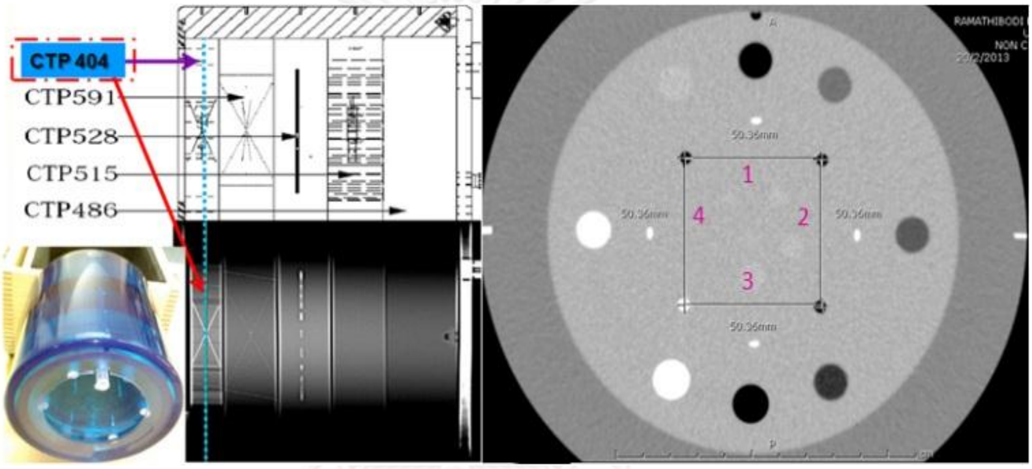

Figure B 19 Accuracy of distance measurements on axial image.

Results:

Table B 13 The accuracy of distance measurement.

Indicated distance (mm)	Measured distance (mm)	Difference (mm)	Criteria	Conclusion
50 mm	50.36	0.36	≤ 1 mm	Pass
50 mm	50.36	0.36		Pass
50 mm	50.36	0.36		Pass
50 mm	50.36	0.36		Pass

Tolerance: The measured distance should be within ± 1 mm. (NCRP No.99: Quality control test for CT scanner, Section 14).

Comment: ☑ Pass

13. Image uniformity

Method:

1. Set up the Catphan phantom as described in beam alignment.
2. Select the section containing the image uniformity module (Select the CTP 486 section: solid image uniformity module).
3. Select the head technique and perform a single transverse scan.
4. Measure the mean value and the corresponding standard deviations in CT numbers within a region of interest (ROI) approximately 400mm^2
5. These measurements are taken from different locations within the scan field.

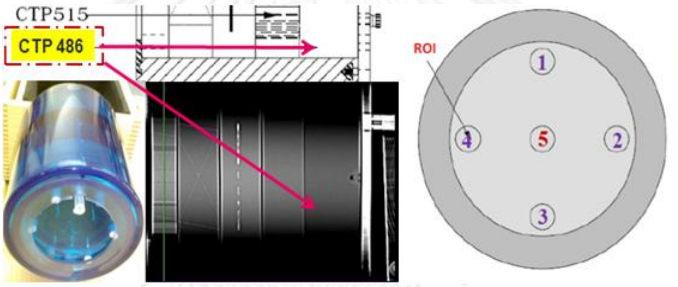

Figure B 20 Catphan phantom setting and reference line of CTP 486 section (Solid image uniformity module) and five positions for measured the image uniformity in Catphan phantom**.**

Technique: 120 kV$_p$, 300mA, 1.0sec, 240mm FOV, 2 and 5mm Slice thickness.

Results:

Table B 14 Image uniformity (Slice thickness 2 mm).

Position	Mean C.T. Number	S.D.	Difference (HU)
1	5.48	4.88	-0.40
2	4.24	4.86	0.84
3	3.89	4.26	1.19
4	4.4	4.71	0.68
5 (center)	5.08	5.14	0.00

**Difference = |CT number center–CT number peripheral |*

Table B 15 Image uniformity (Slice thickness 5 mm).

Position	Mean C.T. Number	S.D.	Difference (HU)
1	4.45	2.85	0.00
2	3.87	2.77	0.58
3	3.58	2.92	0.87
4	3.84	2.86	0.61
5 (center)	4.45	3.54	0.00

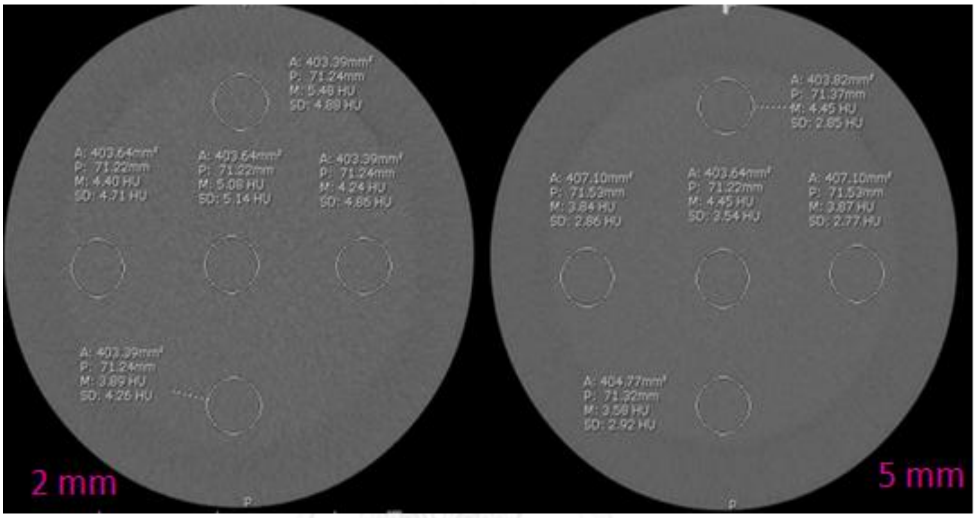

Figure B 21 Five positions for mean CT number measurement measured the image uniformity in Catphan phantom at 2mm (left) and 5mm (right) slice thickness.

Tolerance: The difference of CT number between center and periphery position should be within ± 5 HU (IAEA Human Health Series No.19).

Comment: ☑ Pass

VITA

NAME	Miss Saifhon Admontree
DATE OF BIRTH	April 20, 1980
PLACE OF BIRTH	Khonkaen, Thailand
EDUCATION	Bachelor of Science Program in Radiological Technology, Faculty of Medical Technology, Mahidol University, 2003
POSITION HELD&OFFICE	Radiological Technologist at Advanced Diagnostic Imaging Center, Faculty of Medicine, Ramathibodi Hospital, Mahidol University. 270 Rama VI Rd, Phayathai, Ratchatewi, Bangkok. 10400

Academic Publication

1. Admontree, S., Krisanachinda, A., Laothamatas, J.and Trinavarat, P. Radiation Dose in Whole Brain Computed Tomography in Comprehensive Stroke Imaging using Axial Volumetric 320-detector CT. In proceeding of 13th Asia-Oceania Congress of Medical Physics & 11th South-East Asian Congress of Medical Physics, pp 117-120. Singapore, 2013.